

DIFFUSIVE LOSS OF NAPL FROM A DISK SOURCE

**DIFFUSIVE LOSS OF NON-AQUEOUS PHASE ORGANIC SOLVENTS
FROM A DISK SOURCE**

By
INTAEK YOON, M.S

A Thesis
Submitted to the School of Graduate Studies
In Partial Fulfillment of the Requirements
For the Degree
Masters of Applied Science

McMaster University
Department of Civil Engineering

© Copyright InTaek Yoon, September 2006

Masters of Applied Science (2006)
(Civil Engineering)

McMaster University
Hamilton, Ontario

Title: Diffusive Loss of Non-Aqueous Phase Organic Solvents from
a Disk Source

Author: Intaek, Yoon
M.S (Seoul National University)

Supervisor: Dr. Sarah E. Dickson

No. of Pages: xii, 139

Abstract

Matrix diffusion from planar fractures was studied both mathematically and through physical model experiments. A conceptual model was developed based on previous work by Parker (1994) and Crank (1956). Mathematical models were developed to simulate diffusion from 2D and 3D instantaneous disk sources and a 3D continuous disk source. The models were based on analytical solutions previously developed by Carslaw and Jaeger (1959). Analytical solution is not available for the total mass diffused into the porous matrix for a 3D continuous disk source, and it was therefore calculated through the summation of the iso-concentration lines, which were assumed to be a semi-spherical shape.

The mathematical simulations indicated that the 2D scenario produces significantly different results from the 3D scenario, the time for mass disappearance is significantly larger for continuous sources than for instantaneous sources, the normalized concentration generally decreased over time for instantaneous sources while it increased over time for continuous sources, diffusion rates decrease significantly over time and space, and the normalized mass loss from the source zone never reaches 1 for continuous sources due to the semi-infinite integral. The simulations also showed that disappearance times increase exponentially with increasing source radii and matrix porosity, and decrease with increasing aqueous-phase NAPL solubilities.

The observations from the physical model experiments were very close to the simulated data at $z = 0$, validating the 3D mathematical models for this elevation. A plot of the observed vs simulated data did not reveal any trends, indicating that the majority

of the differences can be attributed to experimental error. The experimental concentrations were below the method detection limit at depths of 3 and 6 cm however, indicating that either the experiments should have been conducted over a longer time period or a more sensitive analytical method should have been employed, to enable model validation at these depths.

Acknowledgements

I wish to express my appreciation to my supervisor, Dr. Sarah E. Dickson for her support and friendship throughout the research and, for affording me the opportunity to work as her student. I would also like to thank Dr. James E. Smith in the School of Geography and Earth Sciences at McMaster University for his advice during the experiments.

The support and encouragement of my entire family is invaluable - without it I could not have come this far. I would like to thank the most important person of all, my wife HaeJin Chang. Without her help and support throughout these last three years this thesis would not have been possible. Also I dedicate this work to my lovely two daughters Kate (SoHyun) Yoon, and Jessica (JiYeon) Yoon. Every time I am writing this thesis I am an insufficient father.

Table of Contents

Chapter 1: Introduction	1
1.1 Introduction	1
1.2 Research Goals and Objectives	6
1.3 Thesis Outline	7
Chapter 2: Literature Review	8
2.1 Literature Review	8
Chapter 3: Conceptual Frameworks and Mathematical Model Development	20
3.1 Conceptual Model Development	20
3.2 Mathematical Model Development	23
3.2.1 Derivation of the Diffusion Equation for a Disk Source	26
3.2.2 Analytical Solution Development : Instantaneous Disk Source in 2D	29
3.2.3 Analytical Solution Development : Instantaneous Disk Source in 3D	34
3.2.4 Analytical Solution Development : Continuous Disk Source in 3D	36
Chapter 4: Computation Results and its Comparison	40
4.1 Computational Results from a 2D Instantaneous Disk Source	42
4.2 Computational Results from a 3D Instantaneous Disk Source	50
4.3 Computational Results from a 3D Continuous Disk Source	56
4.4 Comparison of the 3D Instantaneous and Continuous Disk Source Solutions ..	63
4.5 Parameter Sensitivity Analysis	67
4.5.1 Sensitivity of disappearance time to the Radius of Disk Source and Chemical Properties	68
4.5.2 Sensitivity of Disappearance Times to Matrix Porosity (ϕ_m)	71
4.6 Comparison of the disappearance time between Parker's and this work	74
Chapter 5: Laboratory Experiments	77
5.1 Materials and Methods	77
5.1.1 Silica Flour	77

5.1.2 N-Butanol	80
5.2 Experimental Apparatus	81
5.3 Experimental Conditions	84
5.4 Sampling Locations	85
5.4.1 Sampling Locations	85
5.4.2 Sampling Methodology	89
5.4.3 Quantification of n-Butanol	92
5.5 Observations and Results	94
5.5.1 Percent Saturation	94
5.5.2 Diffusive Loss of n-Butanol	95
5.5.3 Comparison of Experimental Observations and Model Simulations	101
6. Conclusions	106
6.1 Achievements of Present Study	106
6.2 Recommendations for Future Work	108
7. References	109
Appendix I: Fortran and Maple Codes for calculations of the diffusion	117
Appendix II: Analysis data for experiment 2 and 3	139

List of Figures

Figure 3.1: Top view of the 2D and 3D conceptual models. Arrows represent direction of diffusion within the porous matrix	21
Figure 3.2: Side view of the 3D conceptual model. Arrows represent the direction of diffusion, which is assumed to be symmetrical about the fracture aperture	21
Figure 3.3: Conceptual model for instantaneous and continuous disk sources in a 3D cylindrical coordinate system	22
Figure 3.4: Parker's conceptual model (1994) for NAPL disappearance in fractured porous media. a) early time, b) intermediate time, and c) later time	22
Figure 3.5: Schematic diagram of a ring source	27
Figure 3.6: Schematic diagram of a disk source	28
Figure 3.7: A schematic diagram for the calculation of diffused mass at any time t	32
Figure 3.9: A schematic diagram for interpolation of the concentration profile at depth	39
Figure 4.1: Comparison of the approximate solution (3.14f) with orders of 4, 8, 12, and the exact solution (3.12, 3.17) for a 2D instantaneous disk source at $t = 3600$ sec. Values of variables are given in Table 4.2	43
Figure 4.2: Concentration profile at $r=0$, for a 2D instantaneous disk source	44
Figure 4.3: Concentration profile versus distance at $r = 0$ for a 2D instantaneous disk source with boundary conditions given by (3.11)	45
Figure 4.4: Concentration profiles for an instantaneous disk source in 2D with boundary conditions given by 3.11	46
Figure 4.5: Comparison of mass diffused from the source zone at time t computed by equation (3.18a) and (3.16c)	47
Figure 4.6: The total mass diffusing away from the disk source (hatched area) and remaining in the disk source (white area) as a function of time for a 2D instantaneous disk source with boundary conditions given by (3.12)	48
Figure 4.7: Relative concentration profiles from a 2D instantaneous disk source at times. (a) $t = 5$ days,(b) $t=10$ days,(c) $t =15$ days,(d) $t =20$ days,(e) $t =25$ days, and (f) $t =30$ days	49
Figure 4.8: Concentration profile at $r = 0.0$ cm, $z = 0.0$ cm, for a 3D instantaneous disk source (dashed line) with boundary conditions given by (3.19), and a 2D instantaneous disk source (solid line) with boundary conditions given by (3.11)	51

Figure 4.9: Concentration distributions for instantaneous disk sources in 2D and 3D, with boundary conditions and variable values listed in Table 4.1 and 4.2 respectively	52
Figure 4.10: The relative mass diffusing into the porous matrix for the 2D and 3D instantaneous disk sources	53
Figure 4.11: Relative concentration profiles from a 3D instantaneous disk source at times. (a) $t = 5$ days, (b) $t = 10$ days, (c) $t = 15$ days, (d) $t = 20$ days, (e) $t = 25$ days, and (f) $t = 30$ days	54
Figure 4.12: The vertical section of the concentration profile from a 3D instantaneous disk source at times (a) $t = 5$ days, (b) $t = 10$ days, (c) $t = 15$ days, (d) $t = 20$ days, (e) $t = 25$ days, and (f) $t = 30$ days	55
Figure 4.13: Concentration profile at $r = 0.0$, $z = 0.0$ cm for a 3D continuous disk source with boundary conditions given by equation (3.25)	57
Figure 4.14: Relative concentration profiles as a function of dimensionless time for a 3D continuous disk source with boundary conditions given by equation (3.25) at $z = 0$ and $r = 0, 0.25, 0.5, 0.75,$ and 1 cm	58
Figure 4.15: Relative concentration profiles as a function of dimensionless time for a 3D continuous disk source with boundary conditions given by equation (3.25) at $z = 0$ and $r = 1.5, 2, 4, 8, 12, 16,$ and 20 cm	59
Figure 4.16: Normalized concentration profiles versus radial distance for a 3D continuous disk source with boundary conditions given by (3.25), at $t = 15$ days, 1 yr, and infinity	59
Figure 4.17: Total amount of diffusing substance on continuous disk source in 3D at $z = 0$	61
Figure 4.18: The mass diffused from a 3D continuous disk source with boundary conditions given by (3.25)	61
Figure 4.19: Relative concentration profile sections, through the origin, for a 3D continuous disk source with boundary conditions given by equation (3.25) at (a) $t = 1$ day, (b) $t = 5$ days, and (c) $t = 10$ days	62
Figure 4.20: Comparison of the relative concentration as a function of time for the 3D instantaneous and 3D continuous disk source solutions at $r = 0$ and $z = 0$	64
Figure 4.21: Comparison of cumulative normalized mass diffused from 3D instantaneous and continuous disk sources as a function of time	64
Figure 4.22: Comparison of mass diffused as a function of time for 3D instantaneous and continuous disk sources	65

Figure 4.23: Comparison of the normalized concentration profiles as a function of time for 3D instantaneous and continuous disk sources at $r = 2.0$ cm and $z = 0.0$ cm	66
Figure 4.24: NAPL disappearance times expressed in terms of the radius of disk source for a 3D instantaneous disk source with (a) a clay matrix ($R=1$), (b) a shale/sandstone matrix ($R=1$), and (c) a granite matrix ($R=1$)	70
Figure 4.25: NAPL disappearance times for a 3D continuous disk source for four chemicals expressed in terms of equivalent radius of disk source	71
Figure 4.26: Effect of matrix porosity on the rate of DNAPL disappearance for a 3D instantaneous disk source with no sorption ($R=1$)	73
Figure 4.27: Effect of matrix porosity on NAPL disappearance time expressed as equivalent radius of a continuous disk source for a clay matrix with no sorption ($R=1$) at $t = 10$ days	73
Figure 4.28: Comparison of the Parker <i>et al.</i> , (1994) model and this work as a function of the mass diffused into matrix at disappearance times of $t = 1$ day, $t = 10$ days, $t = 100$ days, and $t = 1000$ days	76
Figure 5.1: Results of a sieve analyses for the silica flour employed in these experiments(Source : U.S Silica Company)	80
Figure 5.2: (a) Schematic and (b) photograph of the experimental apparatus	83
Figure 5.3: Results of simulations employed to determine the size of experimental apparatus required for these experiments	83
Figure 5.4: Sampling locations for experiment 1, $z = 0$	85
Figure 5.5: Surface sampling locations ($z = 0$) for experiments 2 and 3	86
Figure 5.6: Sampling locations at 3cm depth ($z=3$ cm) for experiments 2 and 3	87
Figure 5.7: Sampling locations at 6cm depth ($z=6$ cm) for experiments 2 and 3	88
Figure 5.8: Coring device	90
Figure 5.9: GC-MSD calibration curve for n-butanol	93
Figure 5.10: Variations in the percent saturation at depths of 0 cm, 3 cm, and 6 cm	95
Figure 5.11: Top view of the experimental apparatus for experiment 1 at a) $t = 0$, b) $t = 1$ hr, c) $t = 4$ hrs, d) 9 hr and e) $t = 24.5$ hrs	96
Figure 5.12: Top view of the experimental apparatus for experiment 2 at a) $t = 0$, b) $t = 1$ hr, c) 5 hrs and d) $t = 10.5$ hrs	97
Figure 5.13: Top view of c the experimental apparatus for experiment 3 at a) $t = 0$, b) $t = 1$ hr, c) 5 hrs and d) 10.5 hrs	98

Figure 5.14: The diffused mass of n-butanol per hour versus experimental time for experiment 1	100
Figure 5.15: Mass loss comparisons as calculated from observed data and by mathematical simulation for experiment 1	100
Figure 5.16: Comparison between calculated and observed data at the end of experiment 1 (t = 12.5 hrs)	102
Figure 5.17: Comparison between calculated and observed data at the end of experiment 2 (t = 10 hrs 10 min.)	103
Figure 5.18: Comparison between calculated and observed data at the end of experiment 3 (t = 10 hrs 5 min.)	103
Figure 5.19: Concentration profiles at various experimental times	104
Figure 5.20: Comparison between calculated and observed data for experiment 1, 2 and 3	105

List of Tables

Table 1.1 Regulations for chlorinated solvent concentrations present in soil and groundwater, set by US EPA	2
Table 1.2 Physical and chemical properties of selected chlorinated solvents. (Mackay <i>et al.</i> , 1993)	5
Table 4.1 Summary of analytical solutions for diffusive mass transfer in porous media	40
Table 4.2 Values assigned to variables for computational purposes	41
Table 4.3 Chemical properties for selected organic compounds used for diffusive mass loss calculations	67
Table 4.4 Characteristics of various geologic media	68
Table 4.5 Effect of the radius of an instantaneous disk source on TCE disappearance time for types of geologic media	69
Table 4.6 Effect of the matrix porosity on TCE disappearance time for the four different chemicals	72
Table 4.7 Comparison of the disappearance time for four chemicals between the Parker <i>et al.</i> , (1994) model and this work	75
Table 5.1 Chemical Breakdown of Silica Flour	79
Table 5.2 Typical Physical Properties of Silica Flour	79
Table 5.3 Physical properties of n-butanol	81
Table 5.4 Summary of the experimental conditions	84
Table 5.5. Variations of the mass for MeOH and samples in experiment 2 and 3.....	91
Table 5.6 Analysis conditions for GC-MSD	92
Table 5.7 Percent saturation at 0, 3, and 6 cm depths for experiments 1, 2 and 3	94
Table 5.8 Summary of the diffusive mass loss from experiment 1, calculated from visual observation	99

Chapter 1: Introduction

1.1 Introduction

Many kinds of petroleum products and chlorinated solvents were produced after the industrial revolution of the late nineteenth century. Chlorinated solvents were first produced in Europe in the nineteenth century, and production of these chemicals began in the early twentieth century in the United States (Pankow and Cherry, 1996). Carbon tetrachloride (CTC), the first chlorinated solvent, was generally used as dry cleaning and spot-removing agent in the late nineteenth century, and at that time it was imported from Germany into the United States (Doherty, 2000). After the use of CTC as a dry-cleaning solvent, perchloroethylene (PCE) and trichloroethylene (TCE) also became widely used in Europe and the United States. Production of PCE and TCE as chlorinated solvents began in the U.S in 1923. Doherty (2000) stated that *“PCE was introduced to the dry-cleaning industry during the 1930’s, and became widely accepted due to its low toxicity relative to carbon tetrachloride, and its low flammability and less persistent odor relative to petroleum solvents”*. However, due to improvements in the dry-cleaning process, the demand for PCE in the dry-cleaning industry began to significantly decrease. As a result, TCE became one of the most widely used chlorinated solvents in North America and Europe due to its properties; including effectiveness, noncorrosivity, and nonflammability (Kirk-Othmer, 1964). Over 90 percent of TCE consumption was for cleaning and degreasing, and widespread use of chlorinated solvents in dry-cleaning and manufacturing industries began in the 1940s, and increased markedly in the 1950s and 1960s (Pankow and Cherry, 1996). According to the U.S International Trade Commission (1991), the use of TCE peaked in the U.S. in 1970, and PCE and DCM

peaked in the U.S. in 1980. The decline in the use of these substances in the following years was mainly due to increased evidence of toxicity, recognition of the risk to human health, and the advent of environmental regulations.

From the environmental regulations point of view, CTC was banned from use in US commercial goods in 1970, and it was identified by the International Agency for Research on Cancer (IARC) as an animal carcinogen and a potential human carcinogen in 1972. The National Cancer Institute released evidence of TCE carcinogenicity in March 1975 (National Cancer Institute, 1975). The 1992 amendments to the Montreal Protocol included a complete ban on CTC production and use in Canada as of January 1, 2000. To reduce the risk to human health due to chlorinated solvents, the Residential Preliminary Remediation Goals - Soil (PRGs), the Public Health Goals - Groundwater (PHGs), and the drinking water limits (or Maximum Concentration Limits, MCLs), for many chlorinated solvents were set by the US Environmental Protection Agency (EPA) in 1987; these limits are given in Table 1.1.

Table 1.1 Regulations for chlorinated solvent concentrations present in soil and groundwater, set by US EPA.

Chemical Name	Residential Preliminary Remediation Goals-Soil (PRGs) (mg/kg)	Public Health Goals – Groundwater (PHGs) (µg/L)	Regulatory Levels	
			California(US A) drinking water MCL (µg/L)	US drinking water MCL(µg/L)
Tetrachloroethene(PCE)	5.7	60	5	5
Trichloroethene(TCE)	2.8	800	5	5
1,1,1-Trichloroethane	630	No PHG	200	200
1,2-Dichloroethane	0.35	400	0.5	5
DichloroetheneCarbon	0.054	10,000	6	7
Tetrachloride (PCM)	0.024	100	0.5	5
Vinyl Chloride (VC)	0.15	50	0.5	2

Many chlorinated solvents have not been properly treated, or were disposed of directly into the environment. In spite of the widespread use of chlorinated solvents, their presence in soil and groundwater went largely unrecognized until the late 1970s. Kueper *et al.* (2003) explained that the primary reason for this lack of recognition by the research community was the lack of availability of analytical methods and equipment for detecting low concentrations of chlorinated solvents in groundwater. Analytical methods and equipment with the required sensitivities did not become widely available until relatively recently (1980s). Since the mid 1980s, many industrial organic chemicals such as creosote, coal tar, polychlorinated biphenyls (PCBs) and chlorinated solvents have been recognized as common cause of soil and groundwater contamination in industrialized areas. It has been estimated that there are thousands of sites impacted by non-aqueous phase liquids (NAPLs) in North America, continental Europe and other industrialized areas of the world (Kueper *et al.*, 2003).

There are three primary differences between dense non-aqueous phase liquids (DNAPLs) and light non-aqueous phase liquids (LNAPLs) in terms of groundwater contamination. When LNAPLs (*e.g.*, petroleum products) are spilled in significant volumes, being less dense than water, they float on the water table. This property enables them to be located in the subsurface relatively easily (Marinelli and Durnford, 1996). In contrast, when DNAPLs are spilled into the subsurface, they are often difficult to locate as they sink below the water table. Secondly, DNAPLs are often not detectable by taste, odor, or sight, as they exist in the dissolved form at very low concentrations (concentration levels ranging from ppm to ppb). Conversely, most LNAPLs are relatively

easy to detect by taste, odor and sight at typical aqueous phase concentrations. The third principal difference is mobility. LNAPLs float on the water table; they move in the horizontal direction and the main driving force is surface tension. However, DNAPLs do not stop at the water table. They migrate both vertically and laterally in the subsurface due to gravitational and viscous forces. Their high densities, and often low viscosities, enable them to migrate considerable distances. Migration ceases when the gravitational and viscous forces are exceeded by capillary forces.

Chlorinated solvents (e.g., trichloroethene (TCE), tetrachloroethene (PCE), 1,1,1-trichloroethane(1.1.1-TCA)) form a class of DNAPL compounds; Table 1.2 gives the physical properties of a selection of these compounds. Chlorinated solvents are highly toxic, and are characterized by low aqueous phase solubilities, viscosities, degradabilities and K_{oc} values. Therefore, small volumes of chlorinated solvents have the ability to contaminate large volumes of groundwater over a long period of time. As stated above, when DNAPLs are released at the ground surface they migrate both vertically and laterally due to gravitational and viscous forces in the unsaturated and saturated zones. As the DNAPL migrates through the subsurface, residual DNAPL is formed in both the unsaturated and saturated zones. Residual DNAPL, in the form of disconnected blobs and ganglia, dissolves slowly into flowing groundwater due to its low aqueous phase solubility, consequently giving rise to aqueous phase plumes in subsurface systems (Kueper *et al.*, 2003). DNAPL pools form at the top of capillary barriers in subsurface systems, and also act as a source of long-term contamination for massive volumes of ground water.

Table 1.2 Physical and chemical properties of selected chlorinated solvents.(Mackay *et al.*, 1993)

Solvent	Molecular weight	Aqueous solubility (mg/L)	Density (g/cm ³)	Vapour pressure (Pa@°C)	Viscosity (cP)	K _{oc} (l/kg)
Trichloroethene	131.4	1,100	1.46	9,000	0.57	126
tetrachloroethene	165.8	200	1.62	2,600	0.90	364
tetrachloromethane,	153.8	790	1.59	15,000	0.97	439
trichloromethane	119.4	8,000	1.48	26,000	0.56	44
chlorobenzene	112.6	500	1.11	1,580	0.80	330
1,1,1-trichloroethane	133.4	1,320	1.33	16,000	0.84	152

In fractured subsurface systems, fractures are typically the main avenue for fluid flow, even though the majority of the porosity exists in the matrix blocks between the fractures. DNAPL will enter a water-saturated fracture if the capillary pressure at the leading edge of the DNAPL body exceeds fracture entry pressure, as determined by the properties of the fluid and of the medium (Kueper *et al.*, 1991). The dissolved-phase mass can diffuse from the fracture itself into the pore water within the matrix.

For common chlorinated solvents, mass loss from the fracture to the matrix block can eventually result in complete disappearance of the DNAPL from the fracture (Parker *et al.*, 1994). In general, dissolution in combination with diffusion is the mechanism responsible for the change in the physical state of the solvent, from the DNAPL phase to the aqueous and sorbed phases. The disappearance rate and its implications are the subjects of Parker's work (e.g., Parker *et al.*, 1994, 1997). Dissolution occurs at the fluid-fluid interface. The rate of dissolution of DNAPL in the subsurface will depend on the

effective solubilities and diffusivities of the DNAPL components, the physical distribution of the DNAPL in the porous or fractured medium, and the rate of groundwater flow through and around the DNAPL zone (Pankow and Cherry, 1996). Once dissolution occurs within a saturated fracture, the dissolved DNAPL will diffuse into the porous matrix surrounding the fracture due to a concentration gradient.

Several researches have indicated that it is extremely difficult to remediate DNAPL sites, particularly in highly heterogeneous environments such as fracture systems. (e.g., Parker *et al.*, 1994; Keuper *et al.*, 2003). In the absence of remedial strategies, the dissolution and subsequent diffusion mechanisms will remove trapped DNAPL from fractured environments. Although Parker *et al.*,(1994, 1997) conducted numerical simulations to estimate NAPL disappearance times in fractured environments, these models were never validated through experimentation. Additionally, numerous simplifying assumptions were employed in these models, which likely lead to error in the predicted NAPL disappearance times.

1.2 Research Goals and Objectives

The goal of this research was to further the understanding of diffusive loss of NAPLs in fractured media through computer simulations of the dissolution and subsequent diffusion mechanisms, and to verify these computer simulations through physical model experiments. To achieve this goal, several specific research objectives were defined:

- 1) Establish conceptual and mathematical models for diffusion from instantaneous

and continuous disk sources in 2D and 3D.

- 2) Compare the analytical solutions for the instantaneous and continuous disk source cases in both 2D and 3D.
- 3) Conduct physical model experiments to quantify matrix diffusion in fractures.
- 4) Compare the results of the physical model experiments to those from the mathematical models.

1.3 Thesis Outline

This thesis contains six chapters in addition to this one. Chapter 2 contains a review of background literature pertaining to NAPL entrapment in fractures, as well as the dissolution and diffusion mechanisms in subsurface environments. Chapter 3 presents the conceptual framework and mathematical model development for diffusion from instantaneous disk sources in 2D and 3D, and for continuous disk sources in 3D. Chapter 4 gives the computational results for the three cases (i.e., instantaneous disk source in 2D and 3D, and continuous disk source in 3D), and presents a sensitivity analysis for the 3D instantaneous disk source. Chapter 5 presents the experimental materials and methods employed for the laboratory experiments, and also Chapter 5 presents the results of these experiments, and compares these results to the computational results. Chapter 6 gives the conclusions, and identifies areas in need of further study resulting from this work.

Chapter 2: Literature Review

2.1 Literature Review

Historically, the term “*NAPL*” was first coined in 1981. A black and denser-than-water, immiscible organic liquid was discovered in the soil and bedrock during studies of a hazardous waste landfill in Niagara Falls, New York (Pankow and Cherry, 1996). Although the groundwater community had become aware of the presence of NAPL in soil and groundwater environments by 1981, they did not know how much existed, or how to remediate the dissolved chlorinated solvents located in the subsurface environments until the late 1980s. Pankow and Cherry (1996) noted that large amounts of pure-phase solvent were present at sites contaminated with chlorinated solvents, and that the presence of pure-phase in subsurface systems leads to many difficult problems for remediation strategies. In terms of the literature, the first published paper addressing the behaviour of chlorinated solvents in the subsurface was by Schwille (1984). After the English version of Schwille’s work (1984) was published in 1988 (Schwille, 1988), the groundwater and environmental science community recognized DNAPLs as an important class of groundwater contaminants. Thus, although the general presence of chlorinated solvents in groundwater had become widely recognized in the 1970’s, it was not realized that pure-phase source zones were present below the water table at many contaminated sites until the early 1980’s.

Since the recognition of the existence of NAPL source zones in subsurface systems, a significant body of research has focused on DNAPL migration and its subsequent fate in subsurface environments (e.g., multiphase flow, entrapment,

dissolution and matrix diffusion of DNAPLs) (e.g., Abriola and Pinder, 1985, 1995; McWhorter and Sunada, 1990; Longino and Kueper, 1995; Smith and Gillham, 1999; Silliman *et al.*, 2001; Dickson and Thomson, 2003; Feenstra, 1984; Cherry, 1984; Miller, 1984; Schroth *et al.*, 1995; Eckberg and Sunada, 1984; Parker *et al.*, 1994, 1997). These investigations have employed laboratory investigations, field experiments, and mathematical models.

An excellent understanding of the physical and chemical mechanisms controlling DNAPL behaviour in subsurface environments is essential in order to locate spilled NAPL masses, gauge the risk to human health, and develop appropriate monitoring and remedial strategies. The theory of two-phase flow and NAPL transport in subsurface systems was investigated extensively by petroleum engineers, who were concerned with the movement of petroleum through reservoirs, before NAPLs were recognized as a contaminant source (Buckley and Leverett, 1942). Subsequently, the environmental industry became interested in two-phase flow and NAPL transport. McWhorter and Sunada (1990) studied DNAPL flow in saturated subsurface systems. They derived exact solutions for both one-dimensional and radial flow for two viscous, incompressible fluids and evaluated them numerically for several different types of porous media. They found that saturation profiles for unidirectional and radial drainage exhibit a remarkable sensitivity to both the pore-size distribution and the injection rate. Abriola and Pinder (1985) investigated three-phase flow in systems consisting of air, water, and NAPL, typical of the vadose zone. They developed a multiphase approach to the modeling of organic compound migration in the subsurface environment. This approach is capable of

describing the simultaneous transport of a chemical contaminant in three physical forms: a nonaqueous phase, a dissolved phase, and a gaseous phase. Abriola *et al.* (1995) noted that as NAPL migrated through subsurface systems, capillary forces act to trap residual masses. The partitioning of this residual NAPL mass into the solid, air and water phases serves as a persistent source of contamination which significantly impedes remedial efforts. The physics and chemistry of NAPL entrapment and mass transfer were, at that time, not fully understood. Since the early 1990s, however, much research focusing on the migration and entrapment of DNAPL has investigated the influence of coupled physical and chemical heterogeneities, and has employed a combination of laboratory and numerical experiments (Abriola *et al.*, 1996).

Multi-phase flow in subsurface systems is largely dependent on the relative densities, viscosities, and interfacial tensions of the relevant fluids. When NAPLs are released into the subsurface, they will migrate vertically through the vadose zone. Some mass will remain in the vadose zone both as a residual saturation, and in the gaseous phase due to volatilization. The degree of phase partitioning is dependant on the relative solubilities and volatilities of the compounds present. If a sufficient mass is released, it will eventually reach the top of the capillary fringe, at which point the behaviour of DNAPLs and LNAPLs differ dramatically. LNAPLs will spread laterally over the capillary fringe, while DNAPLs will displace the water occupying the pore space within the capillary fringe and below the water table and continue to migrate vertically until a capillary barrier is reached. At this point, the DNAPLs will spread laterally until either the source is exhausted or another suitable vertical pathway is reached.

Kueper and McWhorter (1991) presented the physics governing the migration and entrapment of DNAPLs, as well as the formation of DNAPL pools in fractured media. They examined the behaviour of DNAPLs in fractured clay and fractured rock. They used a numerical model to demonstrate the behaviour of DNAPL in a rough-walled fracture plane. According to their simulation results, DNAPLs will migrate through the larger aperture regions of a saturated fracture plane, and then enter progressively smaller aperture fractures with depth, as the driving force increases. Additionally, they found that the time it takes for a non-aqueous phase liquid to traverse a fracture is inversely proportional to the fracture aperture size, the fracture dip, and the height of the pool collected above the aquitard. DNAPL will enter a water-saturated fracture if the capillary pressure at the leading edge of the DNAPL body exceeds the fracture entry pressure, as determined by the properties of the fluid and of the medium.

The capillary pressure (P_c) is defined as the pressure difference between nonwetting fluid (DNAPL, P_{NW}) and wetting fluid (water, P_w) (Bear, 1972),

$$P_c = P_{NW} - P_w \quad (2.1)$$

The entry pressure of a rough-walled fracture is approximated by (Kueper and McWhorter, 1991),

$$P_E = \frac{2\sigma \cos\theta}{e} \quad (2.2)$$

where e is the aperture [L], σ is the interfacial tension between the DNAPL and water [F/L], and θ is the contact angle measured through the wetting phase. Equation 2.2 shows that the entry pressure is directly proportional to the interfacial tension between

the liquids and inversely proportional to the fracture aperture, and that the larger aperture regions of a fracture have the lowest entry pressures.

Once a DNAPL has entered a fracture or fracture network, progressively smaller apertures will be invaded if the DNAPL is allowed to extend itself vertically while remaining in a continuous phase (Kueper and McWhorter, 1992). The maximum height of DNAPL that can accumulate above a capillary barrier without penetrating the saturated zone was studied by Kueper *et al.*, (1991, 1993). They stated that the DNAPL pool height is directly proportional to the capillary pressure difference between the top and base of the pool and the interfacial tension, and inversely proportional to the fracture aperture and density difference between the DNAPL and the groundwater. Longino and Kueper (1995) studied the pool height in a flowing groundwater system. They presented a mathematical analysis and performed one-dimensional column experiments for investigating the dissolution of DNAPL pools from natural silica sand column using solubilizing surfactants under upward-flowing conditions. According to their study, upward hydraulic gradients are capable of arresting downward DNAPL migration in a surfactant flood, and the risk of DNAPL movement downward into previously uncontaminated zones of the subsurface increases with decreasing hydraulic gradient.

When a DNAPL becomes trapped in a fracture, the dissolution and diffusion mechanisms govern the length of the time that the source will persist in the absence of remedial actions. Dickson and Thomson (2003) noted that a good understanding of the dissolution processes for NAPLs entrapped in fracture systems is essential towards understanding and predicting the behaviour and fate of NAPLs in fractured rock systems.

The rate of dissolution of DNAPL is commonly estimated using the following factors: a mass transfer coefficient, the interfacial contact area between the DNAPL and groundwater, and a driving force (Pankow and Cherry, 1996). The three most common models for explaining the dissolution phenomena are the stagnant film model, the film penetration model, and the random surface renewal model (Cussler, 1984). Dickson and Thomson (2003) noted that little research exists regarding the dissolution of NAPLs in fractures; however they noted that the results of work investigating pooled DNAPLs in unconsolidated porous media may be instructive toward the understanding of NAPL dissolution in fractures.

Schwille (1988) conducted a series of laboratory experiments examining the dissolution of a TCE pool with dimensions of 1.5 m in length, 0.5 m in width and 0.5 m in depth. They used medium-grained sand as a bottom material. Water flowed through the tank, passing over the TCE pool at velocities ranging from 0.45 to 2.7 m/day, and the dissolved TCE concentrations were measured. It was found that the dissolved concentrations from the tank effluent were less than saturated dissolved concentrations. Johnson and Pankow (1992) extended Schwille's work to calculate the time required for the complete dissolution of a pool of solvents. They calculated the mass-transfer coefficient and dispersivity using Schwille's data. The time to complete dissolution (τ_p , years) for an ideal pool geometry was developed and given by,

$$\tau_p = 2.43 \times 10^{-5} \rho C_{SAT}^{-1} \sqrt{L_p^3 / D_v \bar{v}} \quad (2.3)$$

where ρ is the density of the solvent [M/L^3], C_{SAT} is the saturation concentration of

the compound of interest $[M/L^3]$, L_p is the length of the pool in the direction of groundwater flow $[L]$, D_v is the vertical dispersion coefficient $[L^2/T]$, and \bar{v} is the average groundwater velocity $[L/T]$. Therefore, the dissolution rates depend on the vertical dispersivity, the length of the pool, the solubility, and the groundwater velocity. Hunt *et al.* (1988) developed analytical solutions for the dissolution of DNAPL ganglia and pools to predict single-component DNAPL dissolution into groundwater. They also presented the results of laboratory experiments, using a 1-D column, 91 cm long with an internal diameter of 5.1 cm, and packed with Ottawa sand. They found that the average effluent concentration decreased with increasing flow velocity due to the decreasing contact time. The time required for DNAPL dissolution into groundwater is on the order of decades because the mass transfer rate decreases over time. Dickson and Thomson (2003) developed a phenomenological model based on their experimental data. They employed two fracture planes that originated from a dolomitic limestone outcrop with dimensions of 30.0 cm and 54.6 cm in length (direction of flow) and 22.5 cm and 28.58 cm in width (perpendicular to flow), respectively. They found that three distinct and characteristic stages of dissolution exist: an initial pseudosteady stage, a transient stage, and a tailing stage. They also stated that approximately 8% of initial volume of NAPL present was removed during the initial pseudosteady stage. They concluded that the model developed provides a useful tool for characterizing mass transfer rates in variable aperture fractures.

Once a NAPL trapped within a fracture dissolves, it will diffuse from the fracture into the porous matrix surrounding the fracture (Parker *et al.*, 1994). Since matrix

diffusion was first recognized in 1975 (Foster, 1975), many researchers have investigated this subject, and have focused mostly on the development of conceptual models and their solutions. Some of these conceptual models have focused on sensitivity analyses examining the effect of matrix diffusion on solute transport in fractured media. The following paragraphs review the literature pertaining to matrix diffusion and the diffusive loss of NAPL in fractured subsurface environments.

Foster (1975) realized the effects of matrix diffusion on contaminant behaviour in fractured rock while analyzing a tracer experiment conducted in fractured porous limestone in England. He was able to fit the experimental data only when his model accounted for the attenuation of tritium into the porous limestone matrix. Following Foster's research, Young *et al.* (1976) used a similar mathematical approach to interpret the behavior of nitrate in the same limestone environment and checked the validity of the model using measured tritium and chloride profiles. Day (1977) used the matrix diffusion concept to account for shallow concentration profiles of tritium and oxygen-18 in fractured clay in central Canada.

In the early 1980s, several mathematical models were developed to predict contaminant transport in fractured media with ideal planar walls where transport is influenced by advection, matrix diffusion, axial dispersion, and geochemical retardation (Neretnieks, 1980; Grisak and Pickens, 1980, 1981; Feenstra *et al.*, 1984). A matrix diffusion model was applied by Neretnieks (1980) to explain the retardation of nuclides from a fuel repository into the rock matrix. The model included both diffusion of the nuclides into the rock matrix and sorption of the nuclides onto the surfaces of the fracture

walls. Grisak and Pickens (1980) described an analytical solution for advective solute transport in a planar fracture coupled with diffusion into the adjacent porous matrix. Their analytical solution was verified through laboratory data from a column tracer test conducted with fractured till.

Solute transport through fractured media is typically explained by an advective-dispersive transport model combined with a diffusive transport model, the former is applied in the fracture and the latter applied in the surrounding porous matrix. Grisak and Pickens (1980) developed a useful solution for conducting sensitivity analyses on the effects of water velocity, fracture aperture size, matrix porosity, matrix distribution coefficient, and the diffusion coefficient on solute transport. They concluded that all of these properties are important in determining the relative amounts of solute transported in the fracture and stored in the matrix. The effective solute velocity in the fracture is affected by the matrix diffusion coefficient and the distribution coefficient. They also pointed out that the fracture aperture size plays a significant role in the analysis of solute transport through fractured media; if the aperture size is reduced, the amount of solute transported in the fracture is also reduced and a greater proportion of the solute enters the matrix pores. Feenstra *et al.* (1984) evaluated the influence of matrix diffusion on the movement of contaminants away from a wastewater injection well. An analytical model was developed to simulate the radial migration of the contaminant front away from the injection point under steady flow conditions in a planar fracture with uniform properties. The effective diffusion coefficient was obtained from laboratory experiments.

The first studies concerning DNAPL disappearance in fractures were performed

by Parker *et al.* (1994, 1997). They developed analytical solutions, in one and three dimensions respectively, to solve for NAPL disappearance time in fractured environments. An analytical solution for 1-D diffusion of an aqueous phase mass from a planar fracture surface into the pore water of the matrix was used to calculate DNAPL disappearance times for single component NAPL (Parker *et al.*, 1994). From this study, it was found that DNAPL disappearance for higher solubility compounds is relatively rapid, and the solubility of a DNAPL has a direct effect on its mass loss from a fracture as well as an indirect effect on its mass loss through its influence on partitioning to the matrix solids. It was also found that the geologic media has a significant impact on the disappearance times of DNAPL. Common chlorinated solvents such as dichloromethane (DCM), trichloroethene (TCE), and tetrachloroethene (PCE) are expected to completely disappear in clayey deposits (with matrix porosities ranging from 25% to 70%) within a few days to weeks. The disappearance times for the same solvents are generally a few years in fractured sedimentary rock, which typically have much lower matrix porosities (5~15%). They also stated that relatively small apertures, high aqueous solubilities, and large porosities and high sorption capacities will contribute to enhancing the rapid DNAPL loss rate. This model applies to matrix blocks of a sufficiently large size, so that diffusion from each fracture is not influenced by diffusion from other fractures.

Parker *et al.* (1997) extended their 1994 analysis to include DNAPL mass flux and disappearance from fractures into matrix blocks of finite size where diffusion effects from fractures bordering the same matrix block are included. They employed an analytical solution for 3-D diffusion of aqueous-phase mass from a fracture into the pore

water of the surrounding matrix block. This model employed rectangular, parallelepipeds to represent the matrix blocks, which were bound by smooth planer fractures. The authors found that the disappearance time for a stationary, single-component NAPL from planar fractures was directly dependent on the ratio of the mass storage capacity (dissolved and sorbed) in the matrix to the initial storage capacity in the fractures; this ratio is known as the mass storage capacity ratio.

The Parker *et al.* (1994, 1997) studies focused on the analytical solutions for rectangular 1-D and 3-D idealized cases. Their studies did not provide a comparison of the analytical solutions to experimental data. Additionally, numerous simplifying assumptions were made, which inherently lead to error in the dissolution times.

In summary, matrix diffusion in fractured media is controlled by several factors, including the mass storage capacity (function of fracture spacing, aperture size and matrix porosity), the diffusion coefficient, the dispersivity coefficient, the distribution coefficient, and the aqueous phase flow rate. Additionally, all of these factors interact with one another. The diffusive flux is mainly controlled by the matrix porosity ϕ_m , the effective molecular diffusion coefficient D_e , and the concentration gradient. Also, the literature generally agrees upon the fact that the most important factors to controlling matrix diffusion are the characteristics of the media as well as the properties of the solute itself. The characteristics of the media include; the matrix porosity, the organic carbon fraction (f_{oc}), the mass storage capacity, and the degree of saturation. Solute characteristics include the molecular diffusion coefficient (D_e), the density, and the solubility.

In conclusion, this literature review indicates that even though the matrix diffusion is an important mechanism for explaining the depletion of DNAPL in fractured porous environments, it is not currently well understood. Additionally, experiments have been conducted to validate existing analytical models. Thus, the focus of the present research is to investigate the diffusive loss of NAPLs in fractured porous media through mathematical models, and to verify these models through physical model experiments.

Chapter 3: Conceptual Frameworks and Mathematical Model Development

3.1 Conceptual Model Development

The present conceptual model is based on the conceptual model for diffusive disappearance of NAPL presented by Parker *et al.*, 1994, as well as the model for heat conductance from a disk source in solids presented by Carslaw and Jaeger (1959). This model employs a saturated porous media that is isotropic, homogeneous, and semi-infinite in all directions. A disk-type source is located at the center of the porous media, thereby establishing a chemical potential at the boundary of the disk source as illustrated in Figures 3.1 and 3.2. A conceptual model for a disk source in a 3D cylindrical coordinate system is shown in Figure 3.3. Mass transfer from the disk source to the porous matrix occurs through dissolution and subsequent molecular diffusion as described in the following paragraphs. The nonwetting fluid (NAPL) contacts a thin film of water (wetting fluid) that exists between disk source (NAPL) and the fracture wall. Dissolution occurs from the NAPL source into the thin aqueous film. The rate of dissolution depends on the solubility of the NAPL, the solute concentration in the aqueous phase, and the temperature of the system. In this conceptual model, the NAPL concentration within the water film quickly reaches the aqueous solubility (Schwille, 1988; Mackay *et al.*, 1991; Anderson *et al.*, 1992; Parker *et al.*, 1994) as shown in Figure 3.4a. At early times, water will penetrate into the disk source and solute will spread out in the direction of the porous matrix simultaneously.

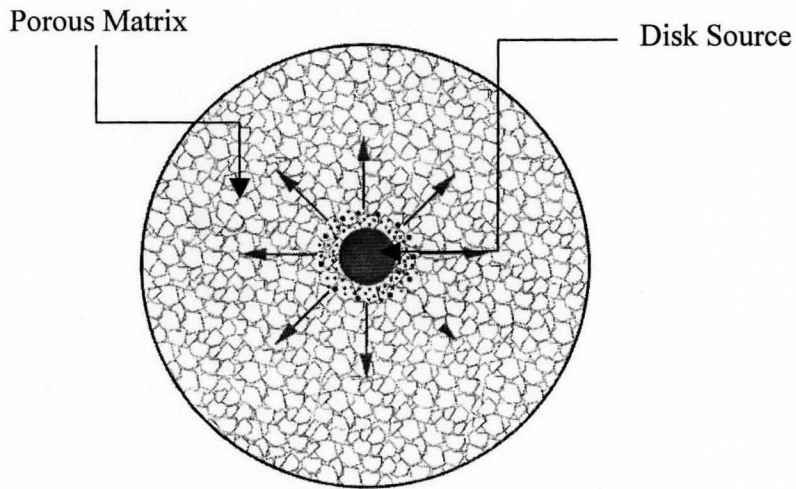


Figure 3.1 Top view of the 2D and 3D conceptual models. Arrows represent direction of diffusion within the porous matrix.

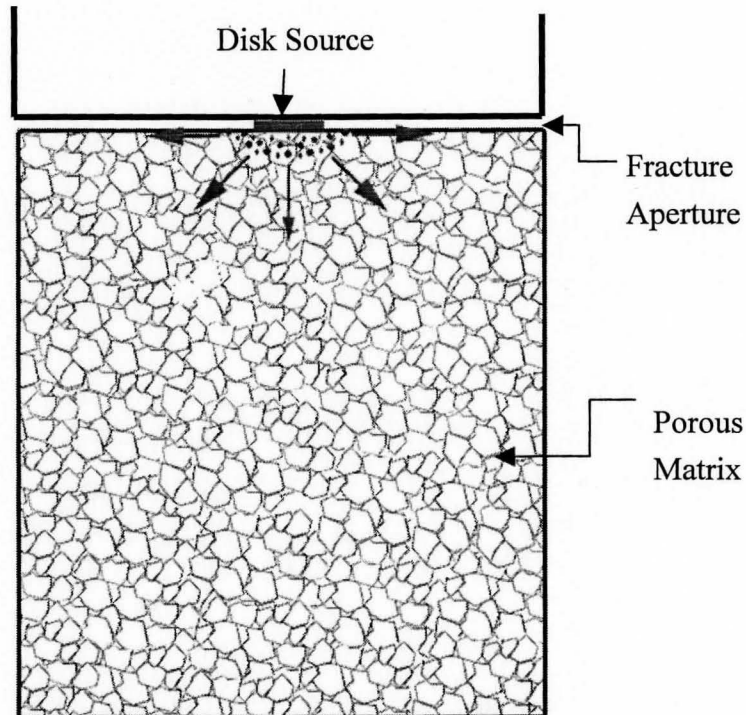


Figure 3.2 Side view of the 3D conceptual model. Arrows represent the direction of diffusion, which is assumed to be symmetrical about the fracture aperture.

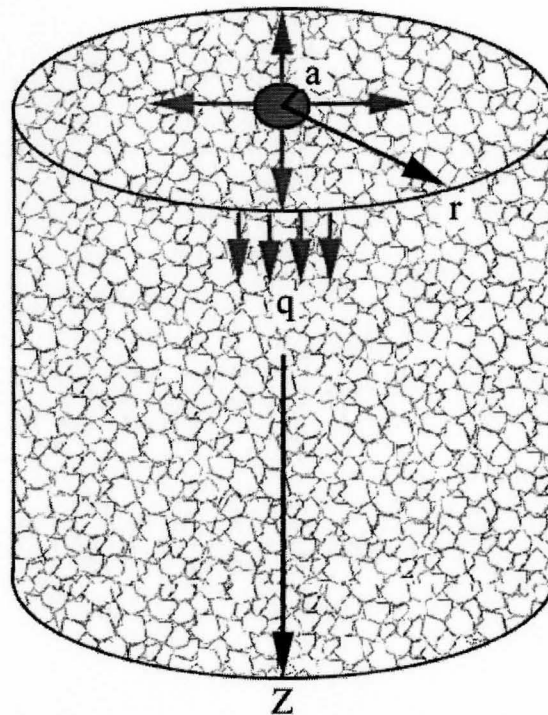


Figure 3.3 Conceptual model for instantaneous and continuous disk sources in a 3D cylindrical coordinate system.

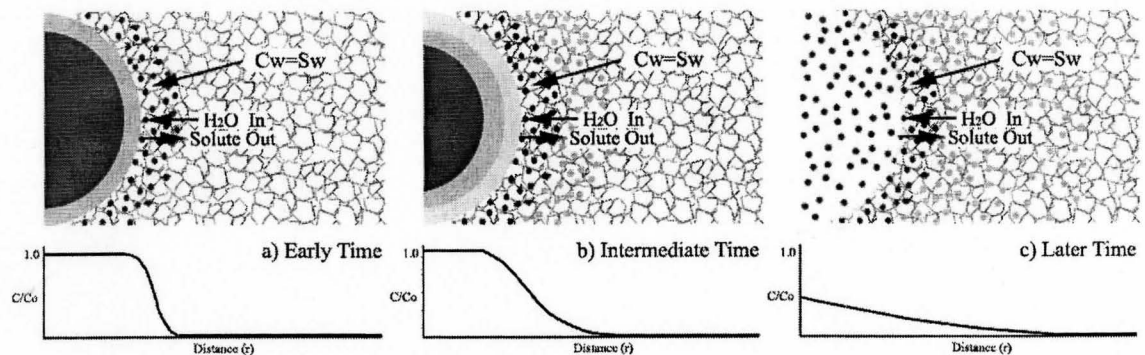


Figure 3.4 Parker's conceptual model (1994) for NAPL disappearance in fractured porous media. a) early time, b) intermediate time, and c) later time.

At intermediate times, the size of the inner part of the disk source diminishes through the continued invasion of the aqueous phase into the disk source. Mass transfer from the immiscible phase to the immobile pore water in the matrix may result in disconnected blobs and ganglia in the boundary regions of the disk source. Disconnection of the immiscible phase due to diffusive mass transfer reduces the concentration gradient at the advancing front, and hence reduces the ability for DNAPL to dissolve and then diffuse into the porous media (Parker *et al.*, 1994). Eventually the disk source will completely dissolve, and continue to migrate through the porous matrix via molecular diffusion as long as a chemical potential continues to exist. At this stage, the NAPL mass exists primarily in the porous media. As clean water comes into contact with the fracture face, the concentration gradient will reverse, resulting in contaminant removal from the matrix at a rate controlled, once again, by the chemical potential. One of the implications of this reverse diffusion process is that additional time will be required to restore contaminated NAPL sites. Parker *et al.*, (1994) and Kueper *et al.*, (2003) noted that complete removal of mass from the matrix blocks via reverse diffusion takes longer than the time period for inward diffusion due to the much lower chemical potentials achievable, on average, in the reverse direction.

3.2 Mathematical Model Development

In studying molecular diffusion in porous media, it is important to understand the basic theory of diffusion. The basic assumptions of this work are that the porous medium is homogeneous, isotropic, and saturated with distilled water, and that diffusion

conditions are such that Fick's 2nd law is valid. The mathematical theory of diffusion in isotropic substances is based on the hypothesis that the rate of transfer through a unit area is proportional to the chemical potential measured normal to the section, and is expressed by Fick's first law as follows:

$$F_{Di} = -\phi_m D_e \left(\frac{\partial C_w}{\partial x_i} \right) \quad (3.1)$$

where F_{Di} [M/L²/T] is the mass flux of the solute,

ϕ_m [-] is the matrix porosity,

D_e [L²/T] is the effective diffusion coefficient,

C_w [M/L³] is the solute concentration, and

x [L] is the distance over which diffusion is occurring.

ϕ_m is defined as the ratio of the volume of the voids (V_v) [L³] to the total volume of the matrix (V) as follows:

$$\phi_m = \frac{V_v}{V} \quad (3.2)$$

D_e is a function of the free-solution diffusion coefficient (D_d) [L²/T], and the tortuosity factor τ ($0 < \tau < 1$) [-], which accounts for the effect of the tortuous pathway due to the presence of the porous matrix ($D_e = D_d \times \tau$) (Bear, 1972). Fick's second law applies to systems where the concentration is changing with time as follows:

$$\frac{\partial C_w}{\partial t} = \frac{D_e}{R} \left(\frac{\partial^2 C_w}{\partial x_i^2} \right) \quad (3.3)$$

where R [-] represents the retardation factor.

The use of a cylindrical coordinate system facilitates the development of an analytical solution for the diffusion equation. Thus, by substituting, $x = r \cos \theta$, $y = r \sin \theta$ into equation (3.3), the equation for diffusion in a cylinder in terms of the cylindrical coordinates r , θ , and z is obtained:

$$\frac{\partial C_w}{\partial t} = \frac{1}{r} \left\{ \frac{\partial}{\partial r} \left(r \frac{D_e}{R} \frac{\partial C_w}{\partial r} \right) + \frac{\partial}{\partial \theta} \left(\frac{1}{r} \frac{D_e}{R} \frac{\partial C_w}{\partial \theta} \right) + \frac{\partial}{\partial z} \left(r \frac{D_e}{R} \frac{\partial C_w}{\partial z} \right) \right\} \quad (3.4)$$

$$\text{or } \frac{\partial C_w}{\partial t} = \frac{D_e}{R} \left[\frac{\partial^2 C_w}{\partial r^2} + \frac{1}{r} \left(\frac{\partial C_w}{\partial r} \right) + \frac{1}{r^2} \left(\frac{\partial^2 C_w}{\partial \theta^2} \right) + \frac{\partial C_w}{\partial z^2} \right] \quad (3.5)$$

If diffusion occurs on the surface of a circular cylinder whose axis coincides with the z axis, and the initial and boundary conditions are independent of the coordinates θ and z , the concentration will be a function of r and t only, and equation (3.5) reduces to

$$\frac{\partial C_w}{\partial t} = \frac{D_e}{R} \left[\frac{\partial^2 C_w}{\partial r^2} + \frac{1}{r} \left(\frac{\partial C_w}{\partial r} \right) \right] \quad (3.6)$$

In this case, the flow of solute takes place in the plane perpendicular to the axis, and the flow lines are radial. Equation (3.6) describes a 2-dimensional disk source. When the initial and boundary conditions are independent of θ alone, the flow of solute takes place in planes through both the vertical and horizontal axes, and the diffusion equation becomes:

$$\frac{\partial C_w}{\partial t} = \frac{D_e}{R} \left[\frac{\partial^2 C_w}{\partial r^2} + \frac{1}{r} \left(\frac{\partial C_w}{\partial r} \right) + \frac{\partial C_w}{\partial z^2} \right] \quad (3.7)$$

Equation (3.7) describes 3-dimensional instantaneous and continuous disk sources. According to equation (3.1), the mass flux will be proportional to the diffusion coefficient,

the matrix porosity, and the chemical potential. It is possible for a solute to migrate through a porous media by diffusion alone when groundwater is not flowing, which is typical of the porous matrix environments surrounding fractures. In these circumstances, diffusive transport may dominate over advective transport.

3.2.1 Derivation of the Diffusion Equation for a Disk Source

The basic assumption for the derivation of the diffusion equation for a disk source is that a disk source is the summation of many ring sources. As shown in Figure 3.5, it is assumed that there is an instantaneous ring source at $t=0$ of mass Q' and radius r' in the plane $z'=0$. If point sources of mass $Q'=Qr'd\theta'$ are distributed around the ring $r=r'$ in the plane $z'=0$, where Q represents the mass per unit length, the concentration at time t ($t > 0$) at the point whose cylindrical coordinates are (r, θ, z) is given by Carslaw and Jaeger (1959) as:

$$C(r, \theta, z) = \frac{Qr'}{8(\pi D_e t)^{3/2}} \int_0^{2\pi} e^{-[r^2+z^2+r'^2-2rr'\cos(\theta-\theta')]/4D_e t} d\theta' \quad (3.8a)$$

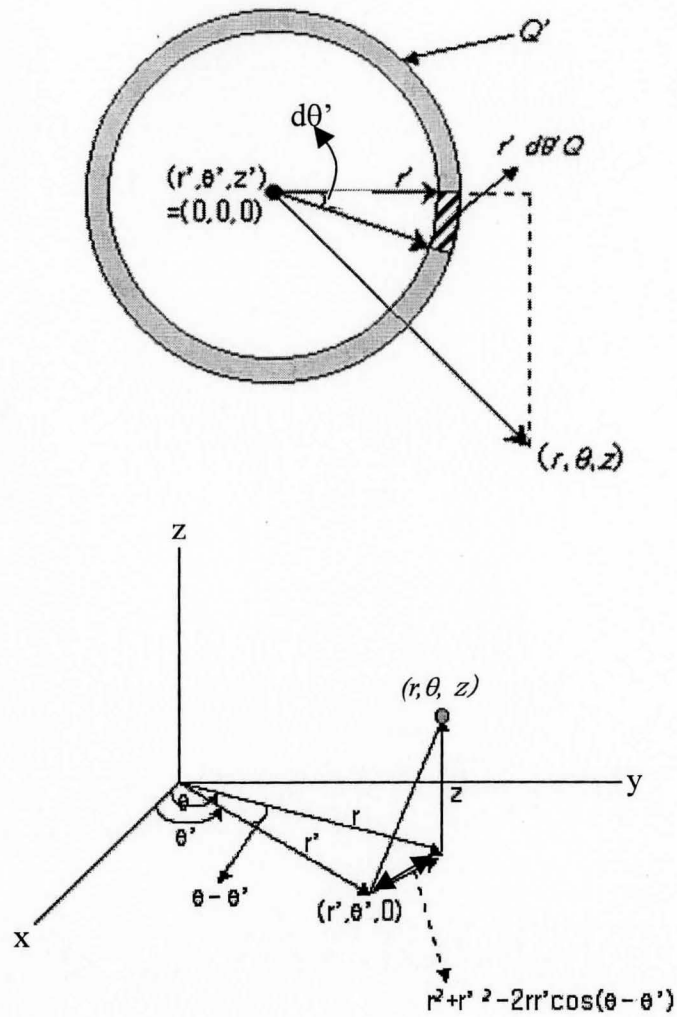


Figure 3.5 Schematic diagram of a ring source.

$$C(r, \theta, z) = \frac{Qr'}{8(\pi D_e t)^{3/2}} e^{-[r^2 + z^2 + r'^2]/4D_e t} \int_0^{2\pi} e^{2rr'\cos(\theta - \theta')/4D_e t} d\theta' \quad (3.8b)$$

$$C(r, \theta, z) = \frac{Q'}{8(\pi D_e t)^{3/2}} e^{-[r^2 + z^2 + r'^2]/4D_e t} I_0\left(\frac{rr'}{2D_e t}\right) \quad (3.8c)$$

where $I_0[-]$ is the modified Bessel function of the first kind of order zero,

t [T] is the time, and

r and z [L] are the axis.

and $Q' = 2\pi r' Q$, $Q' = \text{mass}$, $Q = \text{mass per unit length}$. $Q = q dr' = [M/L^2 \times L = M/L]$, $Q' = 2\pi r' q dr' = [L \times M/L^2 \times L = M]$, and $q = Q/dr' = [(M/L)/L = M/L^2]$, where q is defined as the mass flux per unit area. Therefore Q represents the mass per unit length, Q' represents the mass, and q represents the mass flux. As shown in Figure 3.6, if $Q' = 2\pi r' q dr'$ is substituted into (3.8c), and integrated with respect to r' from 0 to a , the equation becomes:

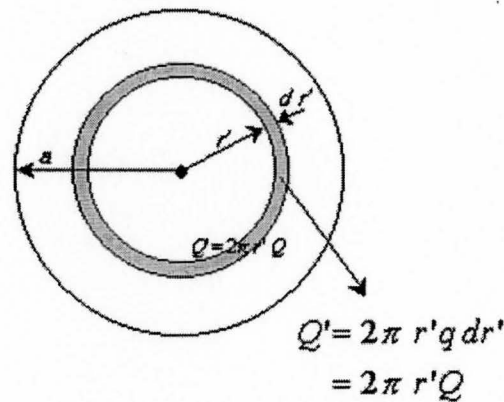


Figure 3.6 Schematic diagram of a disk source.

$$C(r, \theta, z, t) = \frac{2\pi r' q dr'}{8(\pi D_e t)^{3/2}} \exp\left[-\frac{r^2 + z^2 + r'^2}{4D_e t}\right] I_0\left(\frac{rr'}{2D_e t}\right) \quad (3.9a)$$

$$C(r, \theta, z, t) = \frac{q}{4(\pi D_e^3 t^3)^{1/2}} e^{-(r^2+z^2)/4D_e t} \int_0^a e^{-r'^2/4D_e t} I_0\left(\frac{rr'}{2D_e t}\right) r' dr' \quad (3.9b)$$

where $\pi a^2 q$ solute units are released over a disk of radius a . The integral in (3.9b) cannot be expressed in terms of tabulated functions except on the axis $r = 0$ where it becomes

$$C(0, z, t) = \frac{q}{2\sqrt{\pi D_e t}} [1 - e^{-a^2/4D_e t}] e^{-z^2/4D_e t} \quad (3.10)$$

3.2.2 Analytical Solution Development: Instantaneous Disk Source in 2D

As shown in the previous section, for an instantaneous disk source whose central axis coincides with the z -axis, with initial and boundary conditions independent of the coordinates θ and z , the concentration will be a function of r and t only; therefore (3.6) represents a 2D instantaneous disk source in porous media with a constant diffusion coefficient. In this case, solute migration occurs in a plane perpendicular to the z -axis, and the migration lines are radial. The initial and boundary condition are given by

$$C(r, t) = S_w, \quad r \leq a, \quad t = 0 \quad (3.11a)$$

$$C(r, t) = 0, \quad r > a, \quad t = 0 \quad (3.11b)$$

$$C(\infty, t) = 0, \quad t \geq 0 \quad (3.11c)$$

where a [L] represents the radius of the disk source, and S_w [M/L³] represents the aqueous phase solubility. Crank (1956) developed the following analytical solution to equation (3.6) with boundary conditions given by 3.11:

$$C(r,t) = \frac{C_o R}{2D_e t} e^{-r^2 R/4D_e t} \int_0^a e^{-r'^2 R/4D_e t} I_o\left(\frac{R r r'}{2D_e t}\right) r' dr' \quad (3.12)$$

The integral in equation (3.12) must be evaluated numerically except on the axis $r=0$, where equation (3.12) becomes:

$$\int_0^a e^{-r'^2 R/4D_e t} I_o\left(\frac{R r r'}{2D_e t}\right) r' dr' \quad (3.13a)$$

if $r=0$, $I_o\left(\frac{R r r'}{2D_e t}\right) = I_o(0) = 1$, so

$$\int_0^a e^{-r'^2 R/4D_e t} r' dr' \quad (3.13b)$$

$$= \int_0^a e^{-r'^2 R/4D_e t} \frac{1}{2} dr'^2 \quad (3.13c)$$

$$= \int_0^a e^{-r'^2 R/4D_e t} \frac{1}{2} \times (-4D_e t/R) d(-r'^2 R/4D_e t) \quad (3.13d)$$

$$= \frac{-4D_e t}{2R} \int_0^a e^{-r'^2 R/4D_e t} d(-r'^2 R/4D_e t) \quad (3.13e)$$

$$= \frac{-4D_e t}{2R} e^{-r'^2 R/4D_e t} \Big|_0^a \quad (3.13f)$$

$$= (-2D_e t/R)(e^{-a^2 R/4D_e t} - 1) \quad (3.13g)$$

$$= (2D_e t/R)(1 - e^{-a^2 R/4D_e t}) \quad (3.13h)$$

Therefore, equation (3.13a) at $r=0$ becomes

$$C(0,t) = \frac{C_o R}{2D_e t} e^{-r^2 R/4D_e t} \left[(2D_e t/R) \times (1 - e^{-a^2 R/4D_e t}) \right] = C_o (1 - e^{-a^2 R/4D_e t}) \quad (3.13i)$$

Where $r \neq 0$, the integral part of equation (3.13a) becomes:

$$\int_0^a e^{-r^2 R/4D_e t} I_0(x) r' dr' \quad (3.14a)$$

$$\text{where } x = \frac{R r r'}{2D_e t} \quad (3.14b)$$

$$I_0(x) = 1 + \frac{x^2}{2^2} + \frac{x^4}{2^2 \cdot 4^2} + \frac{x^6}{2^2 \cdot 4^2 \cdot 6^2} \quad (3.14c)$$

therefore,

$$I_0\left(\frac{R r r'}{2D_e t}\right) = 1 + \frac{1}{2^2} \frac{R^2 r^2}{(2D_e t)^2} r'^2 + \frac{1}{2^2 \cdot 4^2} \frac{R^4 r^4}{(2D_e t)^4} r'^4 + \frac{1}{2^2 \cdot 4^2 \cdot 6^2} \frac{R^6 r^6}{(2D_e t)^6} r'^6 + \dots \quad (3.14d)$$

$$I_0\left(\frac{R r r'}{2D_e t}\right) r' = r' + \frac{1}{2^2} \frac{R^2 r^2}{(2D_e t)^2} r'^3 + \frac{1}{2^2 \cdot 4^2} \frac{R^4 r^4}{(2D_e t)^4} r'^5 + \frac{1}{2^2 \cdot 4^2 \cdot 6^2} \frac{R^6 r^6}{(2D_e t)^6} r'^7 + \dots \quad (3.14e)$$

The value of $\int_0^a e^{-r^2 R/4D_e t} I_0(x) r' dr'$ can be calculated, and therefore equation (3.13a)

becomes:

$$C(r,t) = \frac{C_o R}{2D_e t} e^{-r^2 R/4D_e t} \int_0^a e^{-r'^2 R/4D_e t} \times \left[\begin{aligned} & r' + \frac{1}{2^2} \frac{R^2 r^2}{(2D_e t)^2} r'^3 + \frac{1}{2^2 \cdot 4^2} \frac{R^4 r^4}{(2D_e t)^4} r'^5 + \dots \\ & \frac{1}{2^2 \cdot 4^2 \cdot 6^2} \frac{R^6 r^6}{(2D_e t)^6} r'^7 + \dots + \infty \end{aligned} \right] dr' \quad (3.14f)$$

As shown in Figure 3.7, the total mass diffused into the porous media at any time t is numerically calculated using the relationships between the initial mass (M_o) in the instantaneous disk source and the remaining mass ($Q(t)$) in the disk source region ($r \leq a$)

at any time $t > 0$. Therefore the total mass diffused is calculated using the concentration profile in the source zone ($r \leq a$) at any selected time t .

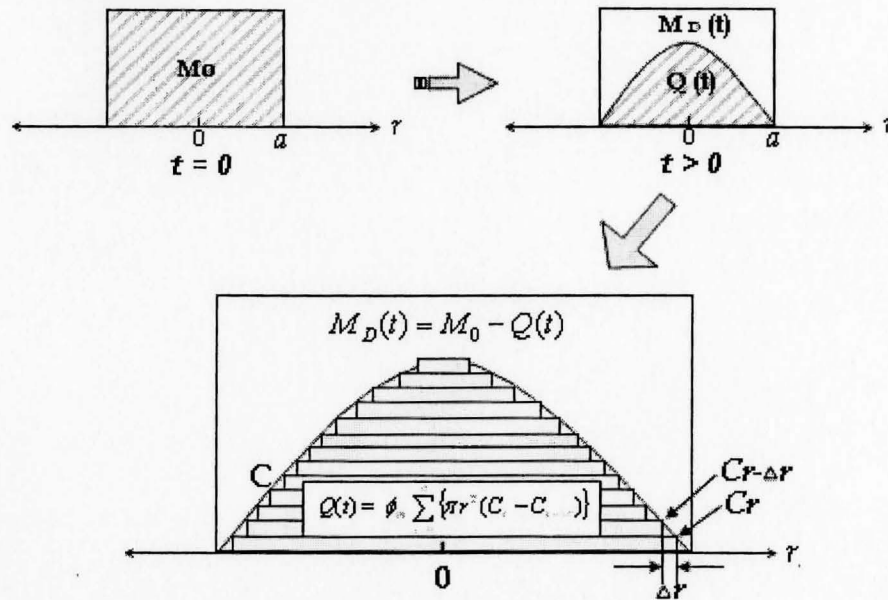


Figure 3.7 A schematic diagram for the calculation of diffused mass at any time t .

Therefore, if the diffusing solute is initially distributed uniformly through a disk of radius a , the total mass of solute (M_0) at time $t = 0$ is:

$$M_0 = \phi_m \pi a^2 C_0 \quad (3.15a)$$

and, $Q(t)$, the mass remaining in the disk source after time t is expressed by:

$$Q(t) = \phi_m \sum_{r=a}^0 \{ \pi r^2 (C_r - C_{r-\Delta r}) \} \quad (3.15b)$$

where C_r is the concentration at distance r , and

$C_{r-\Delta r}$ is the concentration at distance $r - \Delta r$.

The difference between the initial mass and the mass remaining at any time t represents the total mass diffused into the porous media at that time. This can be represented mathematically as follows:

$$M_D(t) = M_0 - Q(t) \quad (r \leq a) \quad (3.16a)$$

$$= \left\{ \frac{M_0 - Q(t)}{M_0} \right\} \times M_0 \quad (r \leq a) \quad (3.16b)$$

$$= \left\{ 1 - \frac{Q(t)}{M_0} \right\} \times M_0 \quad (r \leq a) \quad (3.16c)$$

An alternative solution to equation (3.6) with initial and boundary conditions given by 3.11, developed by Rideal and Tadayon (1954), is

$$C(r,t) = aC_o \int_0^{\infty} J_1(ua) J_0(ur) e^{-D_e u^2 / R} du \quad (3.17)$$

where J_0 , J_1 are Bessel functions of the first kind, of orders zero and one respectively. Rideal and Tadayon also give an expression for the total mass of solute, $Q(t)$, remaining in the source zone after time t :

$$Q(t) = 2\pi a^2 C_o \int_0^{\infty} \frac{J_1^2(ua)}{u} e^{-D_e u^2 / R} du \quad (3.18a)$$

For small values of t , equation (3.18a) becomes

$$Q(t) = \pi a^2 C_o \left\{ 1 - \frac{2}{a} \left(\frac{D_e t}{2\pi R} \right)^{1/2} \right\} \quad (3.18b)$$

and when t is large

$$Q(t) = \pi a^4 C_o R / (4D_e t) \quad (3.18c)$$

3.2.3 Analytical Solution Development: Instantaneous Disk Source in 3D

Carslaw and Jager (1959) developed an analytical solution for diffusion from an instantaneous disk source in 3D with the following initial and boundary conditions:

$$C(r,z,t) = S_w, \quad r \leq a, t = 0, z=0 \quad (3.19a)$$

$$C(r,z,t) = 0, \quad r > a, t = 0, z=0 \quad (3.19b)$$

$$C(r,z,t) = 0, \quad z > 0, t = 0 \quad (3.19c)$$

$$C(\infty, \infty, t) = 0, \quad t \geq 0 \quad (3.19d)$$

Letting $Q' = 2\pi r' q dr'$ in equation (3.8c), and integrating with respect to r' from 0 to a , gives

$$C(r,z,t) = \frac{q(R^3)^{1/2}}{4(\pi D_e^3 t^3)^{1/2}} \int_0^a e^{-R(r^2+z^2+r'^2)/4D_e t} I_0\left(\frac{Rr r'}{2D_e t}\right) r' dr' \quad (3.20)$$

$$C(r,z,t) = \frac{a q}{2(\pi D_e t)^{1/2}} e^{-z^2 R/4D_e t} \int_0^\infty e^{-D_e \lambda^2 / R} J_0(\lambda r) J_1(\lambda a) d\lambda \quad (3.21)$$

when $r=0$ in equation (3.20), $I_0\left(\frac{Rr r'}{2D_e t}\right) = I_0(0) = 1$, therefore

$$\int_0^a e^{-r'^2 R/4D_e t} r' dr' \quad (3.22a)$$

$$= \int_0^a e^{-r^2 R/4D_e t} \frac{1}{2} dr^{1/2} \quad (3.22b)$$

$$= \int_0^a e^{-r^2 R/4D_e t} \frac{1}{2} \times (-4D_e t/R) d(-r^2 R/4D_e t) \quad (3.22c)$$

$$= \frac{-4D_e t}{2R} \int_0^a e^{-r^2 R/4D_e t} d(-r^2 R/4D_e t) \quad (3.22d)$$

$$= \frac{-4D_e t}{2R} e^{-r^2 R/4D_e t} \Big|_0^a \quad (3.22e)$$

$$= -(2D_e t/R)(e^{-a^2 R/4D_e t} - 1) \quad (3.22f)$$

$$= (2D_e t/R) \times (1 - e^{-a^2 R/4D_e t}) \quad (3.22g)$$

Therefore, at $r = 0$ equation (3.20) becomes

$$C(0, z, t) = \frac{q(R^3)^{1/2}}{4(\pi D_e^3 t^3)^{1/2}} e^{-z^2 R/4D_e t} (2D_e t/R) \times (1 - e^{-a^2 R/4D_e t}) \quad (3.23a)$$

$$= \frac{q(R)^{1/2}}{2(\pi D_e t)^{1/2}} (1 - e^{-a^2 R/4D_e t}) e^{-z^2 R/4D_e t} \quad (3.23b)$$

The solution to the system of equations, (3.20) and (3.21), can be obtained for case-specific initial and boundary conditions. Therefore, the concentration at the disk-source is initially constant and equal to the aqueous solubility, S_w ($C = S_w$ at $r \leq a, z = 0, t = 0$), and the initial aqueous concentration in the matrix pore water is zero ($C(r, z, t) = 0$ at $r > a$) (Carslaw and Jaeger, 1959). The total mass diffused into the porous media at any selected time ($M_D(t)$) is calculated as follows:

$$M_D(t) = M_o - Q(t) \quad (r \leq a) \quad (3.24a)$$

$$= \left\{ 1 - \frac{Q(t)}{M_o} \right\} \times M_o \quad (r \leq a) \quad (3.24b)$$

$$= \left\{ 1 - \frac{\pi a^2 C_o - \sum_{r=a}^0 \pi r^2 \Delta C}{\pi a^2 C_o} \right\} \times \pi a^2 C_o \quad (r \leq a) \quad (3.24c)$$

3.2.4 Analytical Solution Development: Continuous Disk Source in 3D

Carslaw and Jager (1959) developed an analytical solution for diffusion from a continuous disk source in 3D. The assumptions used in the development of the solution are the same as those used for the instantaneous disk source in 3D. The following initial and boundary conditions were used to describe the continuous disk source for the development of the solution:

$$-K \frac{\partial C(r,0,t)}{\partial z} = \begin{cases} q & \text{for } 0 < r < a \\ 0 & \text{for } r > a \end{cases} \quad (3.25a)$$

$$C(r,z,t) = 0, \quad r \rightarrow \infty \text{ and } z \rightarrow \infty \quad (3.25b)$$

$$C(r,z,0) = 0, \quad z > 0, \quad r > a \quad (3.25c)$$

Where K is the hydraulic conductivity, and has the same value in all directions due to the assumption of assumed media. The exact solution is given by Carslaw and Jaeger (1959):

$$\frac{C(r,z,t)}{qa/K} = \frac{1}{2} \int_0^\infty J_0(\lambda r) J_1(\lambda a) \times \left\{ e^{-\lambda z} \operatorname{erfc} \left[\frac{z}{2(D_e t)^{1/2}} - \lambda((D_e t)^{1/2}) \right] - e^{-\lambda z} \operatorname{erfc} \left[\frac{z}{2(D_e t)^{1/2}} + \lambda((D_e t)^{1/2}) \right] \right\} \frac{d\lambda}{\lambda} \quad (3.26)$$

Equation (3.26) is valid for all r , and for z greater than zero. At $z=0$, equation (3.26) reduces to:

$$\frac{C(r,0,t)}{qa/K} = \int_0^\infty \operatorname{erf}[\lambda(D_e t)^{1/2}] \frac{J_0(\lambda r) J_1(\lambda a)}{\lambda} d\lambda \quad (3.27)$$

Equation (3.26) is too difficult to evaluate numerically. For convenience, it can be rewritten in dimensionless form with the following variables:

$$r^+ = \frac{r}{a}, \quad z^+ = \frac{z}{a}, \quad \lambda^+ = \lambda a, \quad t^+ = \frac{D_e t}{a^2}, \quad C^+(r^+, z^+, t^+) = \frac{C(r^+, z^+, t^+)}{qa/K}$$

James (1981) stated that equation (3.26) is not valid for all times and locations within the system, and developed a series solution to equation (3.26), with initial and boundary conditions given by equation 3.25 for all z at $r = 0$:

$$C(0,z,t) = 2t^{1/2} \left[\operatorname{ierfc} \left(\frac{z}{2t^{1/2}} \right) - \operatorname{ierfc} \left(\frac{(z^2+1)^{1/2}}{2t^{1/2}} \right) \right] \quad (3.28)$$

as well as a series solution for all r at $z = 0$:

$$C(r,0,t) = C(r,0,\infty) - \frac{1}{2\sqrt{\pi t}} \times \left\{ 1 - \frac{1+2r^2}{24t} + \frac{1}{480t^2} (1+6r^2+3r^4) - \frac{1}{10752t^3} (1+12r^2+18r^4+4r^6) + \dots \right\} \quad (3.29)$$

Thomas (1957) derived an exact steady state solution for the surface concentration in terms of known functions:

$$C(r,0,\infty) = \frac{2}{\pi} E(r) \quad \text{for } 0 < r < 1 \quad (3.30)$$

$$\text{and } C(r,0,\infty) = \frac{2r}{\pi} [E(r^{-1}) - (1-r^{-2})K(r^{-1})] \quad \text{for } r > 1 \quad (3.31)$$

The functions $K[\cdot]$ and $E[\cdot]$ represent the complete elliptic integrals of the first and

second kinds:
$$K(\varepsilon) = \int_0^{2/\pi} [1 - \varepsilon^2 \sin^2 \theta]^{-1/2} d\theta \quad (3.32a)$$

$$E(\varepsilon) = \int_0^{2/\pi} [1 - \varepsilon^2 \sin^2 \theta]^{1/2} d\theta \quad (3.32b)$$

From equation (3.28) and equations (3.29, 3.30, and 3.31), concentration profiles at the surface, $(C(r,0,t))$, and various depths for $r = 0$, $(C(0,z,t))$, can be calculated at any time t in the body. The concentration distribution within the system is required to calculate mass diffused from the source zone at any time, t . Because 3.28 and 3.29 are only valid at $(z, r = 0)$ and $(z = 0, r)$ respectively, the concept of iso-concentration lines within the system was employed to calculate mass diffused, as illustrated in Figure 3.8.

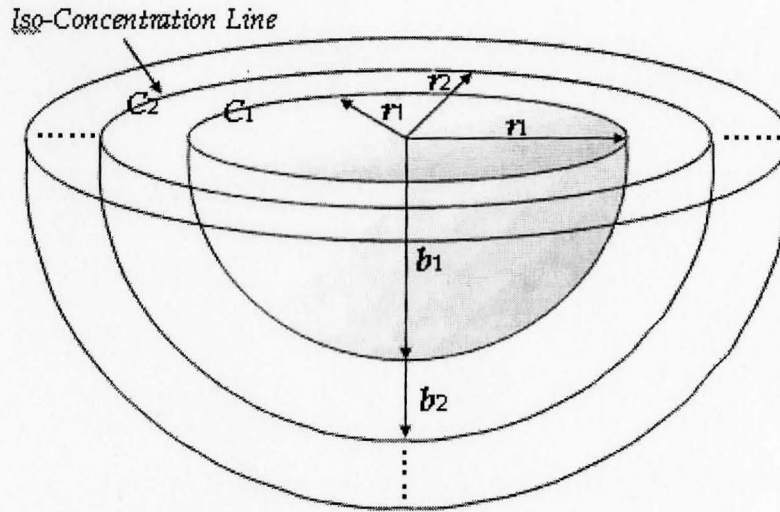


Figure 3.8 A schematic diagram for interpolation of the concentration profile at depth.

In general, the total mass diffused into the porous media at any selected time t can be calculated by the integration of the concentration for r and z directions as given by equation (3.33a). In this study, the total mass diffused into the porous media was calculated by the summation of the iso-concentration lines, which were assumed to be a semi-spherical shape, and subsequent multiplication of the concentrations (equation 3.33b).

$$M_D(t) = \phi_m \int_{-\infty}^{\infty} \int_{-\infty}^{\infty} C(r, z, t) dr dz \quad (3.33a)$$

$$= \phi_m \sum_0^t \left[\left\{ \frac{1}{2} \pi r_1^2 b_1 \times C_1 \right\} + \left\{ \left(\frac{1}{2} \pi r_2^2 b_2 - \frac{1}{2} \pi r_1^2 b_1 \right) \times C_2 \right\} + \dots + \left\{ \left(\frac{1}{2} \pi r_n^2 b_n - \frac{1}{2} \pi r_{n-1}^2 b_{n-1} \right) \times C_n \right\} \right]$$

$$(3.33b)$$

Chapter 4: Computation Results and its Comparisons

This chapter presents the programming methodology and computational results for the three scenarios presented in Chapter 3. (i.e., 2D instantaneous disk source, 3D instantaneous disk source and 3D continuous disk source), and presents a sensitivity analysis for both the 3D instantaneous and continuous disk sources. Table 4.1 summarizes the analytical solutions for the three sets of initial and boundary conditions presented in Chapter 3. The solutions are divided into two categories: general solutions for all values of r and z , and specific solutions for $r=0$. Both the total mass diffused away from the source zone at any time t , $M_D(t)$, and the total mass remaining in the source zone at any time t , $Q(t)$, are also presented in Table 4.1, and are used as a basis for comparing the three scenarios.

Table 4.1 Summary of analytical solutions for diffusive mass transfer in porous media.

Scenario	Representative Physical Conditions	Diffusion Equation	Boundary Conditions	Analytical solution		$M_D(t)$ or $Q(t)$
				General solution	At $r = 0$	
A	2D Instantaneous Disk Source	(3.6)	(3.11a~c)	(3.12), (3.14f), and (3.17)	(3.13i)	(3.16c), (3.15b), (3.18a)
B	3D Instantaneous Disk Source	(3.7)	(3.19a~d)	(3.20) and (3.21)	(3.23b)	(3.24c)
C	3D Continuous Disk Source	(3.7)	(3.25a~c)	(3.26)	(3.28)	(3.33b)

For computational purposes, typical values were assigned to the variables listed in Table 4.2. These values were held constant between all three scenarios for comparison purposes.

Table 4.2 Values assigned to variables for computational purposes.

Variable	Symbol	Units	Value	Representative Compound
Effective diffusion coefficient	D_e	cm ² /sec	0.96×10^{-5} *	n-Butanol
Water solubility	S_w	g/L	63.2**	n-Butanol
Radius of sample	r	cm	Infinity	N/A
Radius of disk source	a	cm	1.0	N/A
Time	T	days	30	N/A
Initial concentration	C_o	mg/L	63,200	N/A
Retardation factor	R	-	1.0	Silica flour
Matrix porosity	ϕ_m	-	1.0	N/A

* McCall et al., (1959) ** P.H. Howard and W.M. Meylan (1997)

The following sections present the computational results from the three scenarios presented in Table 4.1. Additionally, a comparison of the results from each of the three solutions is conducted. Finally, a sensitivity analysis is presented to examine the sensitivity of the 3D instantaneous and continuous solutions to the radius of the disk source, and the matrix porosity.

4.1 Computational Results from a 2D Instantaneous Disk Source

As presented in Table 4.1, there are three general solutions (equations (3.12), (3.20) and (3.26)) for the initial and boundary conditions describing an instantaneous disk source in 2D. Equations (3.12) and (3.17) are both exact solutions; they differ from (3.14f) only in the order of the series. To reduce computation time, equation (3.14f), which provides an approximate solution, may be solved. Equation (3.14f) was programmed in Compaq Visual Fortran (Professional Edition 6.5.0, Compaq Computer Corporation). Although Fortran is more computationally efficient, equations (3.12) and (3.17) were programmed in Maple commercial software (Version 8.00, Waterloo Maple Inc.) (Appendix I), as they were difficult to code in Fortran due to the infinite integral and Bessel function. These equations were easily solved by Maple codes, however the computational time is much longer than the Fortran program developed to solve equation (3.14f). For example, the computational time for a 30 day diffusion simulation is approximately 30 minutes for Maple codes, and only 5 seconds for the Fortran code. Figure 4.1 compares the exact solution for a 2D instantaneous disk source ((3.12) and (3.17)) to the approximate solution (3.14f) using the 4th, 8th, and 12th orders; it shows that at a minimum, an order of 12 must be used to generate a solution with an acceptable degree of error.

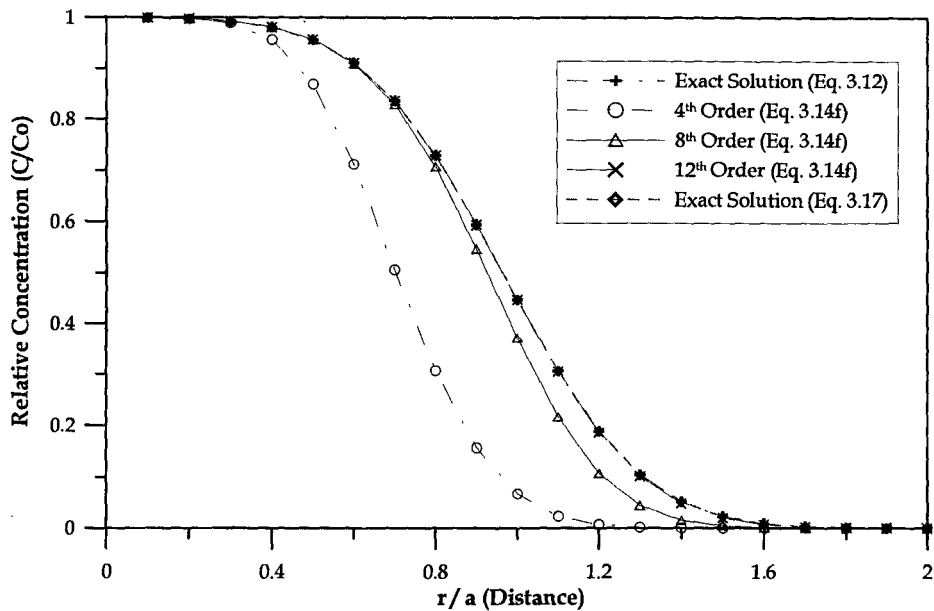


Figure 4.1 Comparison of the approximate solution (3.14f) with orders of 4, 8, 12, and the exact solution (3.12, 3.17) for a 2D instantaneous disk source at $t = 3600$ sec. Values of variables are given in Table 4.2.

Figure 4.1 also compares the two exact solutions (3.12, 3.17) to the 2D instantaneous disk source using the initial and boundary conditions given by (3.11) at $t=3600$ sec. Figure 4.1 shows that there is no difference between (3.12), (3.14f), and (3.17). Therefore, both analytical solutions match one another, which indicate that both solutions were coded correctly. The fact that the 12th order of the approximate solution (3.14f) also matches the two exact solutions indicates that it is coded correctly, and that it is reasonable to use this approximate solution to save computational time. Thus, computational results presented hereafter for 2D instantaneous disk sources with boundary conditions given by (3.11) will be computed by (3.14f) with the 12th order.

When $r=0$ (at the center of the disk source), the concentration profile from a 2D instantaneous disk source is calculated using (3.13i). Figure 4.2 shows the concentration profile generated by (3.13i) using the values defined in Table 4.2 for De , Sw , r , a , Co , R , ϕm , and t . Figure 4.2 shows that the relative concentration at $r=0$ will be reduced to 0.01 after 30 days, with 90% of the solute disappearing within the first 3 days.

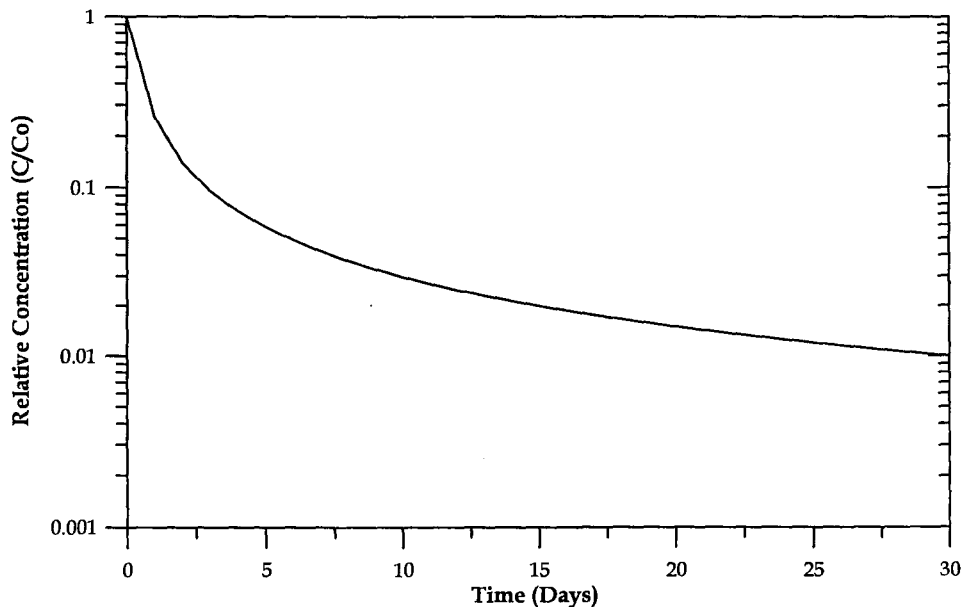


Figure 4.2 Concentration profile at $r=0$, for a 2D instantaneous disk source

The relative concentration profiles versus distance at $r = 0$ are presented in Figure 4.3 for various times, using the variable values specified in Table 4.2. The concentration profile changes significantly at all distances up to 20cm within the 30 day period. The slope of the concentration profile decreases significantly over early time and distance, and flattens out with both time and distance. This is due to the fact that the driving force

for diffusion is the chemical potential, which weakens over time and space, thus the mass of NAPL diffusing will also decrease over time and space.

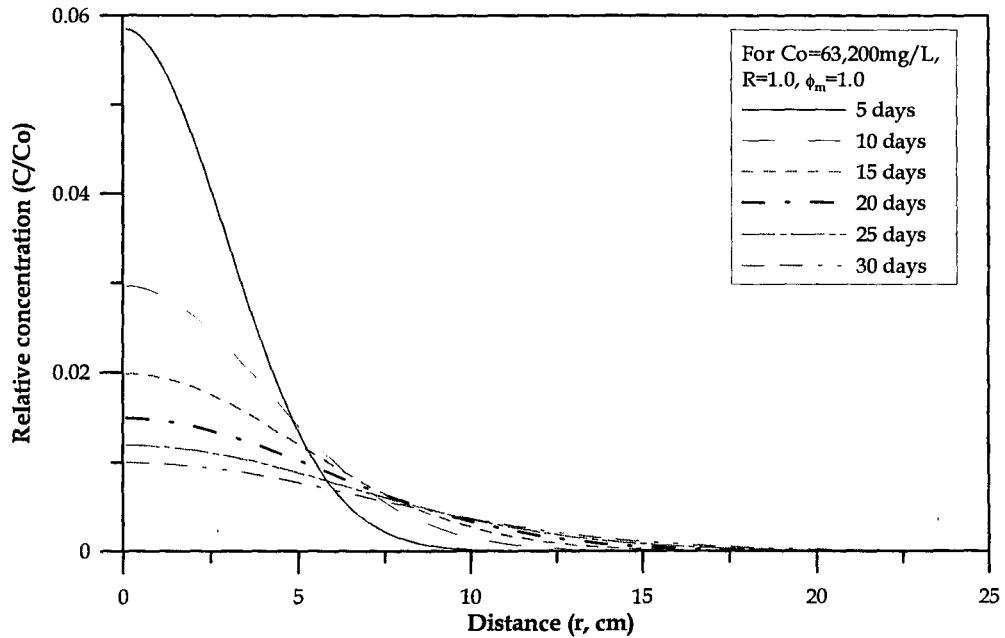


Figure 4.3 Concentration profile versus distance at $r = 0$ for a 2D instantaneous disk source with boundary conditions given by (3.11).

Figure 4.4 shows concentration profiles as a function of distance for a 2D instantaneous disk source at successive times, where the concentration, distance and time are represented by the dimensionless variables C/C_o , r/a , and $(D_e t/a^2)^{1/2}$ respectively.

When $(D_e t/a^2)^{1/2}$ is 0, the actual time $t = 0$, which represents the initial condition. When $(D_e t/a^2)^{1/2} = 1$, the actual time is $104,166 \text{ sec}$ or 28.9 hrs . The total amount of mass diffused from the source zone, $M_D(t)$, and the total mass remaining in the source zone, $Q(t)$, at time t are calculated using (3.16c) and (3.18a) respectively (Table 4.1). The

computation time is much longer for equation 3.18a than it is for equation (3.16c).

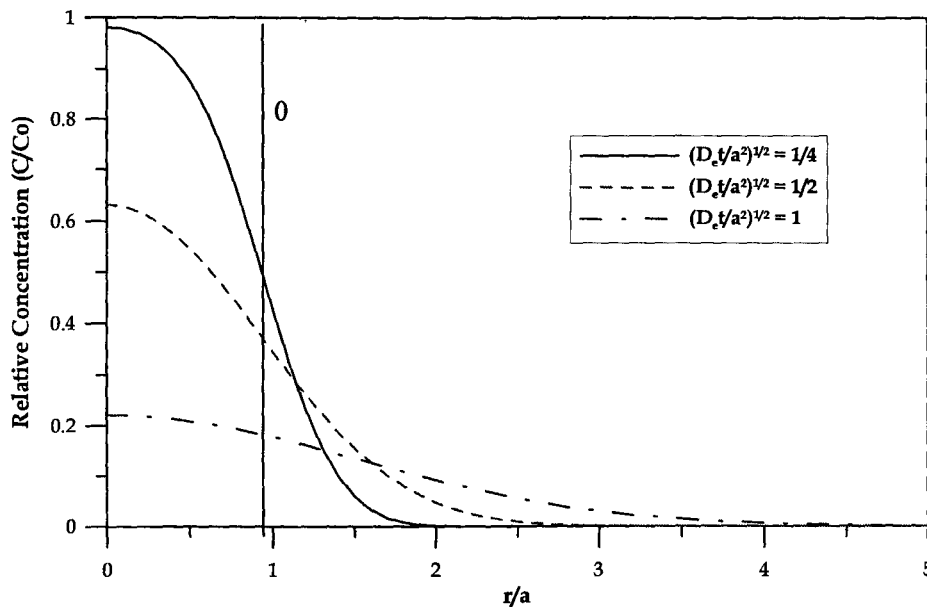


Figure 4.4 Concentration profiles for an instantaneous disk source in 2D with boundary conditions given by 3.11.

Figure 4.5 shows a plot of mass diffused as a function of time, as calculated from both (3.16c) and (3.18a). The results of (3.18a) were plotted using the relationship $M_D(t)/M_o_{at r \leq a} = 1 - (Q(t)_{at r \leq a} / M_o_{at r \leq a})$, where M_o is the total mass of solute present in the disk source at time $t = 0$ (i.e., $M_o = \pi r^2 C_o$). Figure 4.5 shows that both solutions give the same result, indicating that both solutions are coded correctly. Therefore, results presented hereafter will be calculated using 3.16c, as it is much more computationally efficient.

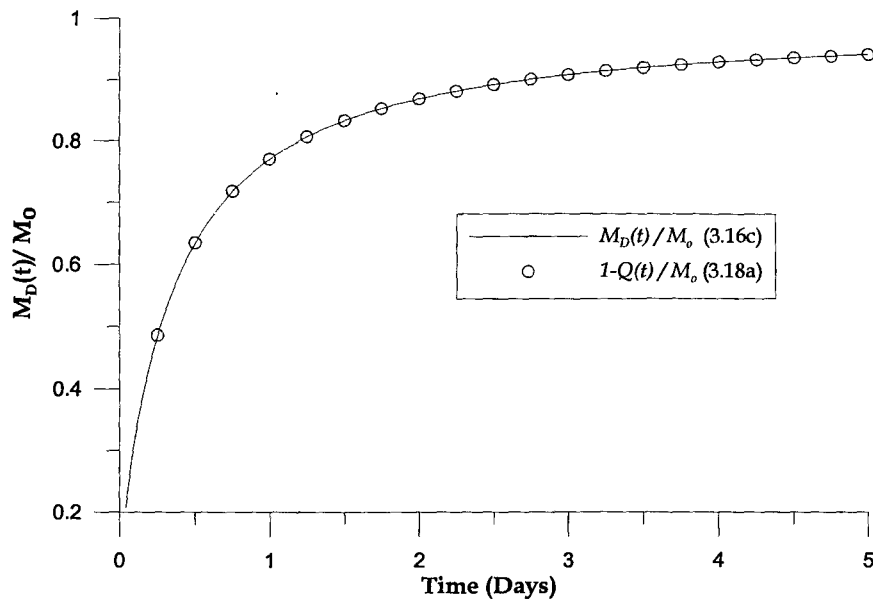


Figure 4.5 Comparison of mass diffused from the source zone at time t computed by equation (3.18a) and (3.16c).

Figure 4.6 shows the normalized mass diffused away from the disk source (hatched area) and the relative mass remaining in the 2D instantaneous disk source (white area) as a function of time. This figure shows that the majority of the instantaneous disk source will be diffused into the surrounding porous media within the first five days. The remaining mass diffuses away from the disk source very slowly (over more than 30 days) due to the decreased chemical potential.

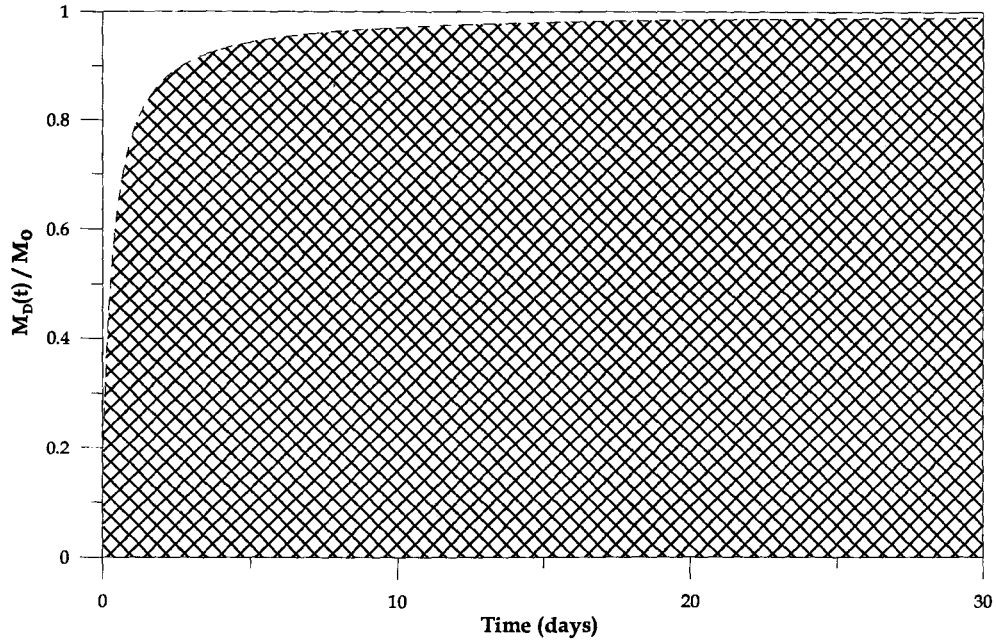


Figure 4.6 The total mass diffusing away from the disk source (hatched area) and remaining in the disk source (white area) as a function of time for a 2D instantaneous disk source with boundary conditions given by (3.12)

Figure 4.7 shows concentration profiles as a function of distance for a 2D instantaneous disk source with boundary conditions given by (3.12). The number on the contour lines represents the normalized concentration at time t . Figure 4.7 shows that the diffusion occurs radially outwards from the source zone. The 0.001 relative concentration contour is at a distance less than $r = 10$ cm at 5 days, and reaches $r = 15$ cm by day 30.

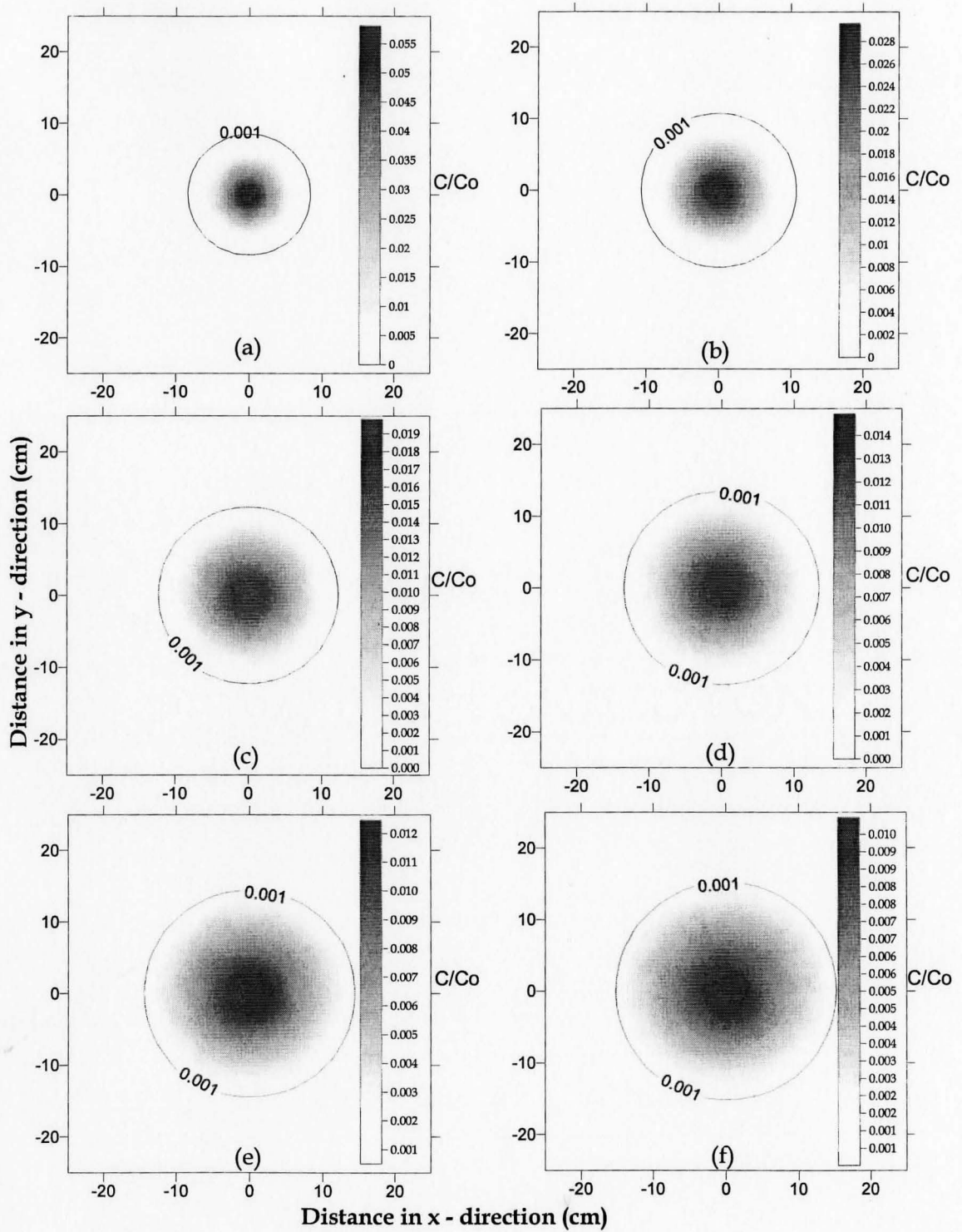


Figure 4.7 Relative concentration profiles from a 2D instantaneous disk source at times. (a) $t = 5$ days, (b) $t = 10$ days, (c) $t = 15$ days, (d) $t = 20$ days, (e) $t = 25$ days, and (f) $t = 30$ days.

4.2 Computational Results from a 3D Instantaneous Disk Source

The exact solution for a 3D instantaneous disk source with boundary conditions given by (3.19) was developed by Crank (1956), and is given by (3.20) and (3.21) (Table 4.1). The primary difference between the 2D and 3D instantaneous disk source solutions is the use of variable q in 3D rather than C_0 in 2D. q is defined as the mass flux,

$$q = \frac{Q}{dr'} = \frac{\pi a^2 C_0}{2\pi a} \left[\frac{M}{L^2} \right],$$

which is defined as the mass diffused into the porous media or matrix per unit area of source zone. (3.20) and (3.21) indicate that the concentration at a given point and time is directly proportional to the radius of disk source (a), the mass flux (q), and the retardation factor (R), and indirectly proportion to the effective diffusion coefficient (De). For consistency and comparison purposes, the computations in this section will use the values assigned to De , Sw , r , a , Co , ϕm and a in Table 4.2.

Figure 4.8 shows the normalized concentration profile as a function of time at $r = 0$ and $z = 0$, where the z -axis represents the vertical distance from the source zone, and the r -axis represents the radial distance from the source zone, as it did in Section 4.1. Figure 4.8 shows that the normalized concentration within the 3D instantaneous disk source at $r = 0$ and $z = 0$ is much lower than the normalized concentration given by the 2D solution at all times with the difference between the solutions increasing over time. This indicates that the mass diffusing in the vertical axis is significant, and will reduce the disappearance time of the source zone.

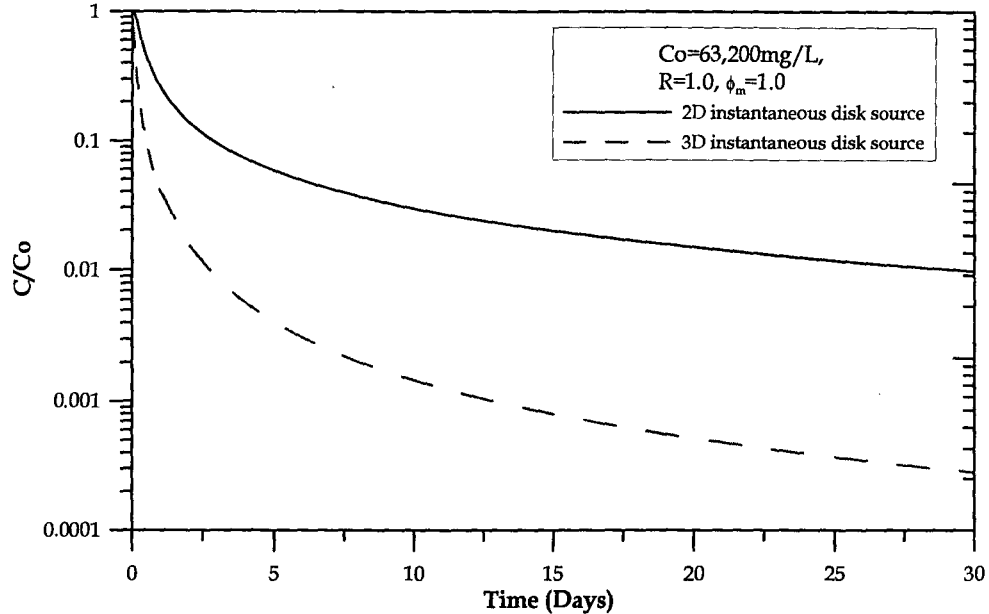


Figure 4.8 Concentration profile at $r = 0.0$ cm, $z = 0.0$ cm, for a 3D instantaneous disk source (dashed line) with boundary conditions given by (3.19), and a 2D instantaneous disk source (solid line) with boundary conditions given by (3.11).

Figure 4.9 represents normalized concentration profiles as a function of dimensionless distance for both 2D and 3D instantaneous disk sources with boundary conditions given by (3.11) and (3.19) respectively, at $z = 0$ and various dimensionless times. The relative concentration at $r = 0$ and $(D_e t / a^2)^{1/2} = 1$ for the 3D instantaneous case approached 0.02, which is more than an order of magnitude lower than for the 2D instantaneous disk source (0.22). This reinforces the fact that vertical diffusion is significant.

The total mass diffused into the porous matrix for the two cases presented in Figure 4.9 is shown in Figure 4.10 as a function of time. The relative mass diffused approached 1 far earlier for the 3D instantaneous disk source than for the 2D

instantaneous disk source, indicating that the solute diffused away from the source zone much more quickly in the 3D case than in the 2D case. Again, this is due to the fact that vertical dispersion is significant, as it represents a significant increase in the area for which the chemical potential is large at early times.

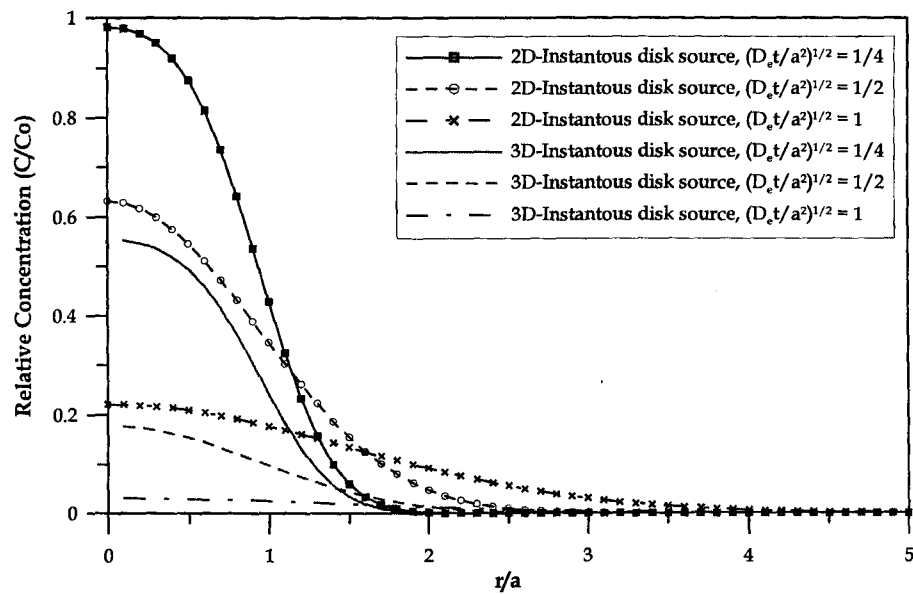


Figure 4.9 Concentration distributions for instantaneous disk sources in 2D and 3D, with boundary conditions and variable values listed in Table 4.1 and 4.2 respectively.

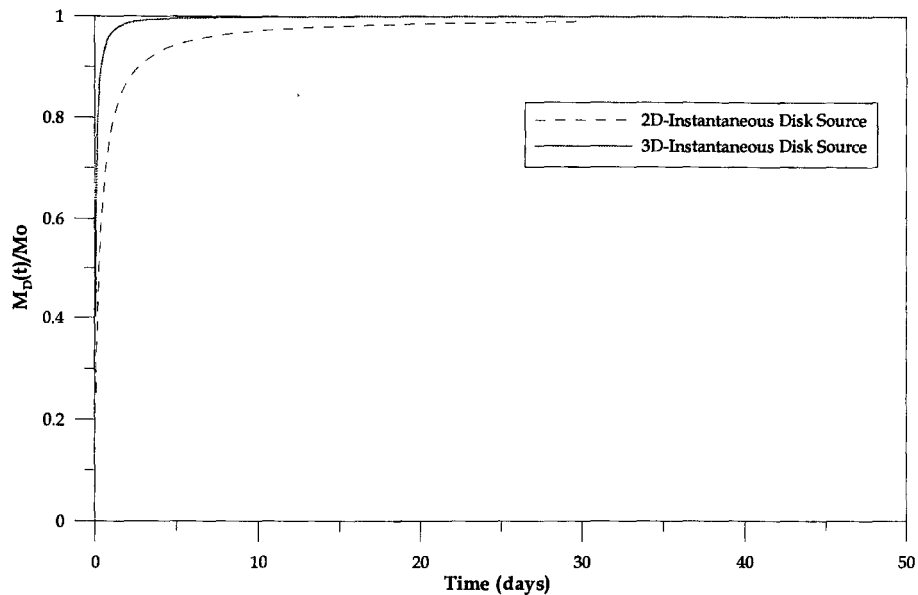


Figure 4.10 The relative mass diffusing into the porous matrix for the 2D and 3D instantaneous disk sources.

Figure 4.11 shows spatial concentration distributions at $z=0$. A comparison of Figures 4.11 and 4.7 indicates that the contour for $C/C_0 = 0.0001$ is much closer to $r = 0$ for the 3D case than for the 2D case. This indicates that in the 3D case, a significant mass diffused in z direction, as the contact area is much greater in this z direction (i.e: surface area of a semi-sphere rather than the perimeter of a circle). Figure 4.12 illustrates this fact through the use of vertical sections, through the origin, of the relative concentration profile at times corresponding to those in Figure 4.11.

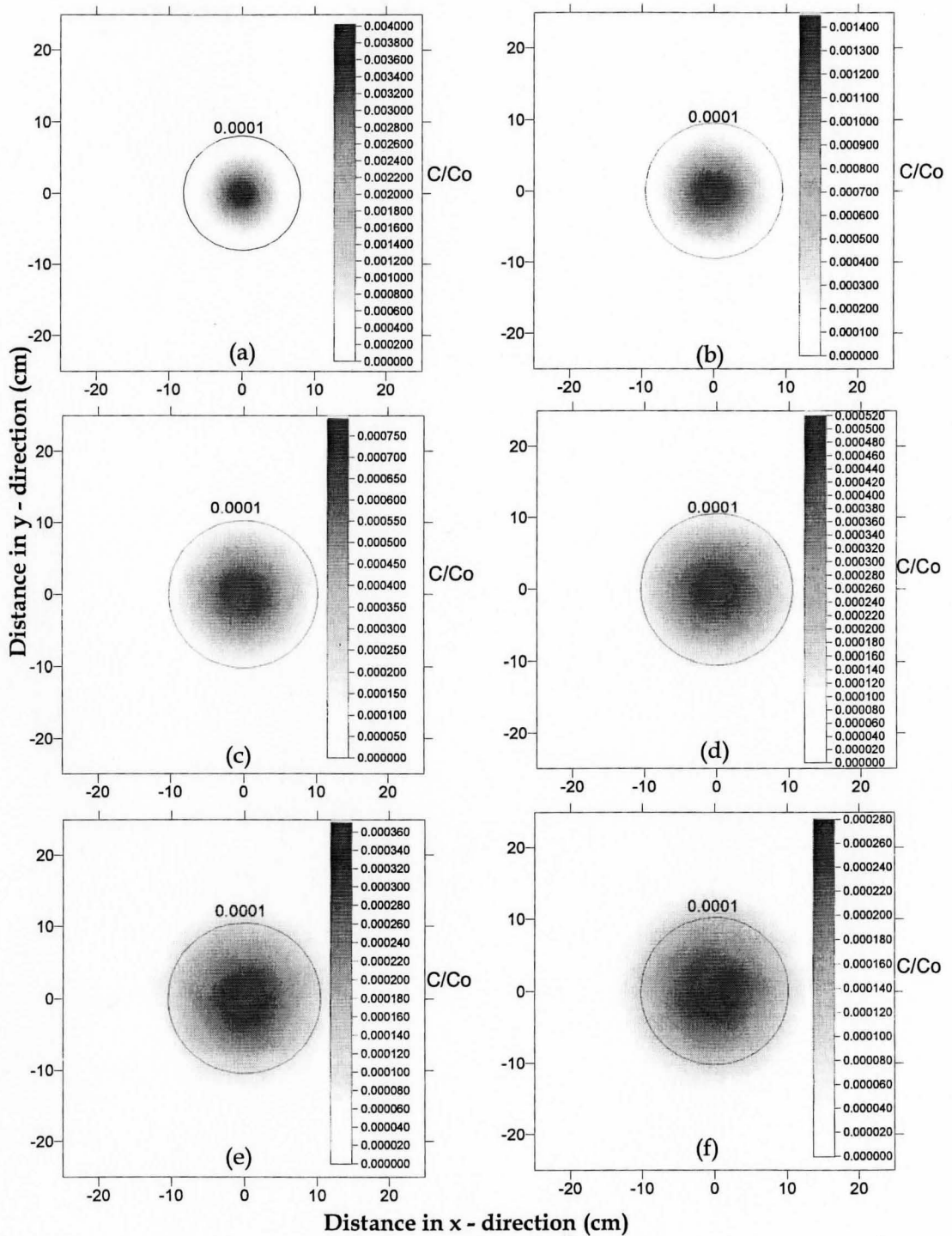


Figure 4.11 Relative concentration profiles from a 3D instantaneous disk source at times. (a) $t = 5$ days, (b) $t = 10$ days, (c) $t = 15$ days, (d) $t = 20$ days, (e) $t = 25$ days, and (f) $t = 30$ days.

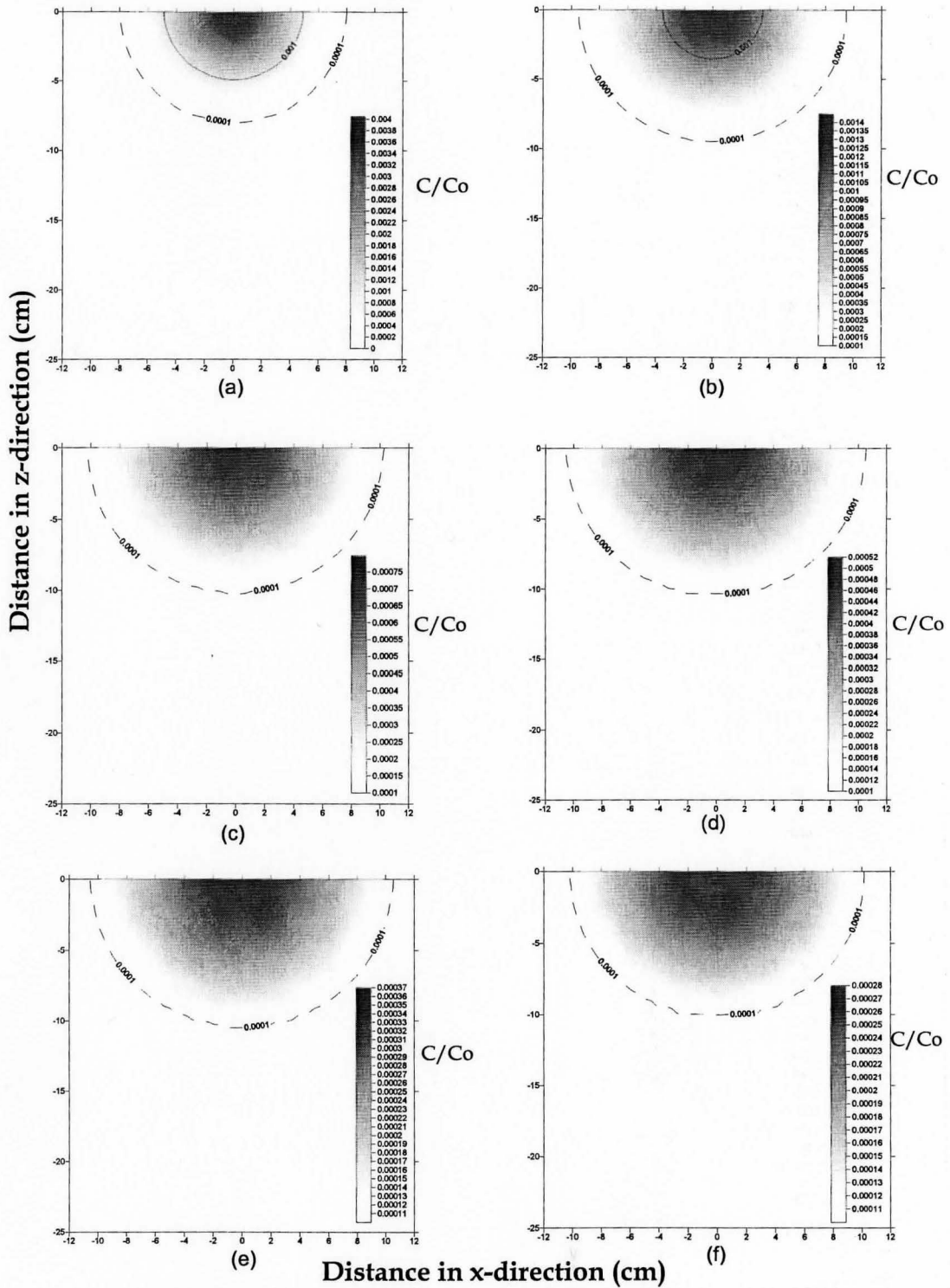


Figure 4.12 The vertical section of the concentration profile from a 3D instantaneous disk source at times (a) $t = 5$ days, (b) $t = 10$ days, (c) $t = 15$ days, (d) $t = 20$ days, (e) $t = 25$ days, and (f) $t = 30$ days.

The comparison between the solutions for diffusion from 2D and 3D instantaneous disk sources presented in this section show that these solutions are significantly different. Therefore, when considering problems of mass disappearance by diffusion, it is necessary to consider the problem in 3D in order to obtain an acceptable degree of accuracy. Therefore, the remainder of this thesis will focus on 3D solutions of NAPL diffusion from disk sources.

4.3 Computational Results from a 3D Continuous Disk Source

As discussed in Section 3.2.4, the exact solution for a 3D continuous disk source with boundary conditions given by (3.25) was given by Carslaw and Jaeger (1959) (3.26). This solution is difficult to solve using a numerical procedure, however, due to the sinusoidal nature of the Bessel function and the fact that the integral has an infinite domain. James (1981) provided series expressions (3.28) and (3.29), for a 3D continuous disk source at $C(r, \theta, t)$ and $C(\theta, z, t)$ respectively. He noted that although (3.26) provides an exact solution, it is difficult to obtain the accurate values anywhere except along the centerline of the domain. Therefore, (3.28) and (3.29) were employed in this work for computing relative concentration profiles from a 3D continuous disk source with boundary conditions given by (3.25). These equations were programmed using Maple software. Again, for comparison purposes, the values assigned to the variables De , Sw , r , a , Co , ϕm and a assigned in Table 4.2 were used in these computations.

Figure 4.13 shows the normalized concentration profile as a function of time for a 3D continuous disk source at $r = 0$ and $z = 0$. This figure shows that the disk source will

provide a continuous driving force into the porous media for a very long time. This contrasts the instantaneous disk source in which the majority of it diffused into the surrounding porous media within the first five days.

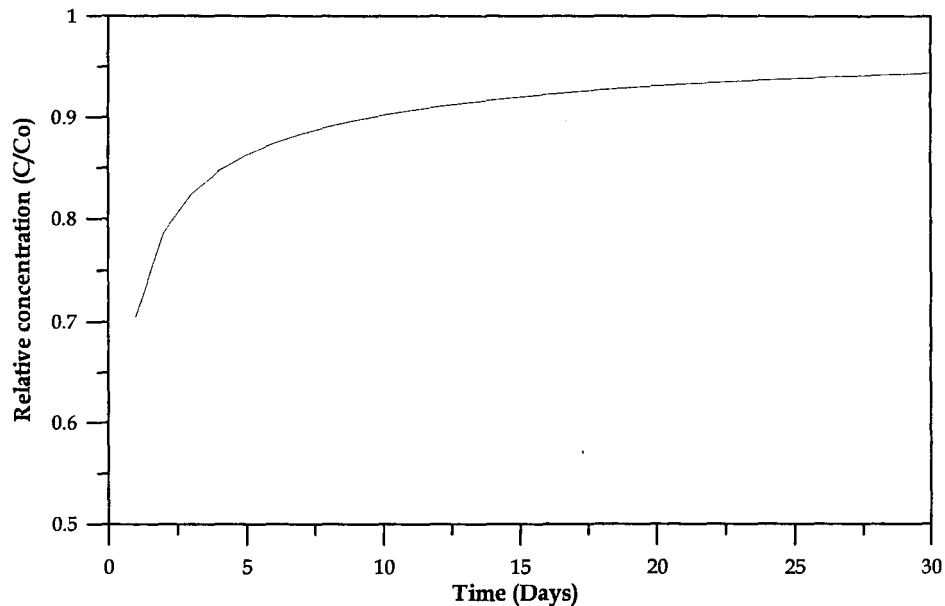


Figure 4.13 Concentration profile at $r=0.0$, $z=0.0$ cm for a 3D continuous disk source with boundary conditions given by equation (3.25)

Figures 4.14 and 4.15 show the normalized concentration profile as a function of dimensionless time, $D_e t / a^2$, for various radial distances at $z = 0$ for a 3D continuous disk source with boundary conditions given by equation (3.25). The concentration profiles for each distance are similar in that they start off by increasing quickly, and then flatten off over time as the chemical potential decreases. The profiles differ, however, in the fact that the further away from $r = 0$, the lower the maximum attainable concentration.

To provide the reader with a sense of real time, the normalized concentrations at $t = 15$ days, $t = 1$ yr, and $t = \text{infinity}$ were calculated, and presented as a function of radial distance at $z = 0$ in Figure 4.16. This figure shows that the rate of diffusion decreases significantly over early time due to decreasing chemical potentials. It also shows that the concentration approaches a maximum based on radial distance, and that maximum decreases with increasing radial distance. This phenomenon can be attributed to the fact that chemical potentials decrease with both distance and time.

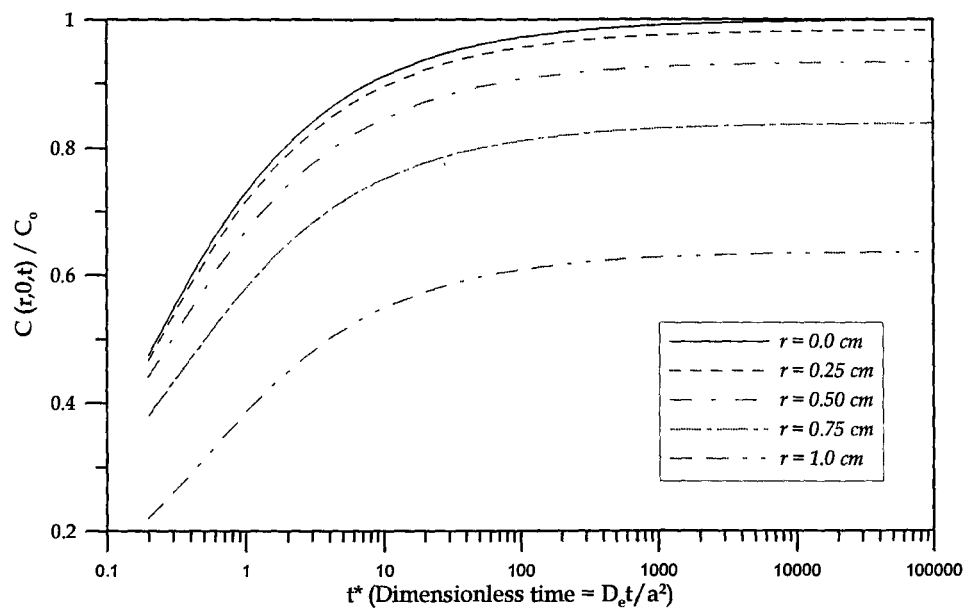


Figure 4.14 Relative concentration profiles as a function of dimensionless time for a 3D continuous disk source with boundary conditions given by equation (3.25) at $z = 0$ and $r = 0, 0.25, 0.5, 0.75,$ and 1 cm.

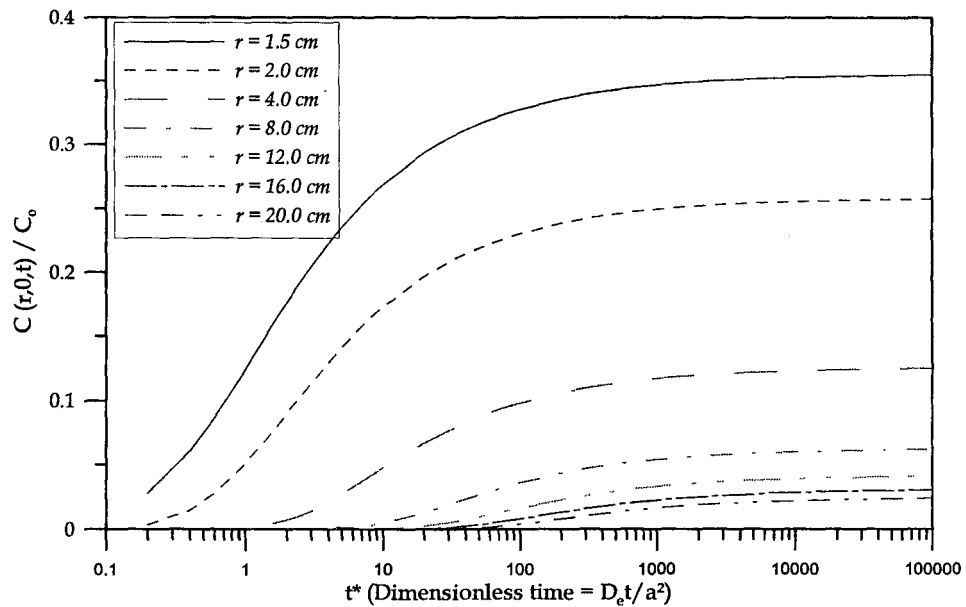


Figure 4.15 Relative concentration profiles as a function of dimensionless time for a 3D continuous disk source with boundary conditions given by equation (3.25) at $z = 0$ and $r = 1.5, 2, 4, 8, 12, 16,$ and 20 cm.

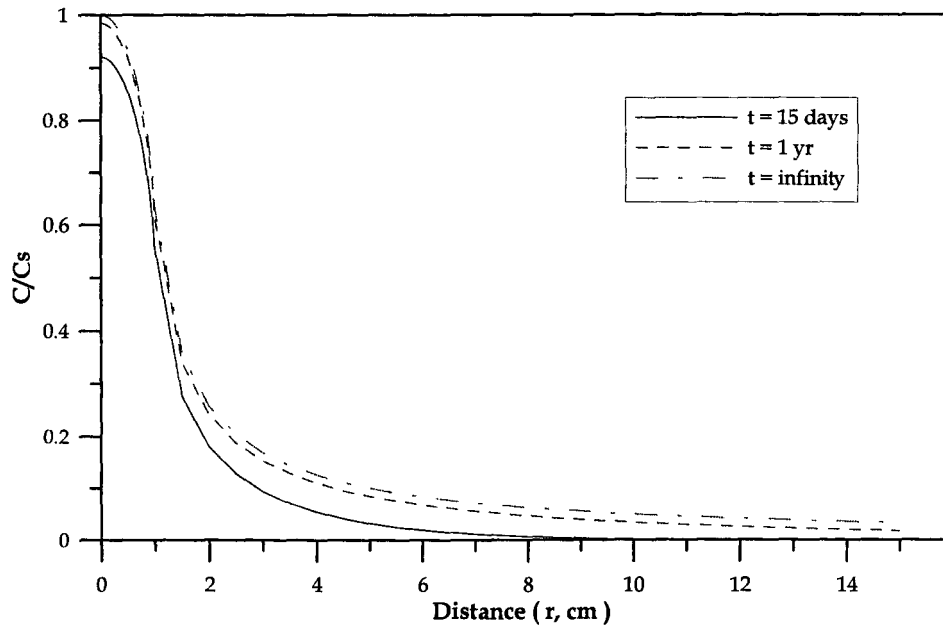


Figure 4.16 Normalized concentration profiles versus radial distance for a 3D continuous disk source with boundary conditions given by (3.25), at $t=15$ days, 1 yr, and infinity.

The total mass diffused through the surface ($z=0$) was calculated using (3.29), which represents integration of the general solution in the z and r directions. Figure 4.17 shows the normalized mass diffusing from a 3D continuous disk source as a function of dimensionless time. This figure shows that the rate of mass diffusion away from the source decreases sharply over early times, and gradually flattens out due to the decreasing concentration gradient over time. Figure 4.18 shows the total mass diffused from a 3D continuous disk source as a function of time. The total mass diffused into porous media varies relatively linearly with time over early times and increases continuously. If the time period in this figure was extended significantly, however, the relationship would flatten out, similar to that shown in Figure 4.17.

Figure 4.19 shows that the concentration profiles with depth for a 3D continuous disk source with boundary conditions given by equation (3.25). This figure shows that the normalized concentration distributions in the z -direction. The relative concentration increases continuously due to the constant concentration provided by the continuous source.

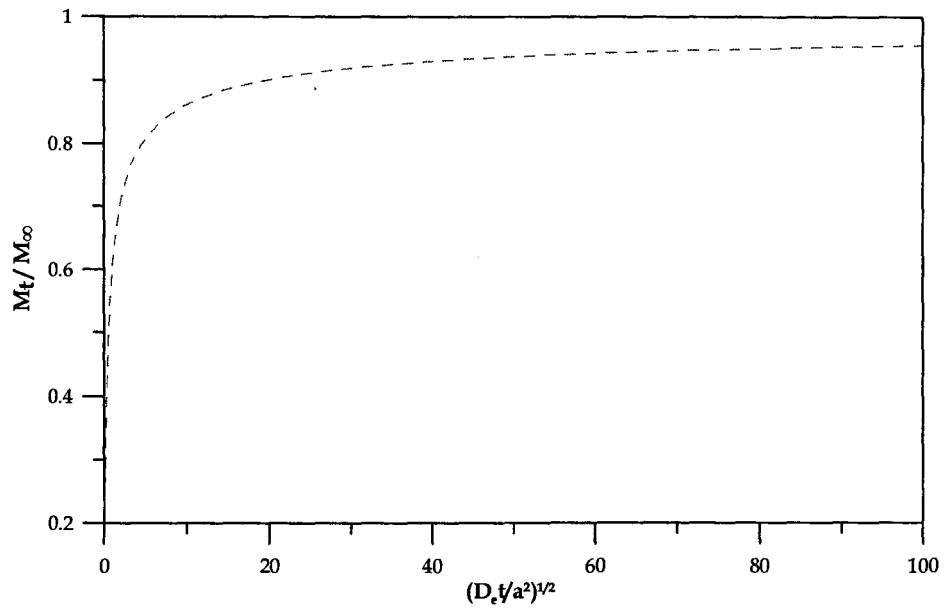


Figure 4.17 Total amount of diffusing substance on continuous disk source in 3D at $z=0$.

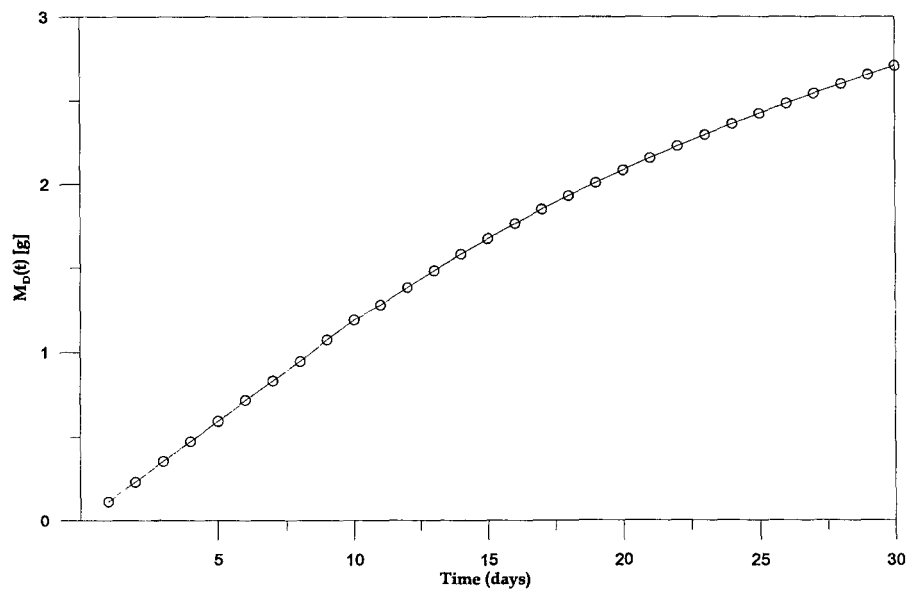


Figure 4.18 The mass diffused from a 3D continuous disk source with boundary conditions given by (3.25).

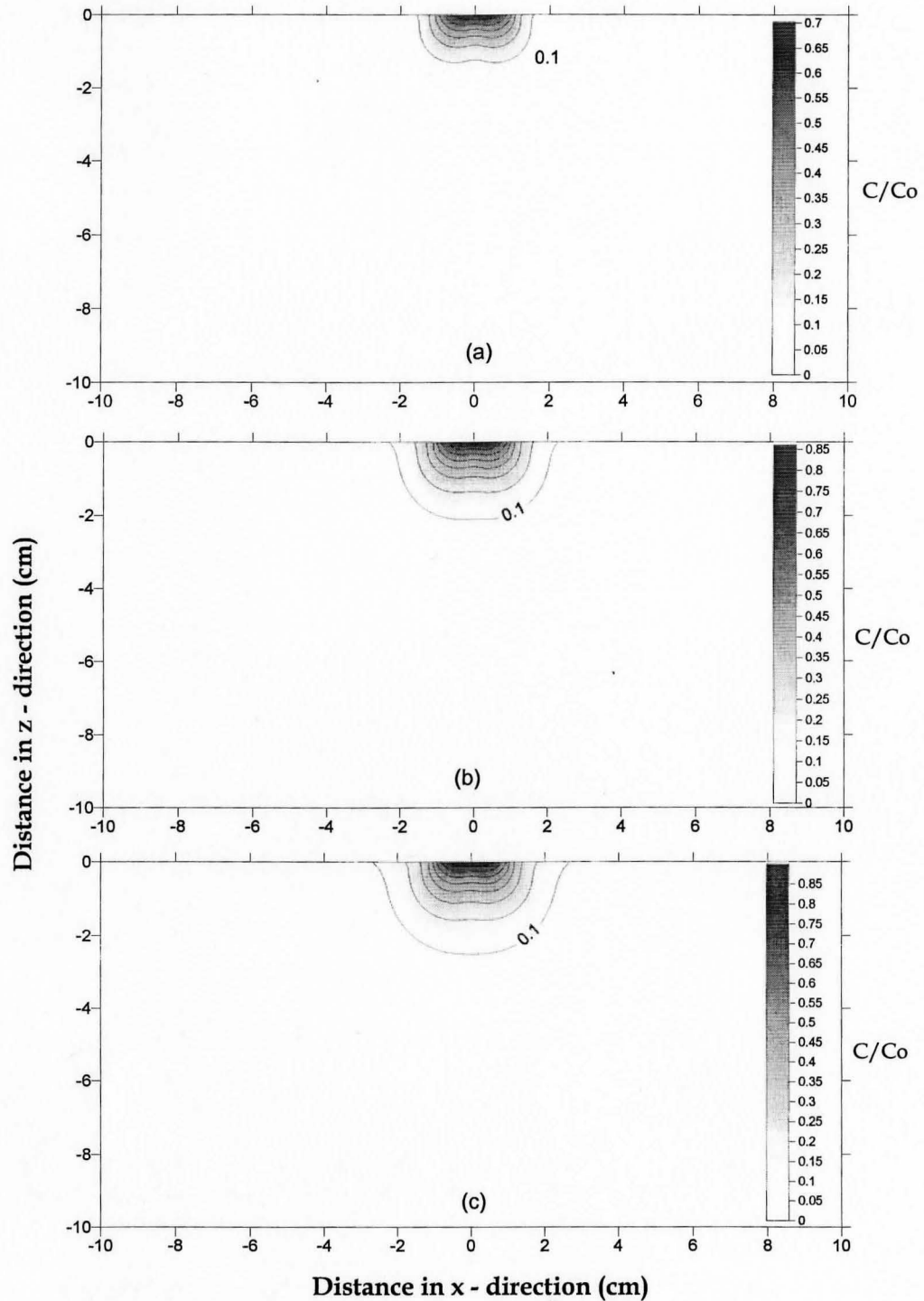


Figure 4.19 Relative concentration profile sections, through the origin, for a 3D continuous disk source with boundary conditions given by equation (3.25) at (a) $t = 1$ day, (b) $t = 5$ days, and (c) $t = 10$ days.

4.4 Comparison of the 3D instantaneous and Continuous Disk Source Solutions

This section presents a comparison between the 3D instantaneous and continuous disk sources as presented in Section 4.2 and 4.3 respectively. For comparison purposes, the values of the parameters listed in Table 4.2 remained constant between all computations.

Figure 4.20 compares the 3D instantaneous and continuous solutions in terms of relative concentration as a function of time at $r = 0$ and $z = 0$. As shown in Figure 4.20, the normalized concentration decreases over time for the instantaneous source and increases over time for the continuous source. The normalized concentration asymptotically approaches one in the continuous case, but never reaches it. Additionally, the rate of diffusion decreases more sharply in the continuous case. This is due to the fact that the chemical potential decreases more quickly in this case because of the constant concentration in the source zone.

Figure 4.21 compares the normalized cumulative mass diffused away from 3D instantaneous and continuous disk sources as a function of time. The calculations for the instantaneous and continuous cases are as presented in Section 4.2 and 4.3 respectively. The normalized mass diffused approached 1 at approximately 50 days for the instantaneous case, however, it is only approximately 0.8 at this same time, and will never reach 1, for the continuous case. This is somewhat misleading, as the mass diffused is not normalized to the same number in the instantaneous and continuous cases; the initial mass present was larger in the continuous case.

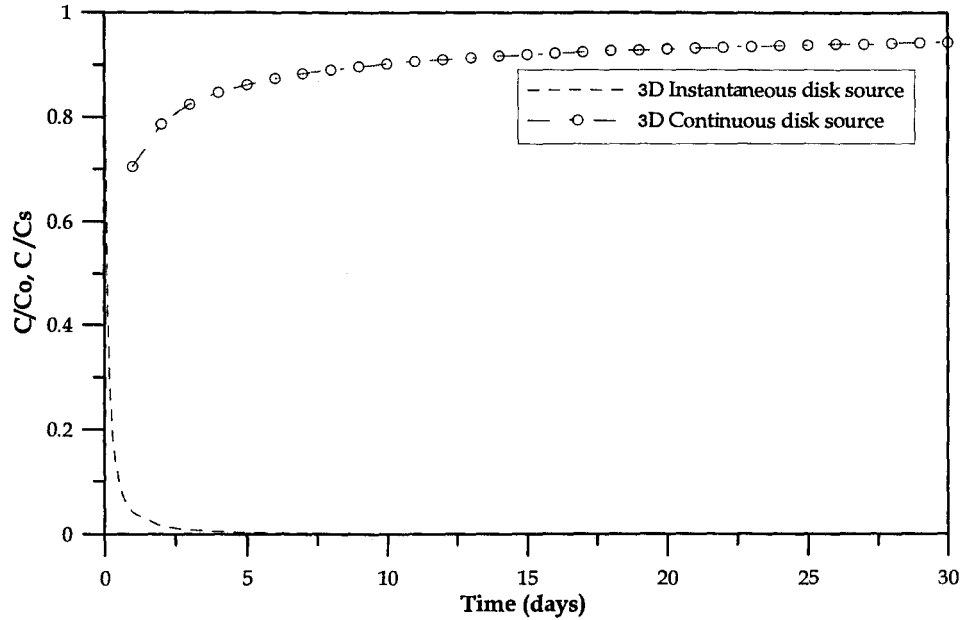


Figure 4.20 Comparison of the relative concentration as a function of time for the 3D instantaneous and 3D continuous disk source solutions at $r = 0$ and $z = 0$.

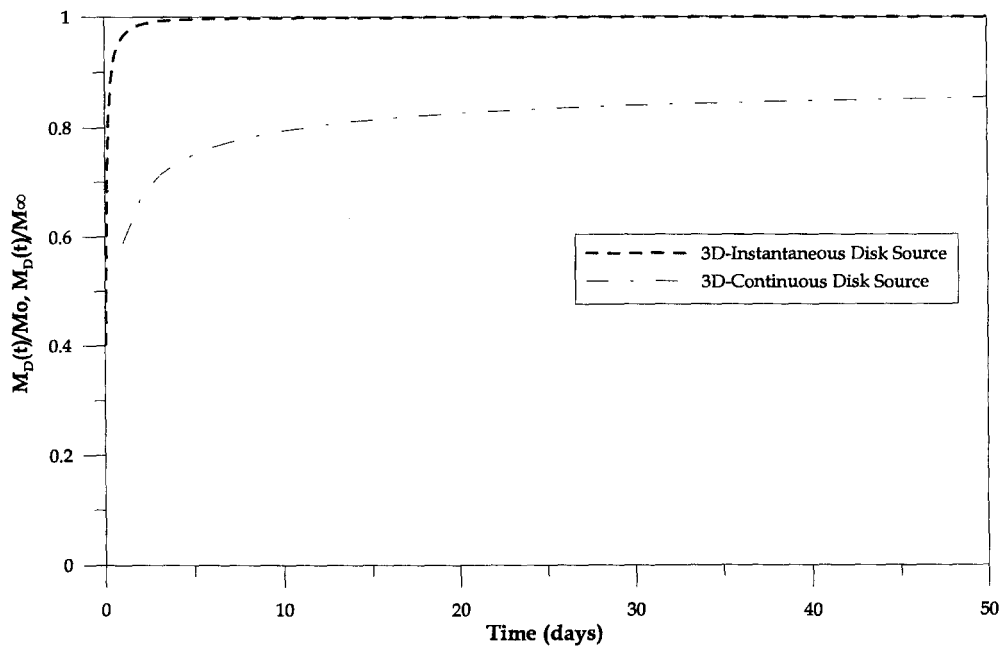


Figure 4.21 Comparison of cumulative normalized mass diffused from 3D instantaneous and continuous disk sources as a function of time.

Therefore, a comparison of the actual mass diffused into the porous matrix in the 3D instantaneous and continuous cases is shown in Figure 4.22. As previously described in Sections 3.2.3 and 3.2.4, the diffusive loss of n-Butanol is calculated using the relationship between the mass diffused and the mass remaining in the source region ($r \leq a$), (i.e., $M_D(t) = \{1 - (Q(t)_{(at r \leq a)} / M_{o(at r \leq a)})\} \times M_{o(at r \leq a)}$) for the instantaneous disk source, and the integration of iso-concentration lines in the r and z directions for the continuous disk source. For the 3D instantaneous and continuous disk sources, the value of $M_D(t)$ is approximately 0.195 mg and 231.9 mg respectively at 40 hours. Therefore, the value of $M_D(t)$ for the 3D continuous disk source is greater than for the 3D instantaneous disk source. The main difference between the instantaneous and continuous disk sources is the shape of the curves with respect to time. The instantaneous disk source curve is exponential whereas the continuous disk source curve varies linearly with time.

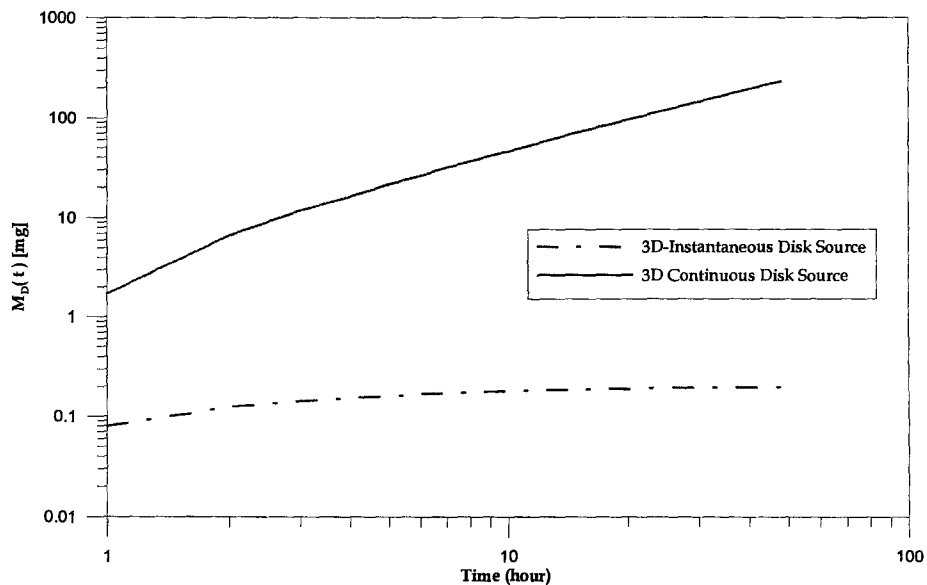


Figure 4.22 Comparison of mass diffused as a function of time for 3D instantaneous and continuous disk sources.

Figure 4.23 shows the normalized concentration profiles as a function of time at $r = 2.0 \text{ cm}$, $z = 0.0 \text{ cm}$ for the 3D instantaneous and continuous disk sources. The concentration at this point, away from the source region, is initially zero, and increases over early time in both cases. The instantaneous disk source, however, reaches a maximum at a relatively early time before decreasing continuously. The 3D continuous disk source, however, increases continuously due to the constant concentration provided by the continuous source; it reaches ~ 0.26 at $t = \text{infinity}$. It should be noted that in this figure, the relative concentrations are normalized to the same number in both the instantaneous and continuous cases.

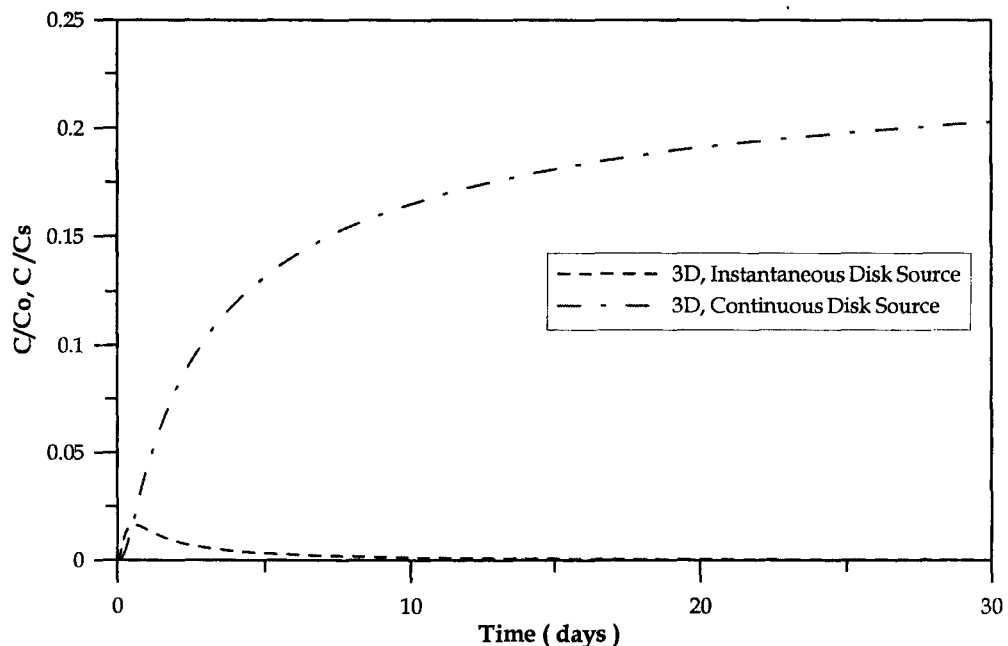


Figure 4.23 Comparison of the normalized concentration profiles as a function of time for 3D instantaneous and continuous disk sources at $r = 2.0 \text{ cm}$ and $z = 0.0 \text{ cm}$.

4.5 Parameter Sensitivity Analysis

As indicated by (3.24c) for a 3D instantaneous disk source and (3.33b) for a 3D continuous disk source, the mass loss from a source zone to the matrix is directly proportional to the matrix porosity (ϕ_m), the aqueous solubility (S_w), the radius of disk source (a), and the time (t) allowed for the diffusion mechanism to take place; it is inversely proportional to the retardation factor (R). In general, the determination of the sensitivity of the mass loss to each of these parameters is difficult. This is due to the fact that the physical properties of both the solute and matrix are not independent of one another. For the purpose of this sensitivity analysis, ranges in parameter values were chosen to be the same as those used by Parker (1994). Trichloroethene (TCE), tetrachloro- ethene (PCE), 1,2,4-trichlorobenzene (TCB) and dichloromethane (DCM) were chosen as the NAPL; its physical properties are given in Table 4.3. The ranges of physical parameters chosen for the porous media are given in Table 4.4. This sensitivity analysis focuses on the effect of the radius of disk source and the matrix porosity.

Table 4.3 Chemical properties for selected organic compounds used for diffusive mass loss calculations.

<i>Chemical</i>	<i>Molecular formula</i>	S_w^1 <i>mg/l</i>	K_{oc} <i>Cm³/g</i>	ρ^1 <i>g/cm³</i>	Do^2 <i>Cm²/sec</i>
TCE	C ₂ HCl ₃	1,420 ³	92 ⁴	1.46	10.1E-06
DCM	CH ₂ Cl ₂	20,000	11 ⁴	1.33	12.4E-06
PCE	C ₂ Cl ₄	240 ³	380 ⁴	1.63	9.4E-06
1,2,4-TCB	C ₂ H ₃ Cl ₃	30 ⁵	3,200 ⁴	1.46 ⁵	5.3E-06

Source : ¹Schulle (1988), ²Bonoli and Witherspoon (1968) for 20°C, ³Broholm *et al.*, (1992) for 23~24°C, ⁴Schwarzenbach *et al.*, (1993) ⁵Mercer and Cohen (1990).

Table 4.4 Characteristics of various geologic media.

<i>Parameter</i>	<i>Clay</i> ¹	<i>Shale / Sandstone</i> ²	<i>Granite</i> ³
Porosity : ϕ	0.35	0.10	0.006
Bulk density : ρ_b (g/cm ³)	1.6	2.4	2.63
Fraction organic carbon : f_{oc}	0.01	0.002	0
Apparent tortuosity : τ	0.33	0.10	0.06
<i>Combined parameters : TCE & Effective diffusion coefficient : De(cm²/s)</i>	<i>geologic</i> 3.3E-06	<i>media</i> 1.0E-06	6.0E-07
Retardation factor : R	5.2	3.2	1

¹ Johnson et al. (1989) ² Feenstra et al., (1984); Barone et al., (1990) ³ Skagius and Neretnieks (1986)

4.5.1 Sensitivity of Disappearance Time to the Radius of the Disk Source and Chemical Properties

Much research has been performed using simplified fractured porous media, which is assumed to be smooth walled. (Parker, 1994, 1997, Grisak et al., 1980, 1981). This assumption makes it easier to evaluate the diffusive mass loss from source zones. Both the fracture aperture and the diameter of the disk source play similar and important roles in NAPL disappearance time.

Table 4.5 and Figure 4.24 show the disappearance time for three geologic media for a 3D instantaneous disk source. To simplify the analysis, the value of R was set to 1 in these simulations. The end point, or disappearance time, was assume to be when $1 - Q(t)/M_0$ equaled 0.9999. Alternatively, it can e interpreted as the point when 0.01% of the initial mass remains in the source zone. Table 4.5 and Figure 4.24 clearly show that disappearance time increases significantly with the size of the source zone. For example,

TCE would disappear from a 3D instantaneous disk source of with a radius of 1cm in 87 days when the surrounding matrix is clay, 122 days when the surrounding matrix is shale/sandstone, and 27 day when the surrounding matrix is granite. NAPL loss from a 3D instantaneous disk source is in the order of the shale/sandstone > clay > granite. These results clearly show that the radius of disk source also plays an important role in NAPL disappearance times, which increase exponentially as the radius increases. Therefore, the larger the disk source, the longer the time required for NAPL disappearance to occur.

Figure 4.25 shows disappearance times for four chemicals in clay materials with no sorption from a continuous disk source. In general, the disappearance time increases with the radius of disk source, and the order of disappearance time is DCM < TCE < PCE < TCB for the same size of the disk source. Figure 4.25 also shows that disappearance times are significantly larger for continuous disk sources than for instantaneous disk sources, all other conditions held equal.

Table 4.5 Effect of the radius of an instantaneous disk source on TCE disappearance time for types of geologic media

Radius of disk source	Disappearance Time (Days)		
	Clay	Shale	Granite
1	87	122	27
10	403	575	143
100	1873	2687	680
1000	8694	12440	3174

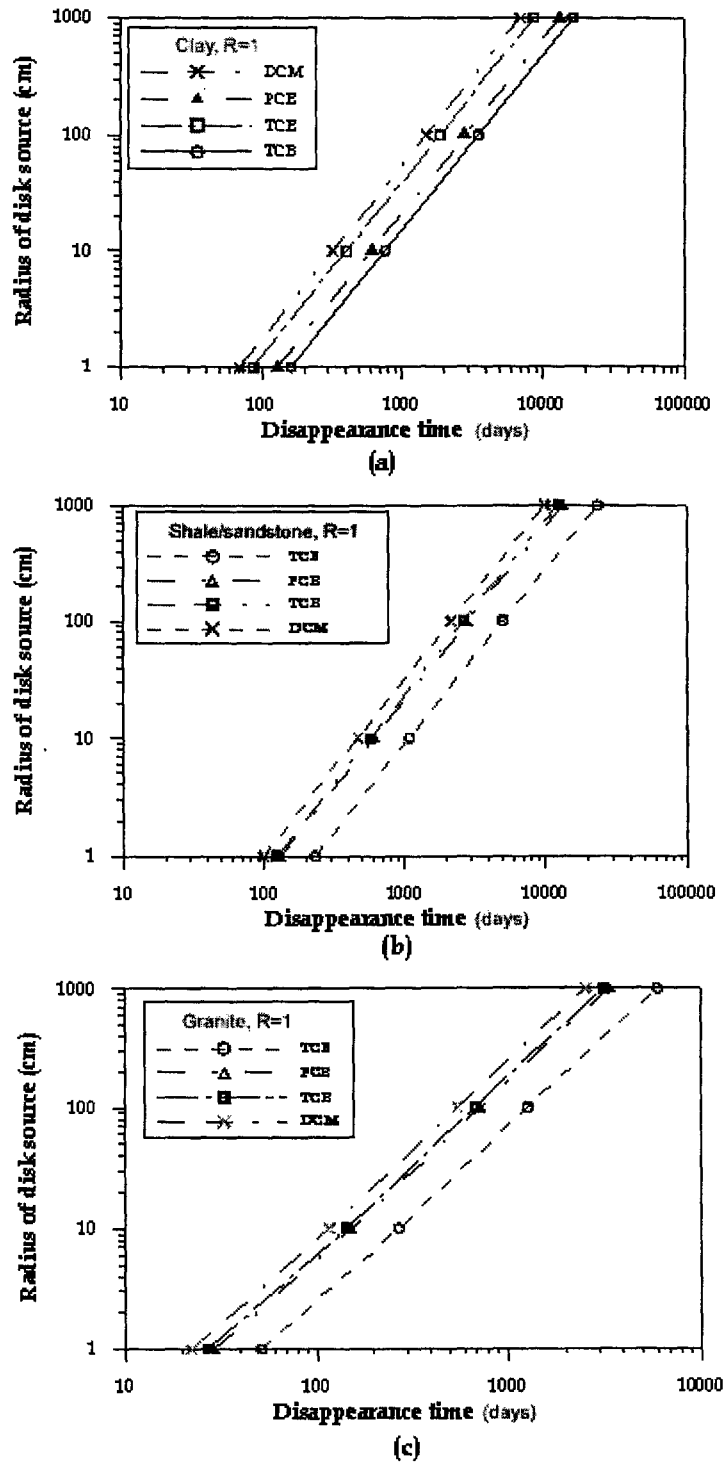


Figure 4.24 NAPL disappearance times expressed in terms of the radius of disk source for a 3D instantaneous disk source with (a) a clay matrix ($R=1$), (b) a shale/sandstone matrix ($R=1$), and (c) a granite matrix ($R=1$)

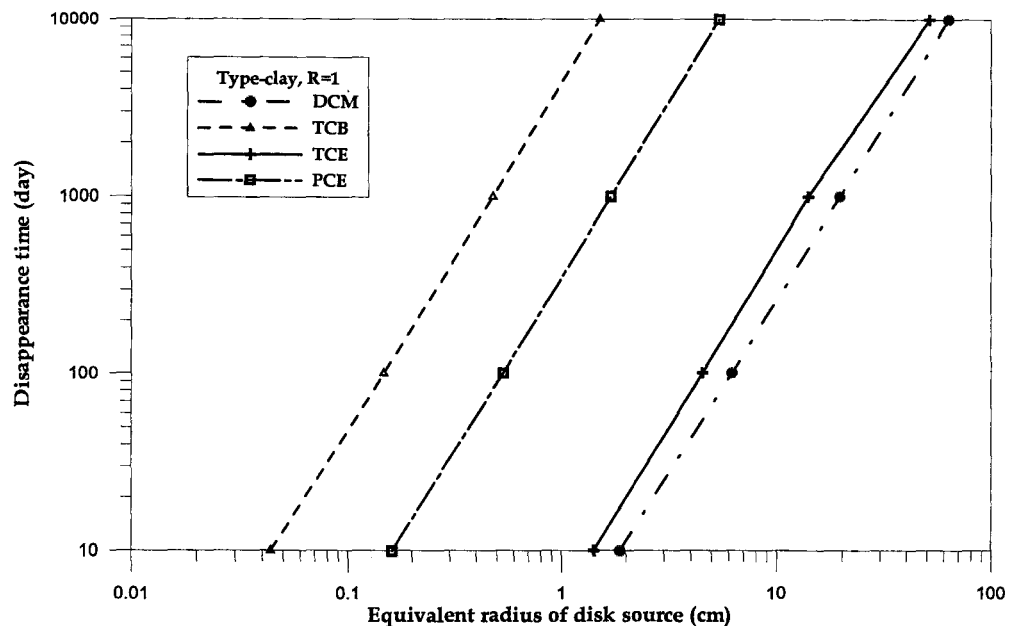


Figure 4.25 NAPL disappearance times for a 3D continuous disk source for four chemicals expressed in terms of equivalent radius of disk source.

4.5.2 Sensitivity of Disappearance Times to Matrix Porosity (ϕ_m)

As stated in section 3.2, porosity is defined as the ratio of the volume of voids to the total volume of the media present. The diffusive loss from the disk source is directly proportional to the matrix porosity. Additionally, the matrix porosity has an indirect effect on the retardation factor (Parker *et al.*, 1994).

To evaluate the disappearance time the four chemicals, the value of $(1 - Q(t)/M_0)$ were calculated using (3.24c) for a 3D instantaneous disk source. The computational results are summarized in Table 4.6 and Figure 4.26 for 3D instantaneous disk source. For the same value of porosity, for instance, the disappearance time for TCE is 38 days, 31 days for DCM, 41 days for PCE, and 71 days for PCB for a instantaneous disk source.

Figure 4.27 shows the effects of matrix porosity on NAPL disappearance times from a 3D continuous disk source expressed as equivalent radius of disk source for four chemical compounds. It is clear that the order of NAPL disappearance is DCM < TCE < PCE < TCB for the same matrix porosity.

Table 4.6 Effect of the matrix porosity on TCE disappearance time for the four different chemicals

Matrix porosity (ϕ_m)	Disappearance Time (Days)			
	TCE	DCM	PCE	PCB
0.001	5	4	5	9
0.01	38	31	41	71
0.1	192	155	204	362
0.3	404	325	430	761
0.5	569	458	606	1073

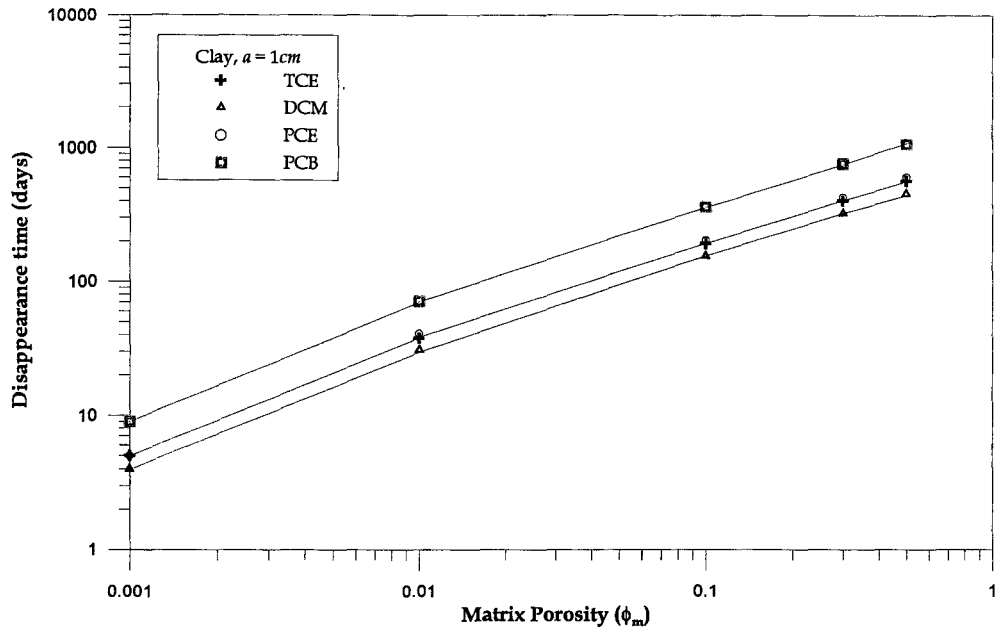


Figure 4.26 Effect of matrix porosity on the rate of DNAPL disappearance for a 3D instantaneous disk source with no sorption ($R=1$).

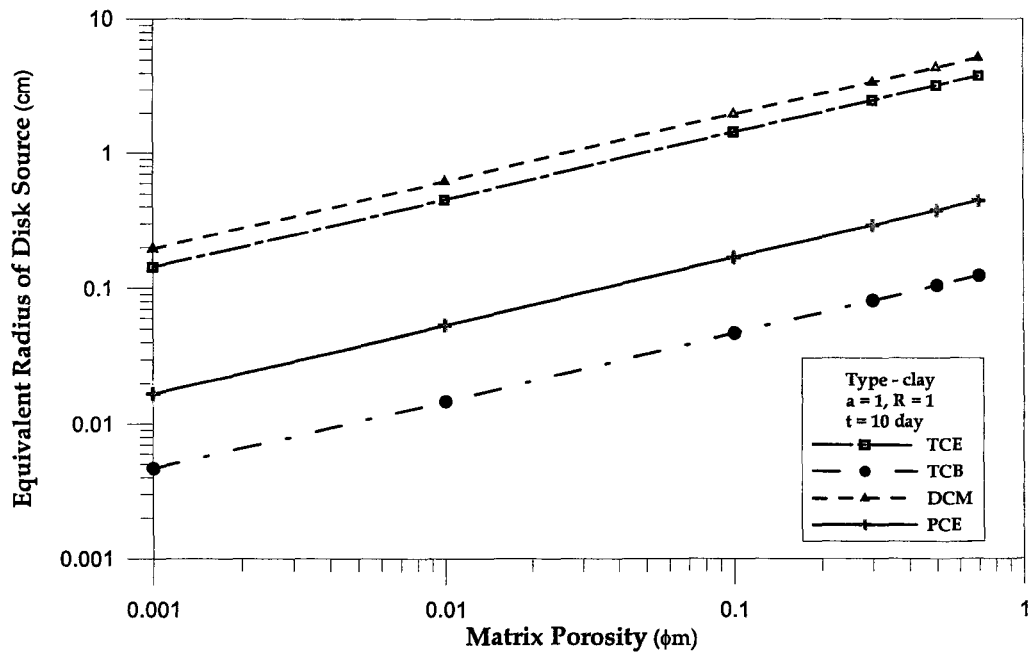


Figure 4.27 Effect of matrix porosity on NAPL disappearance time expressed as equivalent radius of a continuous disk source for a clay matrix with no sorption ($R=1$) at $t = 10$ days.

4.6 Comparison of the disappearance time between Parker's and this work

This section compares disappearance times calculated by Parker *et al.*, (1994) and those calculated here. The primary difference between these two models is that the Parker (1994) model is 1D while the model presented here is 3D. The purpose of this comparison is to determine the error incurred by assuming a 1D system. For comparison purposes, the retardation factor is assumed to be one, and the geologic media is clay. The comparison procedure is as follows: 1) calculate the total mass diffused based on the Parker *et al.*, (1994) model at disappearance times of 1 day, 10 days, 100 days, and 1000 days, for four chemicals; and 2) compare the total mass diffused, for the same disappearance times and chemicals, based on the model presented here. Four chemicals with significantly different diffusion coefficients, DCM, TCE, PCE, and TCB, were chosen for the disappearance time calculations.

Parker *et al.*, (1994) calculated the total mass diffused into the matrix per unit area of fracture surface (Mt) through integration over a specified time period. This model assumed that the matrix diffusion occurs in both x-directions, where the fracture was assumed to be a smooth, parallel-plate fracture. The units of the total mass diffused into the matrix, Mt , is $[M/L^2]$. Conversely, the unit of total mass diffused into the matrix in this work is $[M]$, and the diffusion occurs one direction, and is assumed to be symmetrical. Since the units must be the same to provide a sound basis for comparison between this work and Parker *et al.*, (1994). The total mass diffused into the matrix calculated here was multiplied by two, and divided by the area of the disk source.

Table 4.7 and Figure 4.28 compare the mass diffused into the matrix at the specified disappearance times based on the 1D (Parker et al., 1994) and 3D (this work) models. As shown in Table 4.7 and Figure 4.28, there are differences in the total mass diffused calculated by Parker *et al.* (1994) and this work. These discrepancies arise from the differences between the initial and boundary conditions employed for these two models. Parker et al. (1994) assumed that the concentration at the fracture surface boundary was equal to the aqueous solubility of the relevant NAPL [$C_w(0,t) = S_w$], however this study assumed zero concentration at the surface boundary at the initial time. Therefore, at early times, the total mass diffused calculated by Parker *et al.* (1994) is much greater than that calculated by the model presented here. As time marches forward the total mass diffused as calculated by both models is relatively equal after ten days, at which point the mass diffused by the model presented here begins to exceed the mass diffused calculated by the Parker *et al.*, (1994) model. This is expected, as this model calculates diffusion in 3D, whereas the Parker *et al.* (1994) model calculates diffusion in 1D. The percent difference between the Parker *et al.* (1994) model and this model is dependant on the computational time, the effective diffusion coefficient, and the aqueous solubility of the relevant DNAPL.

Table 4.7 Comparison of the disappearance time for four chemicals between the Parker et al., (1994) model and this work.

	Disappearance Time (days)	Parker et al., ('94) (mg/cm ²)	This Work (mg/cm ²)	% Difference
DCM	1	26.864	9.404	35.01
	10	84.950	102.044	120.12
	100	268.636	1040.720	387.41
	1000	849.501	10629.223	1251.23

	Disappearance Time (days)	Parker et al., ('94) (mg/cm ²)	This Work (mg/cm ²)	% Difference
TCE	1	1.711	0.536	31.31
	10	5.411	5.823	107.61
	100	17.111	59.458	347.47
	1000	54.111	601.451	1111.51
PCE	1	0.280	0.085	30.34
	10	0.886	0.924	104.28
	100	2.803	9.439	336.74
	1000	8.864	95.537	1077.79
TCB	1	0.026	0.005	20.73
	10	0.082	0.062	75.69
	100	0.259	0.646	248.91
	1000	0.821	6.486	790.45

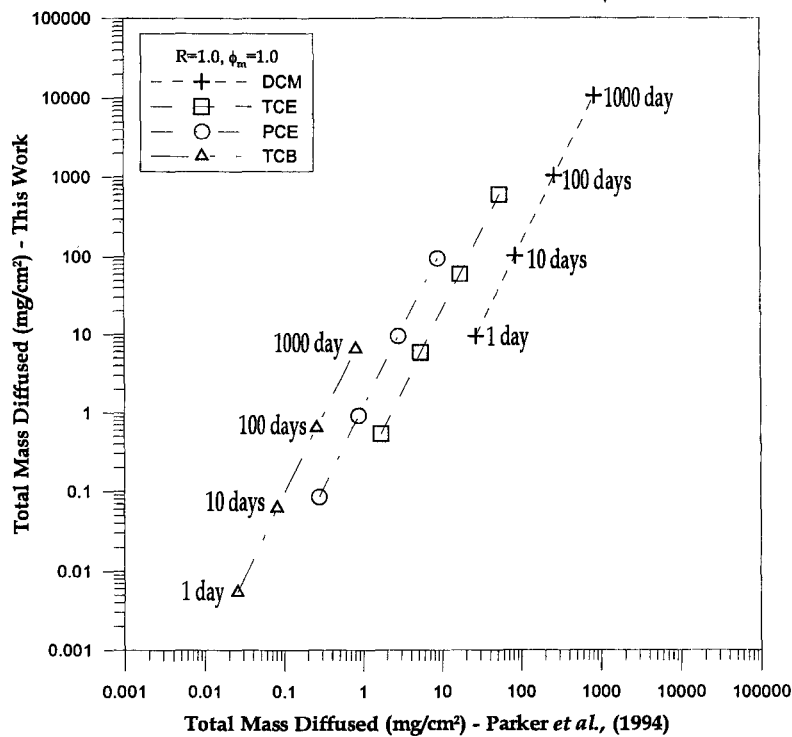


Figure 4-28. Comparison of the Parker *et al.*, (1994) model and this work as a function of the mass diffused into matrix at disappearance times of $t = 1$ day, $t = 10$ days, $t = 100$ days, and $t = 1000$ days.

Chapter 5: Laboratory Experiments and its Results

To verify the diffusion theory presented in Chapter 3, and the models based on this theory developed in Chapter 4, physical model experiments were conducted. These experiments examined 3D diffusion of n-Butanol from both instantaneous and continuous disk sources in a fracture with a silica flour matrix. This chapter presents the experimental materials and apparatus, analyses the observations from these experiments, compares the results of the physical model experiments to those predicted by the models developed in Chapter 4, and offers potential explanations for differences between the physical model experiments and the model predictions.

5.1 Materials and Methods

The purpose of the physical model experiments was to observe and quantify 3D diffusion in a smooth fracture with a clay-like matrix (i.e., high porosity and low hydraulic conductivity). Since diffusion is symmetrical about the centre of the aperture in smooth fractures, only half of the aperture and corresponding matrix were modeled physically. This section describes the materials employed in the physical model experiments, the experimental design, and the methodology used to conduct the experiments.

5.1.1 Silica Flour (290 Flour)

Table 5.1 shows a chemical analysis of the silica flour employed in these experiments. The silica flour is mainly composed of SiO₂ (99.8%), with the remaining

make-up being 0.05% aluminium oxide, 0.04% iron oxide, and 0.02% titanium oxide. Table 5.2 presents the physical properties of silica flour; the colour is white and the specific gravity is 2.65g/cc. Figure 5.1 shows the sieve analysis data for the silica flour; it is fine grained with close to 100% passing at 100 microns.

$$R = 1 + \frac{\rho_b}{\phi} K_d \quad (5.1)$$

where,

R : Retardation factor

ρ_b : the dry bulk density [M / L^3]

ϕ : the matrix porosity [-]

K_d : the distribution coefficient [L^3 / M] = $K_{oc} f_{oc}$

Using the physical properties of silica flour, the entry pressure can be calculated. DNAPL will enter a water-saturated porous media system if the capillary pressure exceeds the entry pressure of the porous media. Dullien (1975) gives the pressure necessary for fluid to enter a pore space, as shown in (5.2). The entry pressure, calculated based on 5.2, is 332.42 Pascals ($\sim 4.18 \times 10^{-5}$ m N-butanol) for the n-butanol / silica flour system employed in these experiments with $\sigma = 0.00167$ N/m, $r = 1.00075 \times 10^{-5}$ m, and $\theta = 5.1^\circ$ (Shripad *et al.*, 2003). Therefore, it is concluded that the N-butanol disk source remained within the fracture plane and did not penetrate the silica flour matrix.

$$P_E = 2\sigma \cos\theta / r \quad (5.2)$$

where

P_E = entry pressure into the fracture (Pascals) (F/L^2)

σ = interfacial tension between DNAPL and water (F/L)

θ = contact angle between DNAPL and water (degrees)

r = pore throat radius (L)

Table 5.1 Chemical Breakdown of Silica Flour.

Silicon Dioxide (total)	SiO ₂	> 99.80
Aluminum Oxide	Al ₂ O ₃	~ 0.05
Iron Oxide	Fe ₂ O ₃	~ 0.04
Titanium Oxide	TiO ₂	~ 0.02
Calcium Oxide	CaO	< 0.01
Loss On Ignition	LOI	~ 0.10

Table 5.2 Typical Physical Properties of Silica Flour.

Colour : White	Mineral : Quartz
Hardness (Mohs) : 7	Moisture : < 0.20%
Specific Gravity (g/cc) : 2.65	Melting Point (°F) : ~3100
pH : 7	Melting Point (°C) : ~1700
Reflectance (%) : ~79	Yellowness Index : 4
f_{oc} : 0.0	

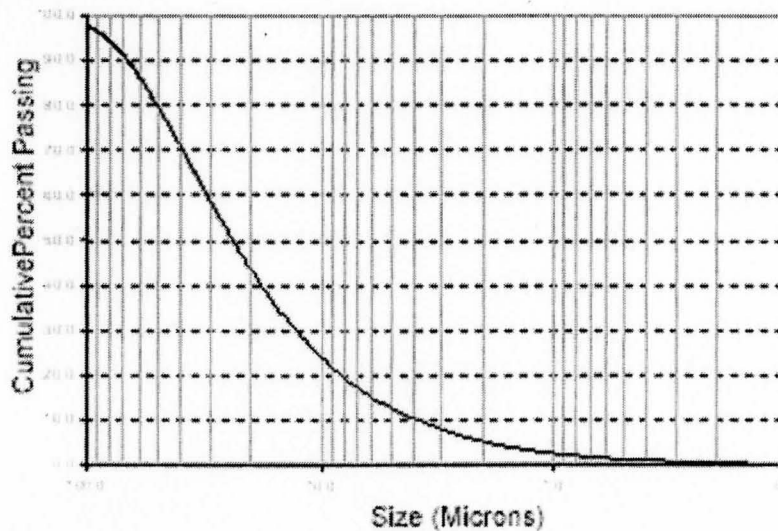


Figure 5.1 Results of a sieve analyses for the silica flour employed in these experiments (Source : U.S Silica Company).

5.1.2 N-Butanol

N-butanol was chosen as the NAPL in these experiments due to its high solubility in water, which enabled the experiments to be conducted relatively quickly in comparison to other potential NAPLs (e.g., TCE, PCE). N-butanol is a colorless liquid with medium volatility and an alcohol-like odor. It has a limited solubility in water and is freely miscible with many other common solvents. Its common uses include coatings, cleaners, textiles, flotation agents, floor polishes, and an extractant in the production of pharmaceuticals and beer. Another major application of n-butanol is as a chemical intermediate for esters (including plasticizers), glycol ethers, butyl-amines, butyl xanthate (ore flotation agent), butyl titanates, and butylated urea resins. The physical properties of n-butanol are given in Table 5.3. The boiling point of n-butanol is 114 ~ 118°C, the

effective diffusion coefficient is $0.96 \times 10^{-5} \text{ cm}^2/\text{sec}$, the solubility in water (S_w) is 63.2g/L, and the specific gravity is 0.810~0.830 g/cm^3 at 20 °C. Synonyms of n-butanol include butanol, 1 -butanol, butanolen, butalol n-, butyl alcohol, and n-butyl alcohol. Since the natural appearance of n-Butanol is clear and colorless, it was dyed with Sudan IV at a concentration of 213 ppm.

Table 5.3 Physical properties of n-butanol

Specific Gravity (a) 20/20°C	0.810 ~ 0.830 g/cm^3
Boiling Point (a) 760mmHg, °C	114~118 °C
Appearance	Clear and colorless
De	$0.96 \times 10^{-5} \text{ cm}^2/\text{sec}$
Sw	63.2g/L

(Source : Technical Data Sheet, BASF Corporation)

5.2 Experimental Apparatus

Figure 5.2 shows a schematic of the apparatus employed for the physical model diffusion experiments. A plastic container, with an inner diameter of 21 cm and depth of 17 cm was fitted with a plastic base of a slightly larger diameter. This container was filled with saturated silica flour to simulate one half of the fracture matrix. The top was sealed with an inert glass plate. Because diffusion is symmetrical about the centre of a smooth fracture aperture, it can be assumed that the glass plate represents the centre line of the fracture aperture. The glass cover was bolted to the flange of the container and sealed using a rubber gasket. The glass cover was also fitted with a glass tube (2 cm ϕ) to enable

the emplacement of either a continuous or instantaneous disk source. The tube was inserted through a hole drilled in the glass cover, and sealed with waterproof sealant. The container was filled with silica flour, and saturated with reverse osmosis (RO) water by partially filling the container with degassed RO water, followed by the addition of silica flour. Degassed RO water and silica flour were added to the container in this manner (in layers) until the container was full. The system was left to equilibrate for a minimum of two days prior to beginning any experiments to ensure that no additional settlement would occur.

Numerical simulations (Scenario C from Table 4.1, continuous 3D disk source) were conducted to determine the size of apparatus required, so that the physical boundaries of the container not affect the experimental results. It was found that the apparatus size could be significantly reduced through controlling the size of disk source or the experimental time. Figure 5.3 shows the computational results for the determination of the dimensions of experimental apparatus. The simulations show that the relative concentration (C/C_0) will be zero at $r = 9$ cm after three days for a 2 cm n-butanol disk source. It was determined that a 21 cm diameter container with a depth of 17 cm would be suitable for the diffusion experiments.

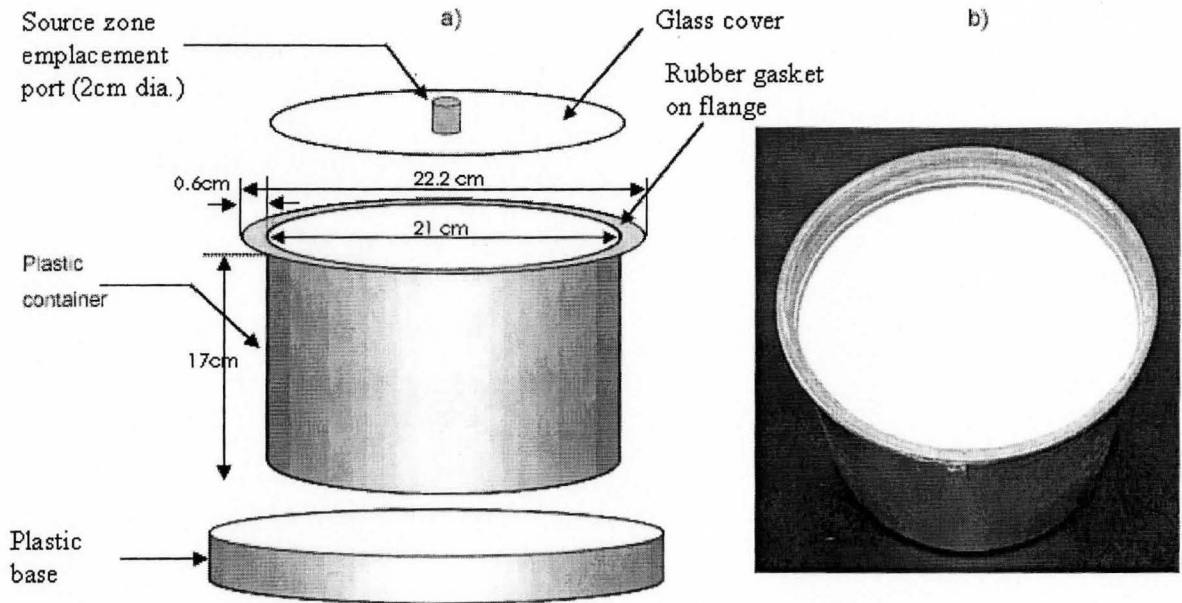


Figure 5.2 (a) Schematic and (b) photograph of the experimental apparatus

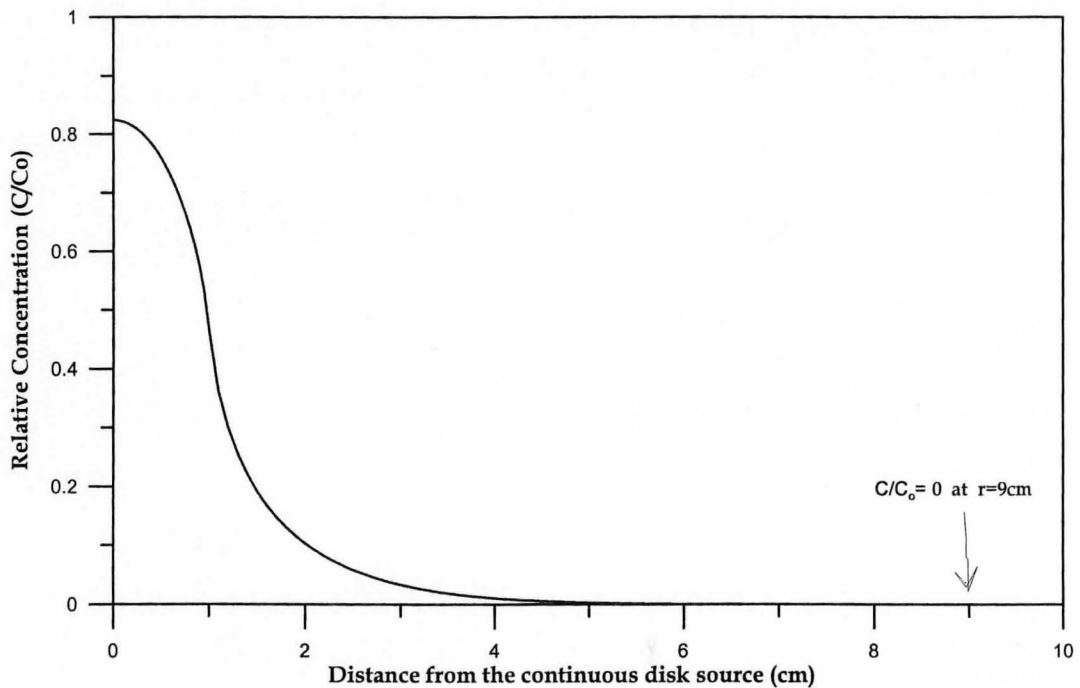


Figure 5.3 Results of simulations employed to determine the size of experimental apparatus required for these experiments.

5.3 Experimental Conditions

Table 5.4 presents a summary of the experiments conducted, as well as the boundary and initial conditions for each experiment. To create an instantaneous disk source, the specified mass of n-Butanol was dissolved into an aqueous phase, and then placed onto the surface of saturated silica flour through the source zone emplacement port located at the center of the glass cover on the container. To create a continuous disk source, the specified mass of n-butanol was placed directly onto the surface of saturated silica flour through the source zone emplacement port.

Table 5.4 Summary of the experimental conditions.

		EXP-1	EXP-2	EXP-3
Method		Inst.	Inst.	Cont.
Input mass of n-Butanol (mg)		257.48	128.74	514.96
Total Experimental Time (hr)	Start	July 23 rd , 11:30	Aug.20 th , 11:50	Aug.20 th , 13:25
	End	July 24 th , 12:00	Aug.20 th , 22:00	Aug.20 th , 23:30
	Exp. Time	24 hrs 30 min.	10 hrs 10 min.	10 hrs 5 min.
Temp(°C)		25	25	25

5.4 Sampling Locations

5.4.1 Sampling locations

Figures 5.4 through 5.7 show the sampling locations for experiments 1, 2 and 3 at various radiuses and depths. In the case of experiment 1, the total number of points sampled was 10. 24 locations were sampled for n-butanol concentrations in experiments 2 and 3 with six additional points sampled for saturation in these experiments.

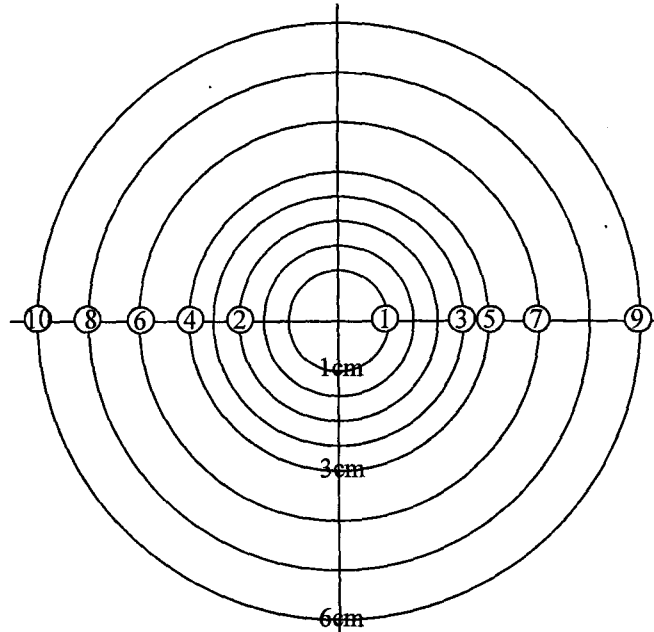


Figure 5.4 Sampling locations for experiment 1, $z = 0$.

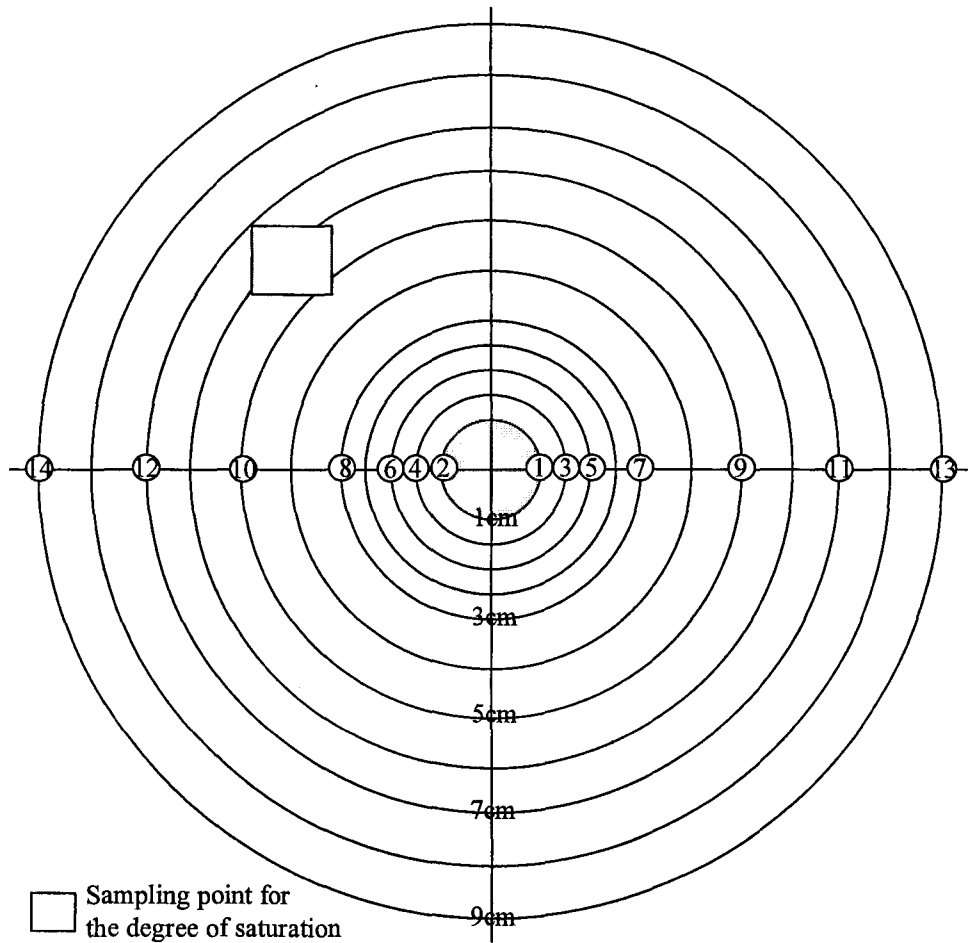


Figure 5.5 Surface sampling locations ($z = 0$) for experiments 2 and 3.

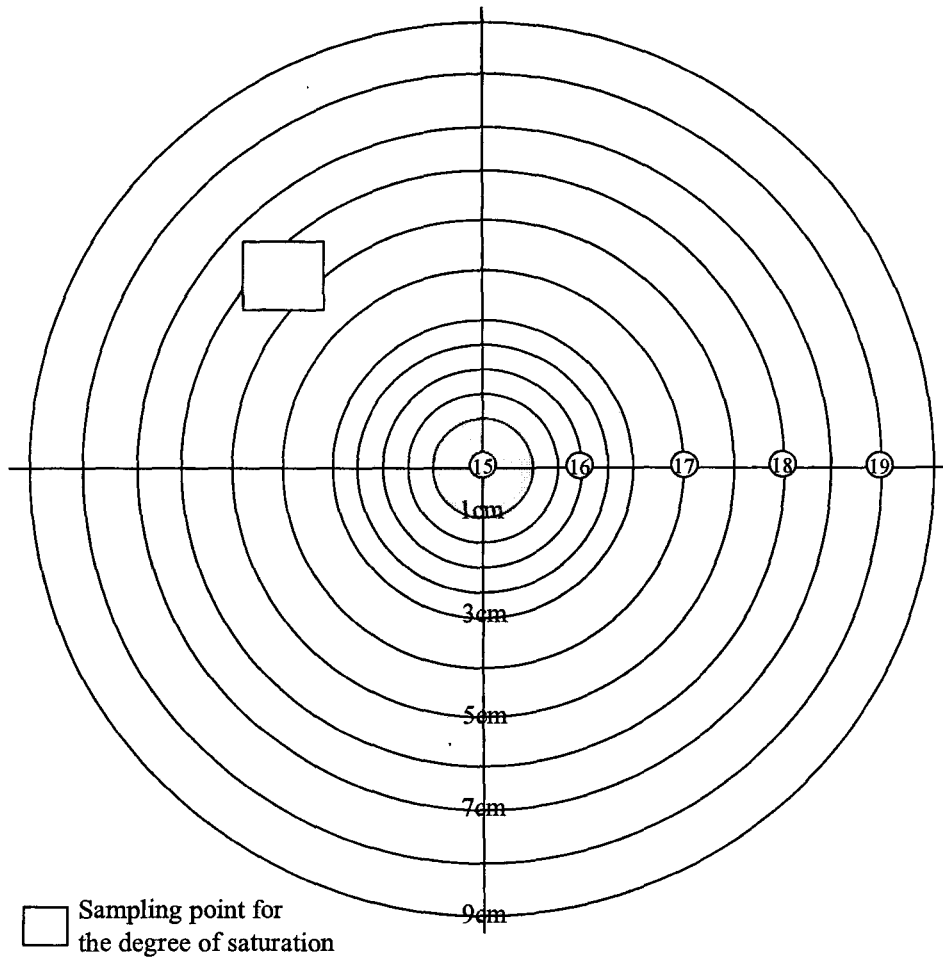


Figure 5.6 Sampling locations at 3cm depth ($z=3$ cm) for experiments 2 and 3.

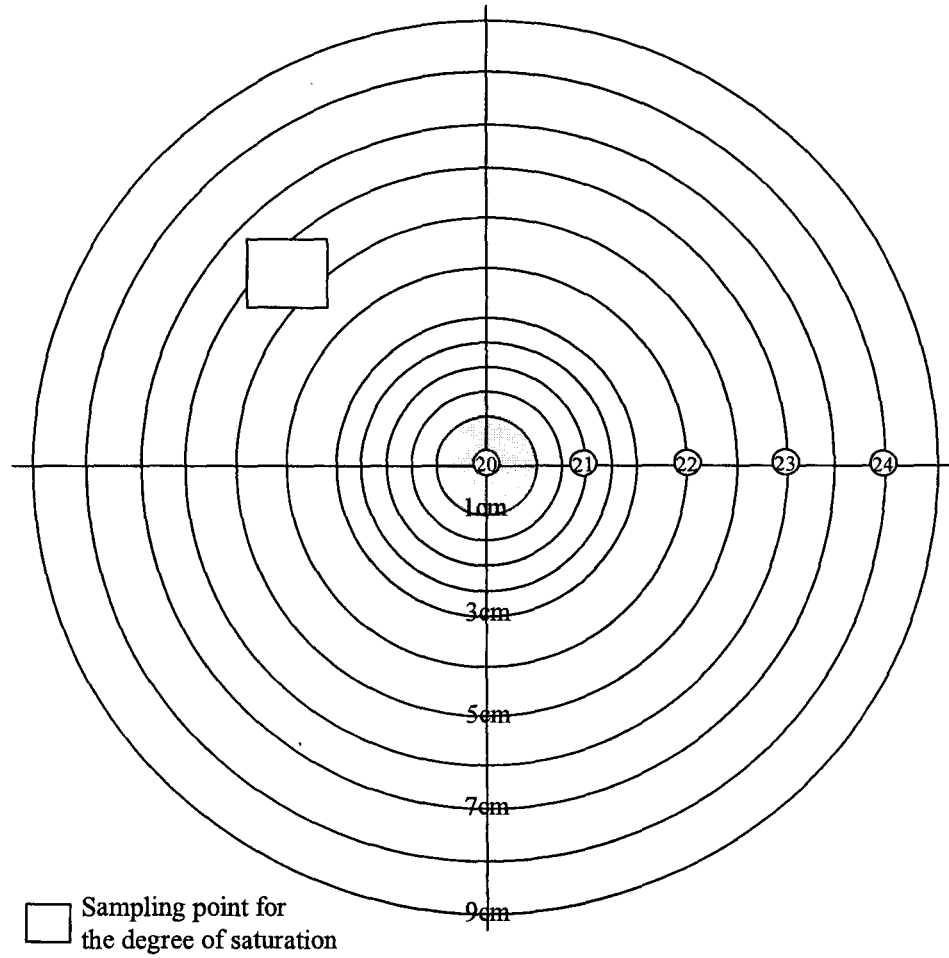


Figure 5.7 Sampling locations at 6cm depth ($z=6\text{cm}$) for experiments 2 and 3.

5.4.2 Sampling methodology

At the end of each experiment, silica flour cores were taken for sampling purposes (quantification of n-butanol) using the specially designed device shown in Figure 5.8. The device is made of a syringe which is connected to a sampling device via a tube. The sampler has an inner diameter of 0.3 cm and a length of 1.5 cm. The suction provided by the syringe protects against losing part of the core. The extracted core was sectioned off into samples for depths of each 0 cm, 3 cm, and 6 cm. The weight of the core withdrawn varied slightly between samples. Therefore, the exact mass of each sample was considered when quantifying n-butanol concentrations.

The n-butanol was extracted from the pore water in each sample by adding 1.5 mL of MeOH to each sample. The masses of the MeOH added and the core sample were then calculated. Table 5.5 shows the variation between samples for both the mass of MeOH added, and the masses of the samples themselves. The concentration of each sample is affected by the mass of MeOH added, as well as by the actual sample mass. Therefore, (5.3) was employed to adjust the measured concentrations to reflect actual values.

Calibrated concentration(ppm) =

$$\left[\left(\frac{\text{average weigh of MeOH}}{\text{real weigh of MeOH}} \times \text{Measured concentration} \right) + \left(\frac{\text{real weight of sample}}{\text{average weight of sample}} \times \text{Measured concentration} \right) \right] / 2 \quad (5.3)$$

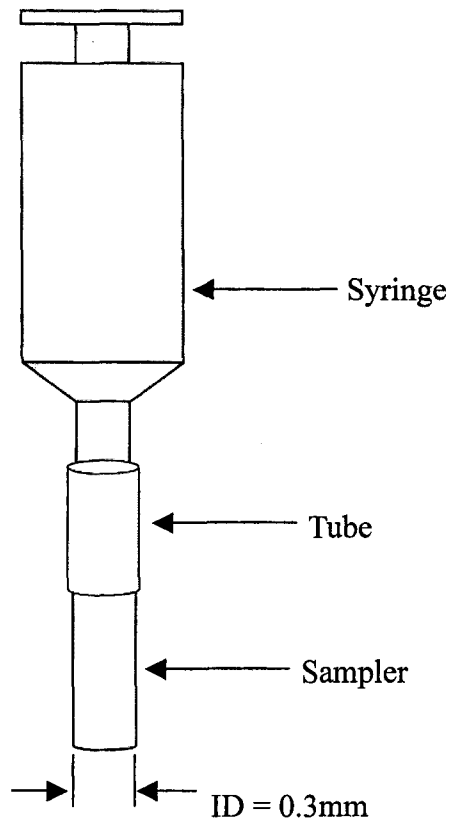


Figure 5.8 Coring device.

Table 5.5. Variations of the mass for MeOH and samples in experiment 2 and 3.

Sample #	Experiment 2		Experiment 3	
	Mass of MeOH (g)	Mass of core sample (g)	Mass of MeOH (g)	Mass of core sample (g)
1	1.1771	0.0645	1.1933	0.0650
2	1.1252	0.0600	1.1445	0.0470
3	1.1283	0.0630	1.1314	0.0431
4	1.1436	0.0612	1.1456	0.0431
5	1.1280	0.0945	1.1427	0.0731
6	1.1480	0.0861	1.2030	0.0887
7	1.1610	0.0770	1.1731	0.0518
8	1.1441	0.0646	1.1570	0.1027
9	1.1259	0.0689	1.2403	0.0525
10	1.1287	0.0632	1.1429	0.0713
11	1.1275	0.0613	1.1553	0.0565
12	1.1248	0.0575	1.1702	0.1089
13	1.1313	0.0834	1.0901	0.0299
14	1.1709	0.0797	1.1721	0.2022
15	1.1490	0.0597	1.1816	0.0506
16	1.1795	0.0680	1.1702	0.0590
17	1.1396	0.0714	1.1543	0.0745
18	1.1175	0.1019	1.1733	0.0668
19	1.1556	0.0223	1.1033	0.0413
20	1.1334	0.0510	1.2161	0.0445
21	1.1678	0.0441	1.1262	0.0513
22	1.1571	0.0486	1.1267	0.0703
23	1.1439	0.0452	1.1479	0.0757
24	1.1374	0.0523	1.1304	0.0576
Mean	1.1436	0.0646	1.1584	0.0678
Std.Dev	0.0179	0.0173	0.0339	0.0344

5.4.3 Quantification of n-Butanol

To quantify the concentration of n-butanol in each core sample, a GC-MSD (Hewlett-Packard, 5973) was used. The analytical method is shown Table 5.6. The temperature program held an initial 45°C column temperature for 3.5 minutes, ramped at 15°C /min to 70°C, which was held for 5.17 min until the end of the run. 10 μ l of 2000mg/L TCE was employed as the internal standard. A sample calibration curve using the internal standard solution is presented in Figure 5.9. Appendix II shows a sample calculation for determining the concentration of n-butanol in a core sample using the GC-MSD output in combination with this calibration curve.

Table 5.6 Analysis conditions for GC-MSD.

Oven Temperature	45°C (3.5min.), 15°C/min. → 70°C (Runtime : 5.17min)
Split ratio	50/1
Split flow	39.1mL/min.
SIM (Select Ion Monitoring)	2.2 min. 55.56 (n-Butanol) 3.0 min. 130.132 (TCE → ISTD)
ISTD(Internal standard)	TCE 2000mg/L → 10 μ l

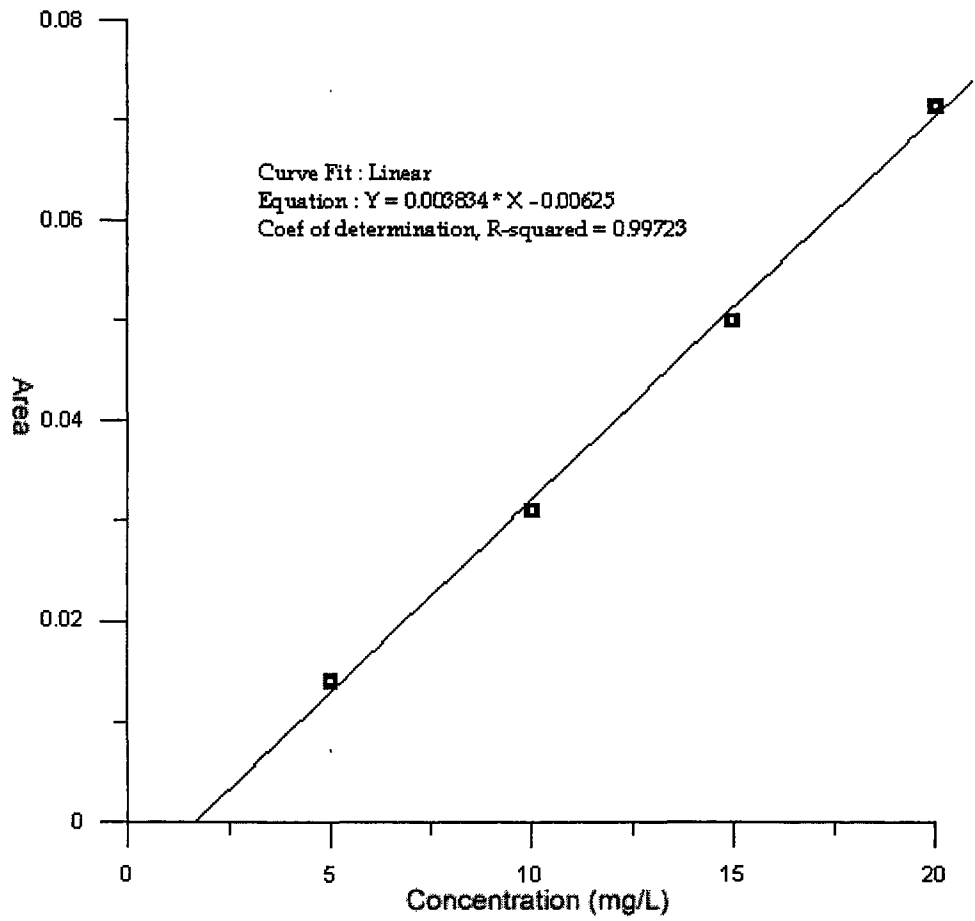


Figure 5.9 GC-MSD calibration curve for n-butanol.

5.5 Observations and Results

5.5.1 Percent saturation

To analyze the degree of water saturation within the container, samples were taken at depths of 0 cm, 3 cm, and 6 cm in experiments 1, 2 and 3. The percent saturation appeared to change over time, even though the silica flour was fully saturated at the beginning of experiment. Table 5.7 and Figure 5.10 present the degree of saturation at varying depths in experiments 1, 2 and 3. From these result, it can be interpreted that the degree of saturation did not reach 100 percent at the surface. The percent saturation varied with time and increased with depth. For example, the range of the percent saturation was 76.4 to 86.99 at the surface and 85.5 to 93.43 at a depth of 6cm. The range of the matrix porosity (ϕ) is 0.34 to 0.42. This value is similar to the value for clay, which has a porosity in the range of 0.35 (Parker *et al.*, '94).

Table 5.7 Percent saturation at 0, 3, and 6 cm depths for experiments 1, 2 and 3.

#	Initial Mass(g)	Dry mass(g)	Air content (%)	Vs	Vv	void ratio	porosity	Percent saturation
Exp1-0cm	1.9240	1.5820	21.618	0.5970	0.4209	0.7050	0.4135	81.26
Exp1-3cm	1.9189	1.5681	22.371	0.5917	0.4261	0.7201	0.4187	82.32
Exp1-6cm	1.9684	1.6212	21.416	0.6118	0.4061	0.6638	0.3990	85.50
Exp2-0cm	1.8854	1.5565	21.130	0.5874	0.4305	0.7329	0.4230	76.40
Exp2-3cm	2.0000	1.6301	22.691	0.6151	0.4027	0.6547	0.3957	91.84
Exp2-6cm	2.0063	1.6300	23.085	0.6151	0.4028	0.6548	0.3957	93.43
Exp3-0cm	1.9609	1.6010	22.479	0.6042	0.4137	0.6848	0.4065	86.99
Exp3-3cm	2.0169	1.6420	22.831	0.6196	0.3983	0.6427	0.3913	94.14
Exp3-6cm	2.0996	1.7746	18.314	0.6697	0.3482	0.5199	0.3421	93.33

* sample volume = 1.01788cm³, G=2.65, rw=1, Vs : volume of solids, Vv : volume of voids

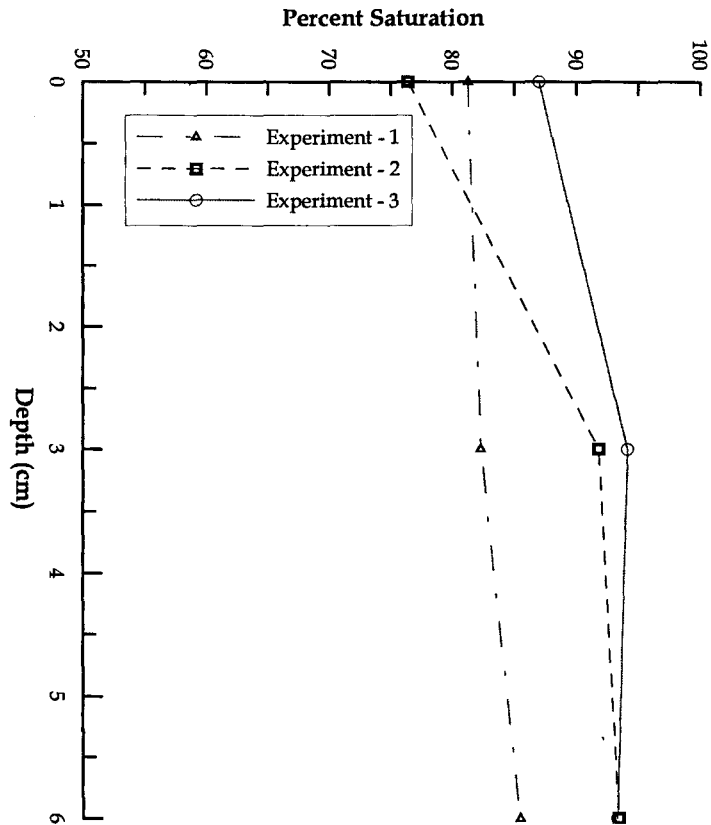
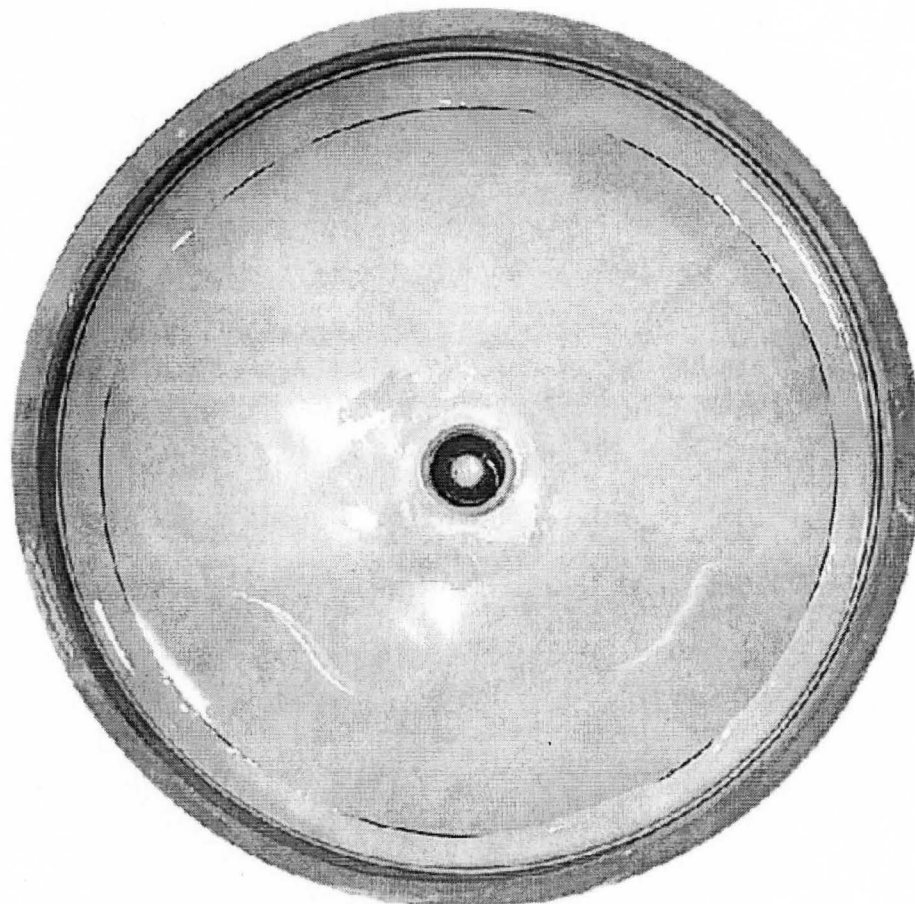


Figure 5.10 Variations in the percent saturation at depths of 0 cm, 3 cm, and 6 cm.

5.5.2 Diffusive loss of n-Butanol

The purpose of these experiments was to quantify the diffusive loss of n-butanol over time. Figures 5.11, 5.12 and 5.13 show the top view of the experimental apparatus at the start of the experiments 1, 2 and 3, as well as the variation in the size of the disk source with respect to experimental time. The area of source region is visible, and therefore easily calculated from the photos. Therefore, in the experiment 1, the diffusive loss of n-butanol is calculated from the area of disk source, as well as from the quantification of n-butanol in the porous matrix.








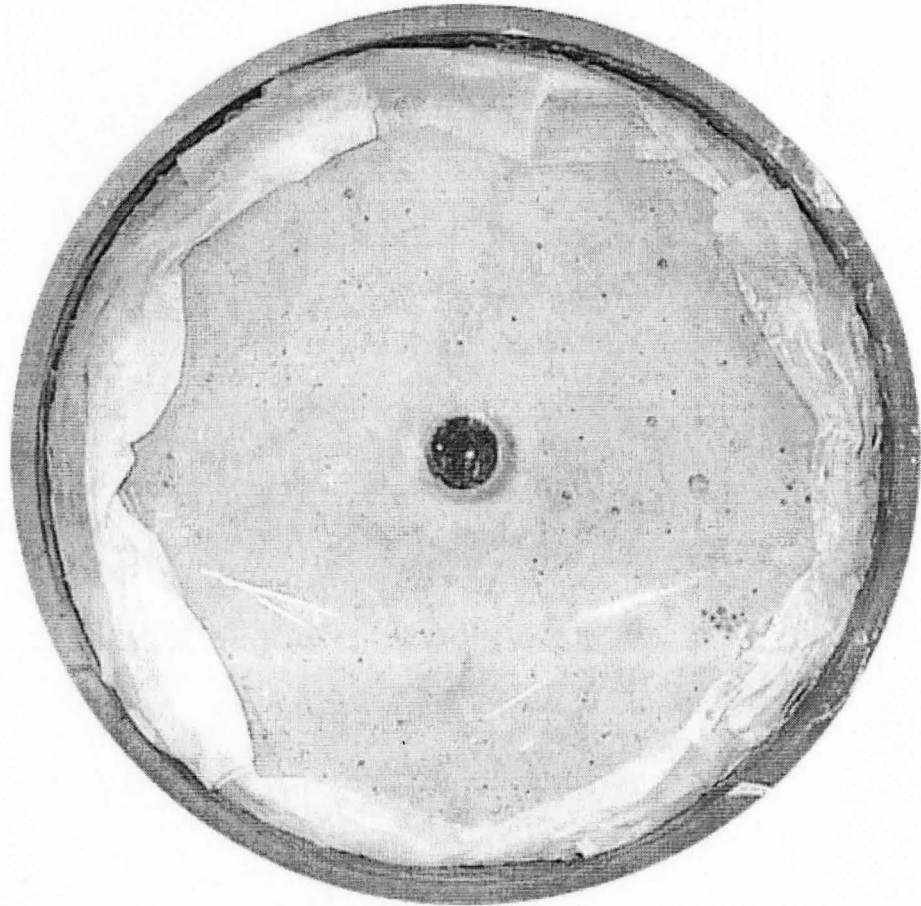
					
	(a)	(b)	(c)	(d)	(e)
Time	t = 0	t = 1 hr	t = 4 hrs	t = 9 hrs	t = 24.5 hr

Figure 5.11 Top view of the experimental apparatus for experiment 1 at a) t = 0, b) t = 1 hr, c) t = 4 hrs, d) 9 hr and e) t = 24.5 hrs.



(a)




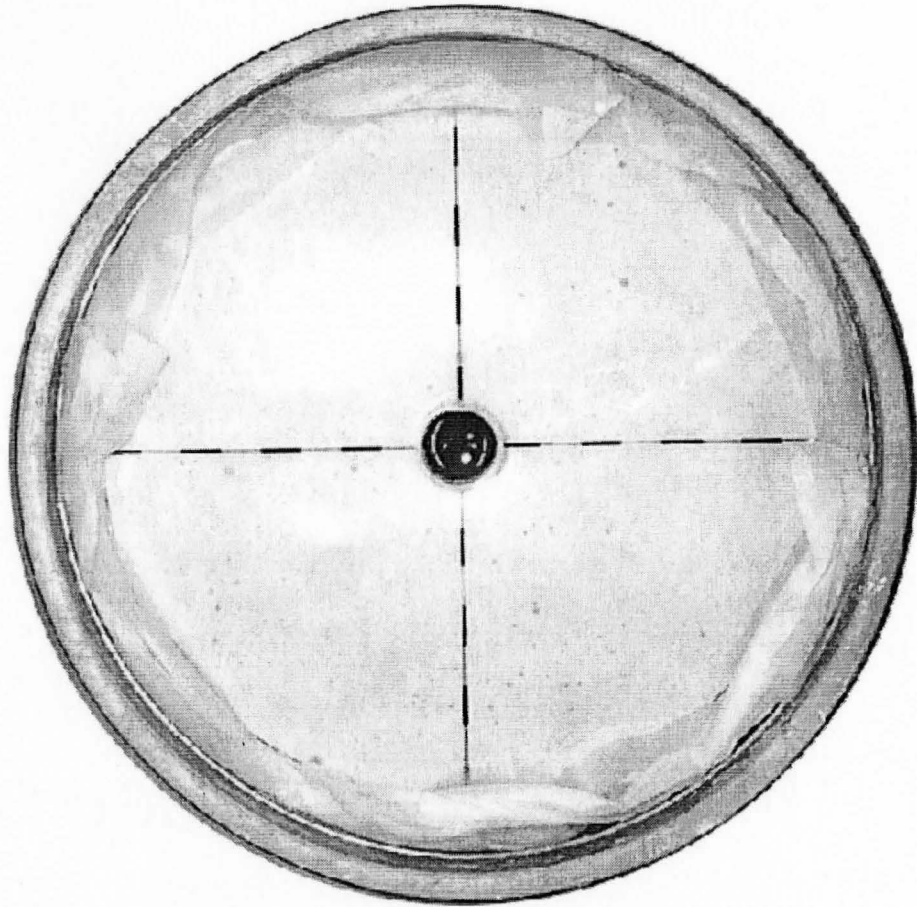
			
	(b)	(c)	(d)
Time	t = 1 hr	t = 5 hrs	t = 10.5 hrs

Figure 5.12 Top view of the experimental apparatus for experiment 2 at a) t = 0, b) t = 1 hr, c) 5 hrs and d) t = 10.5 hrs.



(a)




			
	(b)	(c)	(d)
Time	t = 1 hr	t = 5 hrs	t = 10.5 hrs

Figure 5.13 Top view of c the experimental apparatus for experiment 3 at a) t = 0, b) t = 1 hr, c) 5 hrs and d) 10.5 hrs

Table 5.8 shows the diffusive loss of n-butanol calculated from the analysis of Figure 5.11. Figure 5.14 shows the diffused mass per hour versus experimental time from these calculated data. The diffused mass per hour ranges from 0.0072 g/hr to 0.0218 g/hr; the rate of diffusion decreased with increasing experimental time. This is due to the decreasing chemical potential over time.

Figure 5.15 shows a comparison of the mass loss over time calculated from visual observation to the mass loss over time calculated from model simulations. Two important phenomena are shown in this figure; firstly, there is approximately a 30% of difference between the data calculated from visual observations and that calculated from mathematical simulations, and secondly, the observed data are linear, while the mathematical simulation is not linear. The difference between the observed and simulated data is possibly due to the degree of saturation, the value of D_e , and the matrix porosity. It is more likely, however, that the quantification method using the visual observation technique is inaccurate. Therefore, mass loss will be calculated from n-butanol concentrations in the porous matrix for the remainder of the experiments.

Table 5.8 Summary of the diffusive mass loss from experiment 1, calculated from visual observation.

Time	Disk source area (cm ²)	Volume of Solute (cm ³ =mL)	Diffused Mass (g)	Diffused mass per hour(g/hr)	Total diffused Mass (g)	Diffused mass/Initial mass
0	2.5607	0.3142	0.0000	0.0000	0.0000	0.0000
1	2.3245	0.2837	0.0250	0.0250	0.0250	0.0970
4	2.0848	0.2544	0.0240	0.0080	0.0490	0.1901
9	1.7731	0.2164	0.0312	0.0062	0.0802	0.3112
24.5	0.8450	0.1031	0.0929	0.0060	0.1730	0.6717

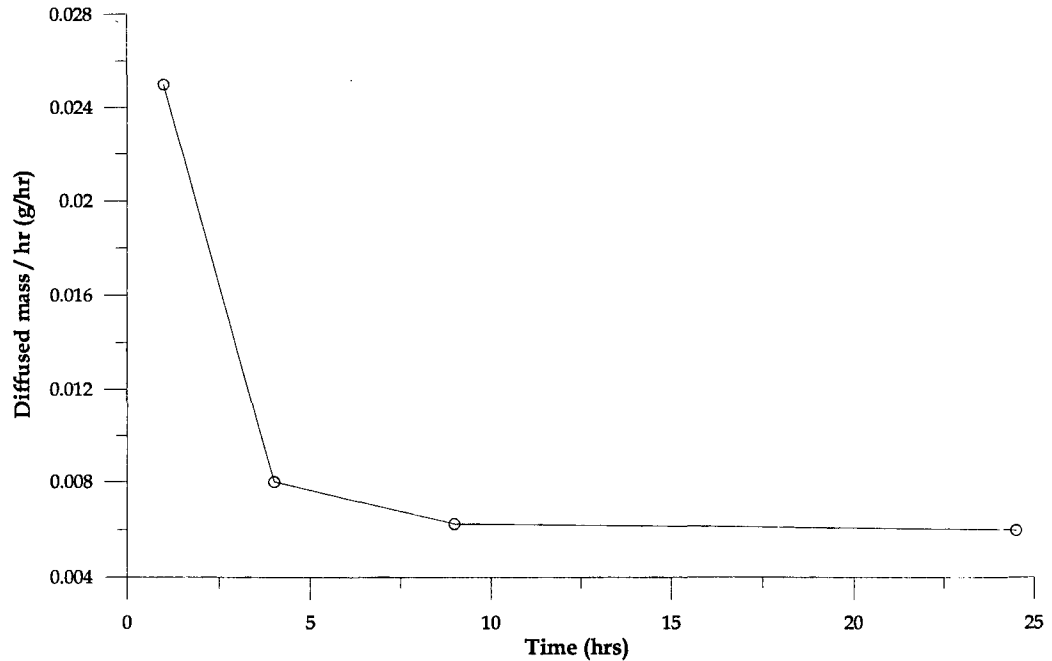


Figure 5.14 The diffused mass of n-butanol per hour versus experimental time for experiment 1.

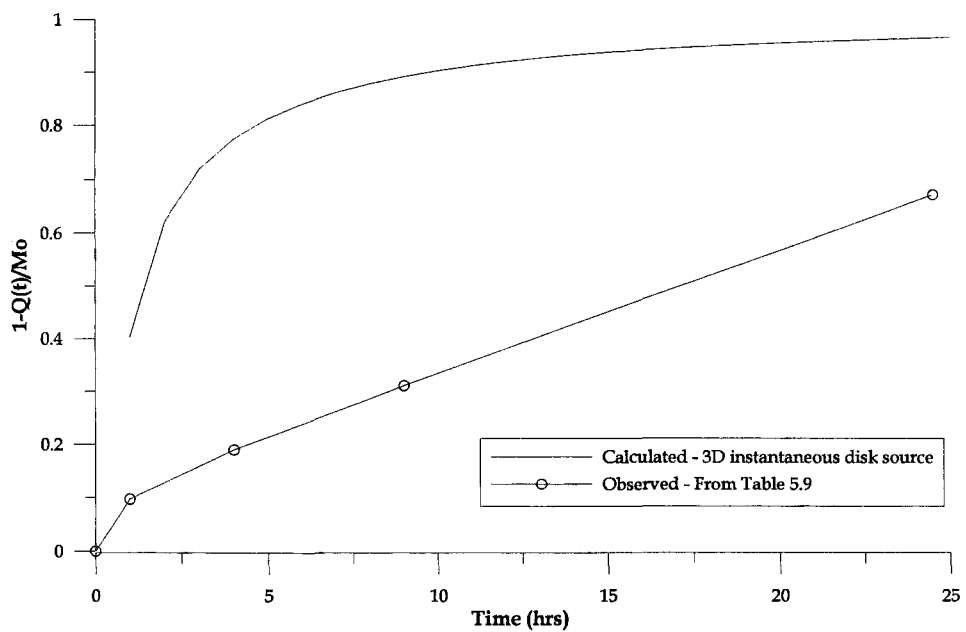


Figure 5.15 Mass loss comparisons as calculated from observed data and by mathematical simulation for experiment 1.

5.5.3 Comparison of Experimental Observations and Model Simulations

As discussed in Chapter 3, the basic assumptions for the numerical model solutions are that the porous medium is homogeneous, isotropic, and saturated with distilled water, and that diffusion conditions are such that Darcy's 2nd law is valid. Although silica flour is well sorted, the degree of consolidation varied over the 17cm experimental depth, which means that a degree of heterogeneity was present in the system. This kind of heterogeneity likely affected the diffusive mechanism over time.

Figures 5.16, 5.17 and 5.18 illustrate both the numerical simulations and the experimental observations for experiments 1, 2 and 3 respectively. These figures show that the calculated and observed data match closely throughout each experiment. The differences between the observed and simulated data can be explained by 1) lower sensitivity of the GC-MSD at lower concentrations, and 2) the slight slope to the surface of the porous matrix in the experiments, as shown in Figure 5.19. This figure shows the surface distribution of solute over time, which is affected by the slope of the media at the surface of the container. As shown in this figure, the diffused area is not exactly symmetrical about the disk source. Diffusion occurred faster to left than to the right, and this difference can be easily seen at the end of the experiment. This asymmetrical diffusion was likely due to the slope of the surface of the porous matrix.

Figure 5.20 shows the general relationship between the calculated and observed data for experiments 2 and 3. The R squared value is 0.871565. The fact that the observed data are equally distributed both above and below the 45° line drawn on Figure 5.20 indicates that there is no systemic error in the model, and the error can be attributed to

experimental error. The results of these experiments do have some limitations, for example, the concentration distribution was not detectable at depths of 3 cm and 6 cm; and are therefore lower than the method detection limit .

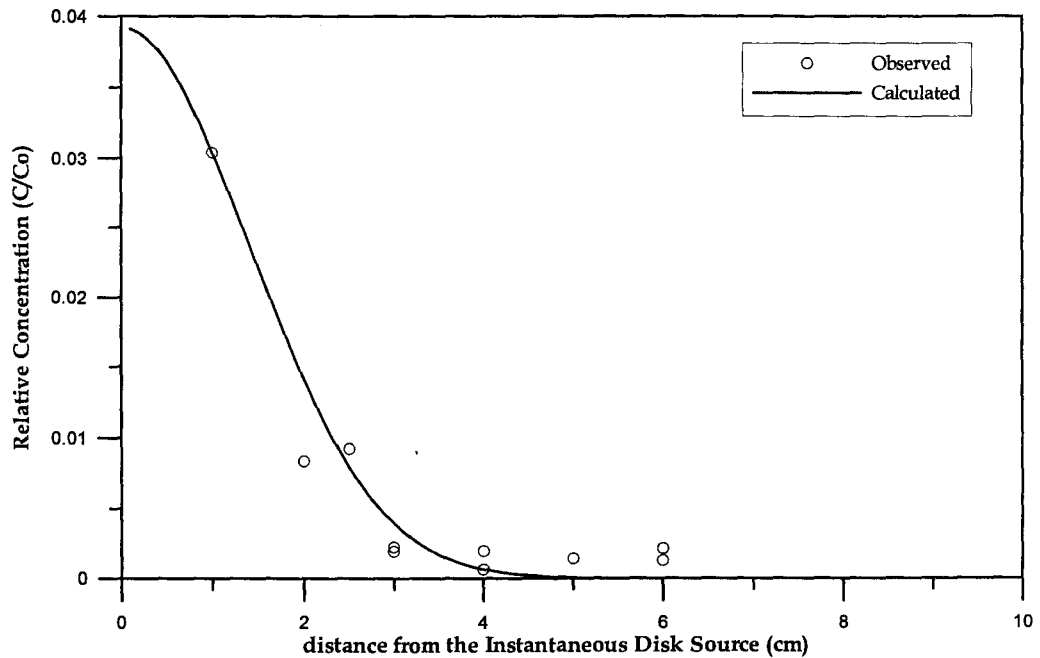


Figure 5.16 Comparison between calculated and observed data at the end of experiment 1 (t = 12.5 hrs).

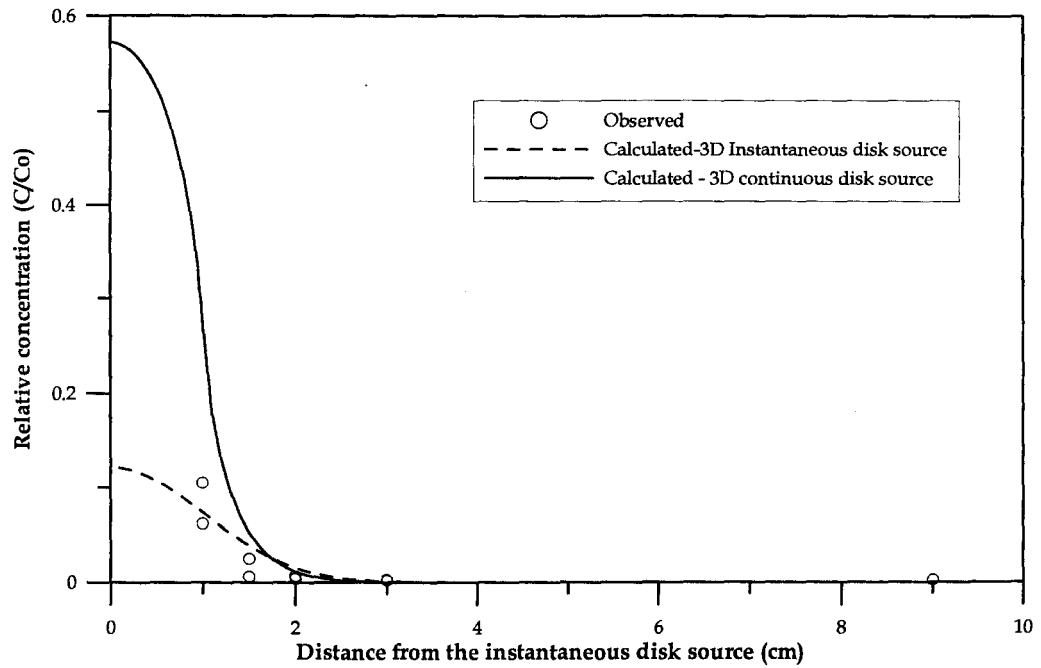


Figure 5.17 Comparison between calculated and observed data at the end of experiment 2 ($t = 10$ hrs 10 min.).

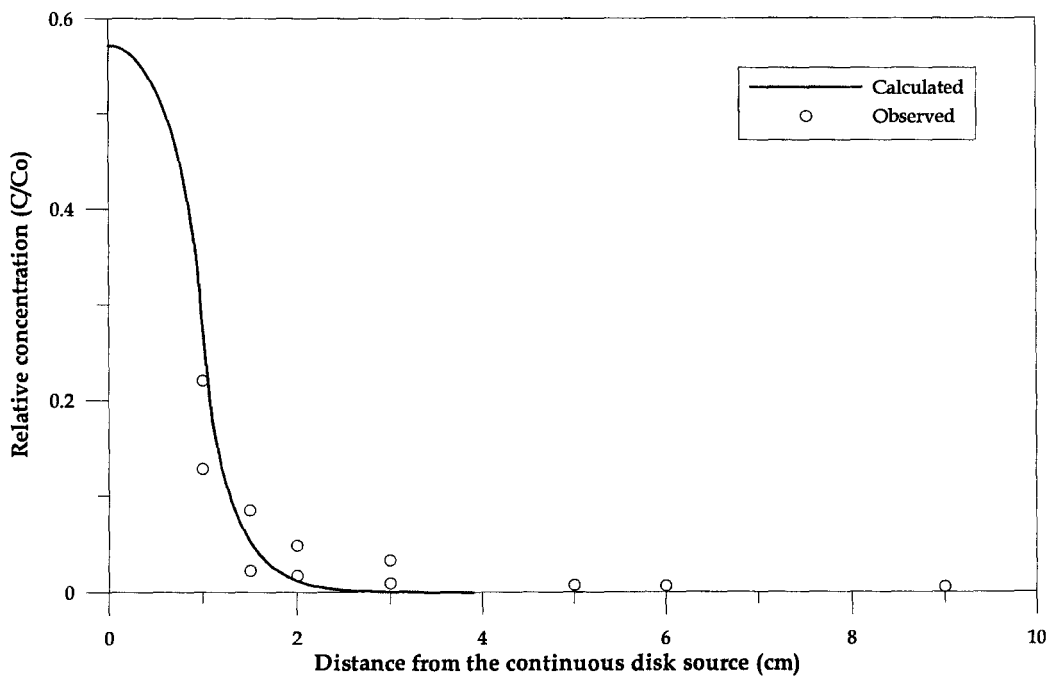


Figure 5.18 Comparison between calculated and observed data at the end of experiment 3 ($t = 10$ hrs 5 min.).

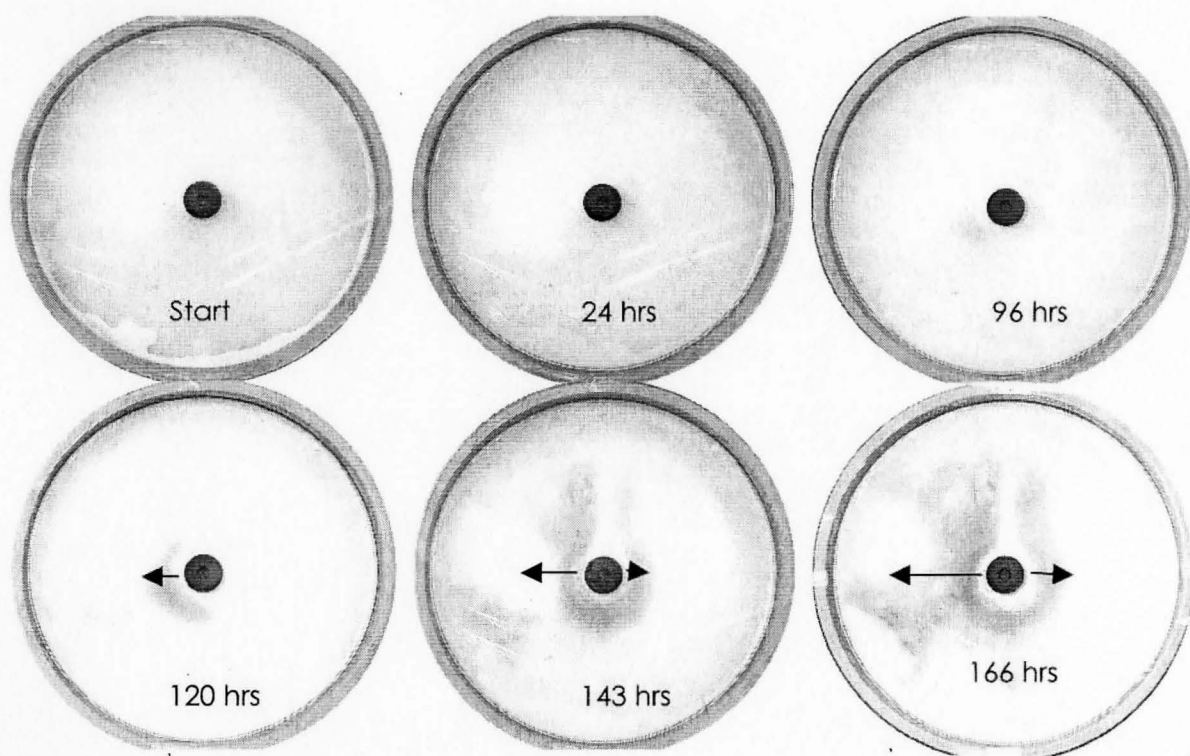


Figure 5.19 Concentration profiles at various experimental times.

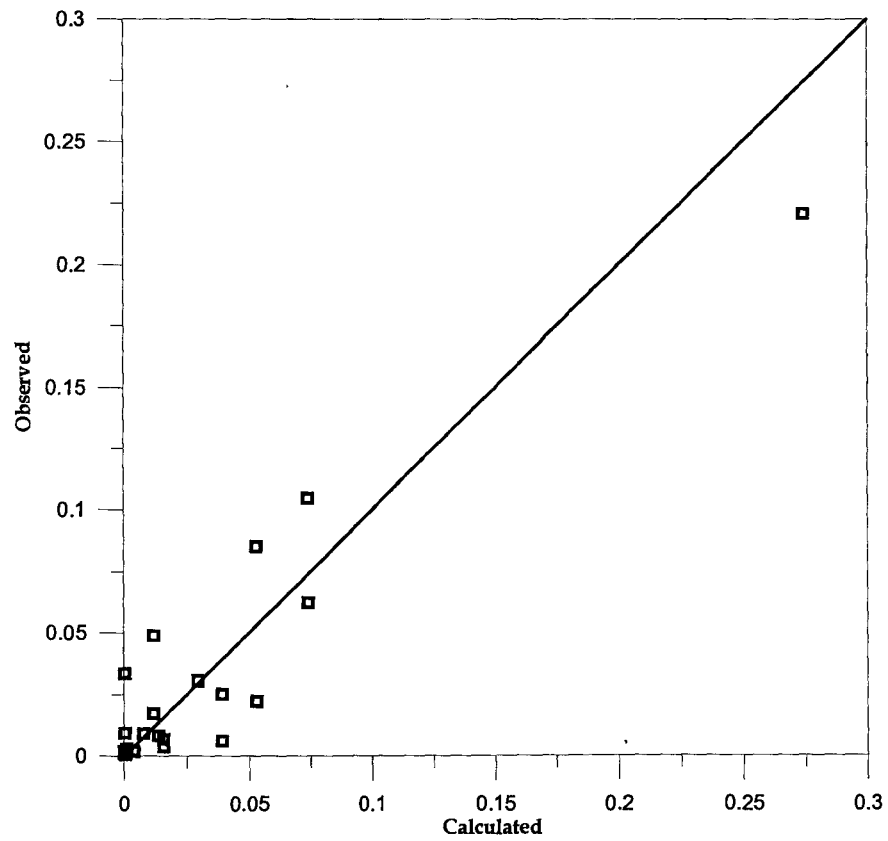


Figure 5.20 Comparison between calculated and observed data for experiment 1, 2 and 3.

Chapter 6: Conclusions

6.1 Achievements of the Present Study

Most of the previous work on matrix diffusion through fractured porous media has been concerned with theoretical approaches. These studies also focused on the understanding of diffusive loss of NAPLs in fractured media through mathematical models, however the mathematical models were verified through physical model experiments. This chapter focuses on the conclusions drawn from this work, and on recommendations for future work.

The results of the simulations of the 2D and 3D instantaneous disk sources, and the 3D continuous disk source indicate the following:

- 1) the 2D approach yields significantly different results from the 3D approach; therefore a 3D modeling approach must be employed to obtain realistic results;
- 2) the rate of n-butanol loss is significantly larger for instantaneous sources than for continuous sources;
- 3) the normalized concentration decreased over time for the instantaneous disk source, while it increased continuously and asymptotically approached 1 for the continuous disk source;
- 4) in both the continuous and instantaneous cases, the diffusion rate decreased over time and space due to the decreasing chemical potential;
- 5) the normalized mass loss from the source zone approached 1 relatively quickly for the instantaneous disk source, however can never reach 1 for the continuous source due to the semi-infinite domain; and

- 6) the sensitivity analysis indicated that disappearance time increased exponentially with increasing disk source radii and matrix porosity, and decreased with increasing aqueous-phase NAPL solubility.

The conclusions derived from the laboratory experiments are:

- 1) the saturation and matrix porosity varied with time and depth, with ranges of .68 - .87 and .36-.42 respectively,
- 2) diffusion rates calculated from visual observation were approximately 30% different from these derived from the model simulations indicating that visual observation is not an accurate method of estimating matrix diffusion.
- 3) the experimental observations matched the model simulations closely for all three physical model experiments in terms of normalized concentration as a function of radial distance at $z = 0$, validating the models at this elevation,
- 4) a plot of the experimental versus simulated data does not reveal any trends, indicating that the majority of the differences can be attributed to experimental error, and
- 5) n-butanol concentrations were not detected at depth, indicating that the duration of the experiments were too short.

6.2 Recommendations for Future Work

- 1) Development of a new approach for packing and saturating the silica flour may simplify the interpretation of the experimental results.
- 2) N-butanol was employed as the NAPL to verify the analytical solutions, which caused difficulty in controlling the source zone at the beginning of each experiment due to the surface. Future experiments should be conducted with a typical DNAPL, which would facilitate the control of the source zone.
- 3) Longer experimental durations, and more sensitive analytical techniques, would enable the verification of the model at depths greater than zero.

7. References

- Abriola, Linda M., and George F. Pinder. (1985) A multiphase approach to the modeling of porous media contamination by organic compounds: 1) Equation development. 2) Numerical Simulation. *Water Resources Research*. Vol. 21. No. 1. pp. 11~26.
- Abriola, Linda. M., Kurt D. Pennell, and Catherine A. Peters. (1995). Persistence and interphase mass transfer of organic contaminants in the unsaturated zone: Experimental observations and mathematical modeling. *Vadose Zone Hydrology : Cutting Across Disciplines*, Kerney Foundation Conference, Davis, CA, 1995
- Abriola, Linda. M., and Avery H. Demond. (1996). The migration and entrapment of DNAPLs in physically and chemically heterogeneous porous media. *Research Plan: U.S Department of Energy* (Grant #DE-FG07-96ER14702)
- Anderson, M.R., R.L. Johnson, and J.F. Pankow. (1992), Dissolution of dense chlorinated solvents into ground water: 1. Dissolution from a well defined residual source. *Ground Water*. V. 30, pp. 250~256
- Baehr, Arthur L., (1987), Selective transport of hydrocarbons in the unsaturated zone due to aqueous and vapour phase partitioning. *Water Resources Research*, 23, No. 10, pp.1926~1938.
- Bear, Jacob, (1972), Dynamics of fluids in porous media, New York; American Elsevier Publishing Company, pp.764
- Bernard H. Kueper and David B. McWhorter, (1992). The behavior of dense, non-aqueous phase liquids in fractured clay and rock, *Ground Water*, Vol. 29, NO. 5, pp. 716-728

- Bernard H. Kueper and David B. McWhorter, (1996). Physics governing the migration of dense non-aqueous phase liquids in fractured media, dense chlorinated solvents, Portland, Oregon: *Waterloo Press.*, 337-352
- Beth L. Parker, Robert W. Gillham, and John A. Cherry, (1994). Diffusive disappearance of immiscible-phase organic liquids in fractured geologic media, *Ground Water*, Vol. 32, No. 5, pp.805-820
- Beth L. Parker, David B. McWhorter, and John A. Cherry, (1997). Diffusive loss of non-aqueous phase organic solvents from idealized fracture networks in geologic media, *Ground Water*, Vol. 35, No. 6, pp.1077-1088
- Buckley, S.E., and M.C. Leverette, (1942), Mechanism of fluid displacement in sand. *Transactions, American Institute of Mining, Metallurgical, and Petroleum Engineering* 146, pp. 107~116
- Carslaw, H.S. and J.C. Jaeger, (1959). Conduction of heat in solids. Second Edition, Clarendon Press, Oxford.
- Cherry, J.A. (1984). Groundwater Contamination. *Mineralogical Association of Canada Short Course in Environmental Geochemistry*. Vol. 10, M.E. Fleet (Ed.), May, 1984, London, Ontario.
- Clausen, J. L., J. Zutman, and N. Farrow. (1993) Characterization of the northwest plume utilizing a driven discrete-depth sampling system. *Report by Martin Marietta Energy Systems Inc. to the US Dept. of Energy*.
- Cohen, R. M., A. P. Bryda, S. T. Shaw, and C. P. Spalding. (1992). Evaluation of visual methods to detect NAPL in soil and water. *Ground Water Monitoring Review*. 12. No, 4. pp. 132~141

- Crank, J., (1956), *The Mathematics of Diffusion*, Oxford University Press
- Cussler, E.L. (1984) *Diffusion, mass transfer in fluid systems*, Cambridge University Press, New York, New York.
- Day, M.J, (1977). *Analysis of movement and hydrochemistry of groundwater in the fractured clay and till deposits of the Winnipeg area*, M/Sc, Thesis, Dept. of Earth Sciences, University of Waterloo, Waterloo, Ontario.
- Doherty, Richard E., (2000). A history of the production and use of carbon tetrachloride, tetrachloroethylene, trichloroethylene and 1,1,1-trichloroethane in the United States: Part 1 - historical background; carbon tetrachloride and tetrachloroethylene, *Journal of Environmental Forensics*, Vol.1, June 2000, pp. 69-81.
- Dullien, F.A.L, (1979). *Porous media : fluid transport and pore structure*, New York : Academic Press, 1979
- Eckberg, David K., and Daniel K. Sunada, (1984), Nonsteady three-phase immiscible fluid distribution in porous media, *Water Resources Research* 20, No. 1, pp.1891-1897
- Feenstra, S. (1984). Groundwater contamination by dense non-aqueous phase liquid chemicals. *Geological Association of Canada, Annual Meeting, May 14~16, 1984*, London, Ontario
- Feenstra, Stan J.A. Cherry, E.A. Sudicky, and Zia Haq, (1984). Matrix diffusion effects on contaminant migration from an injection well in fractured sandstone, *Ground Water*, Vol. 22, No. 3, pp.307-316

- Feenstra, S., Mackay, D.M., and Cherry, J.A., (1991). Presence of residual NAPL based on organic chemical concentrations in soil samples. *Ground Water Monitoring Review II*. No.2. pp.128~136
- Fetter, C.W., (1988). Applied Hydrogeology, 2nd edition, Merrill Publishing Company, Columbus, Ohio
- Fetter, C.W., (1999). Contaminant Hydrogeology, 2nd edition, Prentice Hall, pp 45~47
- Foster, S.S.D. (1975). The chalk groundwater tritium anomaly – A possible explanation. *Journal of Hydrology*. V. 25, pp.159-165
- Grisak G.E. and J.F. Pickens, (1980). Solute transport through fractured media. 1. The effect of matrix diffusion, *Water Resources Research*, Vol. 16, No. 4, pp. 719-730
- Grisak G.E. and J.F. Pickens, (1981), An analytical solution for solute transport through fractured media with matrix diffusion, *Journal of Hydrology*, 52, pp.47-57
- Hunt, J. R., N. Sitar and K. S. Udell. (1988). Nonaqueous phase liquid transport and cleanup. 1. Analysis of mechanisms. *Water Resources Research*, 24. pp. 1247~1259
- James, V.B., (1981). Large time solutions for temperatures in a semi-infinite body with a disk heat source. *Int. J. Heat Mass Transfer*. V. 24. pp.155~164.
- Karickhoff, S.W., D.S. Brown, and T.A. Scott. (1979). Sorption of hydrophobic pollutants on natural sediments. *Water Research*. V. 13, pp.241-248.

- Karickhoff, S.W (1981). Semi-empirical estimation of sorption of hydrophobic pollutants on natural sediments and soils. *Chemosphere*. V. 10, pp. 833~846
- Karickhoff, S.W (1984). Organic pollutant sorption in aquatic systems. *Journal of Hydraulic Engineering*. V. 110, pp. 707~735.
- Kirk-Othmer Encyclopedia of Chemical Technology. John Wiley and Sons, Inc., New York, Vol. V, p. 183, 1964
- Kueper, B.H. and D.B. Mcwhorter. (1991). The behaviour of dense, non-aqueous phase liquids in fractured clay and rock. *Ground Water*. 29, no. 5: 716~728
- Kueper *et al.*, (2003). An illustrated handbook of DNAPL transport and fate in the subsurface
- Mackay, D., W.Y. Shiu, and S. Feenstra. (1991). Dissolution of non-aqueous phase liquids in groundwater. *Journal of Contaminant Hydrology*. V.8, pp. 23~42
- Mackay, D.M., P.V. Roberts, and J. A. Cherry (1993). Transport of organic contaminants in groundwater, *Environ. Sci. Technol.*, 19, 384-392
- Marinelli and Durnford (1996), LNAPL thickness in monitoring wells considering hysteresis and entrapment, *Ground Water*. 34, no. 3:4055-414
- McCall *et al.*, (1959). Physical and Chemical Data, pp. 3-258
- Miller, D. W. (1984). Groundwater Contamination : A Special Report. *American Assoc. for Advancement of Science*. Washington, D.C., pp.25

- Neretnieks, I. (1980). Diffusion in the rock matrix : An important factor in radionuclide retardation , *Journal of Geophysical Research*, v. 85, no. B8, pp. 4379~4397
- Pankow, J.F and J.A. Cherry, (1996), Dense chlorinated solvents and other DNAPLs in groundwater: History, behavior, and remediation, Waterloo Press
- Parker, B.L., R.W. Gillham, and J.A. Cherry. (1994). Diffusive disappearance of immiscible phase organic liquids in fractured geologic media. *Ground Water* 32, no. 5: 805-820.
- Parker *et al.*, 1996, The effects of molecular diffusion on DNAPL behavior in fractured porous media. Pp 355-390
- Parker, B.L., D.B. Mcwhorter, and J.A. Cherry. (1997). Diffusive loss of non-aqueous phase organic solvents from idealized fracture networks in geologic media. *Ground Water* 35, no. 6: 1077~1088.
- Poulson, M.M. and B.H. Kueper. (1992). A field experiment to study the behaviour of tetrachloroethylene in unsaturated porous media. *Environmental Science and Technology*, 26, No.5, pp.889~895
- Reitsma S., and Kueper B. H., (1991). Laboratory measurement of capillary pressure-saturation relationships in a rock fracture. *Water Resources Research*. Vol.30 No.4. pp.865~878
- Rideal, E.K., and Tadayon, (1954). *J., Proc. Roy. Soc.* **225** A, 357
- Rivett, M. O. (1995). Soil-gas signatures from volatile chlorinated solvents: Borden field experiments. *Groundwater*, Vol. 33. pp. 84~98

- Sarah E. Dickson and Neil R. Thomson. (2003). Dissolution of entrapped DNAPLs in variable aperture fractures: Experimental data and empirical model. *Environ. Sci. Technol.*, Vol. 37, No. 18, 4128~4137
- Schneider, G. W and J. P. Greenhouse. (1992). Geophysical detection of PCE in a sandy aquifer using resistivity and nuclear logging techniques. *Proceedings. Society of Engineering and Mineral Exploration Geophysics*, April 26~29, 1992, pp.619~628
- Schwarzenbach, R.P., and J. Westall, (1981). Transport of nonpolar organic compounds from surface water to groundwater: Laboratory sorption studies. *Environmental Science and Technology*. V. 15, pp. 1360~1367.
- Schwille, F. (1984). Migration of organic fluids immiscible with water in the unsaturated zone. Springer-Verlag, Germany.
- Schwille, F. (1988). Dense chlorinated solvents in porous and fracture media – model experiment. Translated by James F. Pankow. Lewis Publishers, Chelsea, MI. pp. 146.
- Shripad J. Gokhale, Joel L, and Peter C. Wayner Jr. (2003). Experimental investigation of contact angle, curvature, and contact line motion in dropwise condensation and evaporation. *Journal of Colloid and Interface Science*, 259, pp354~366.
- Silliman S. E., Berkowitz B., Simunek J., and Genuchten M. Th. (2001). Fluid flow and solute migration within the capillary fringe. *Ground Water*. Vol. 40, No.1, pp.76~84
- Smith J. E., and Gillham R. W., (1999). Effects of solute concentration-dependent surface tension on unsaturated flow: Laboratory sand column experiments. *Water Resources Research*. Vol. 35 No. 4 pp.973~982

Thomas, P.H., (1957). Some conduction problems in the heating of small areas on large solids. *Q. J. Mech. Appl. Math.* 10, pp.482~493

United States International Trade Commission (1991). Synthetic Organic Chemicals: United States Production and Sales, USITC Publication 2470, Washington, D.C.

Unpublished preliminary report issued by the National Cancer Institute, Bethesda, Maryland 1975.

Young, C.P., Oakes, D.B, and Wilkinson, W.B., (1976). Prediction of future concentrations in groundwater, *Ground Water*, 14; pp. 426~438

Appendix I : Fortran and Maple Code for calculations of the diffusion

• Program (2D – Instantaneous Disk Source): Equation 3-14f

```

double precision t0,c,de,c0,a,t,r1,s1,s2,s3,s4,s5,s6,s7,s8
Open(11,file="2D-Diffusion.dat")
De=0.96*10E-06
C0=63200.0
a=1.0
pi=3.141592654
R1=1.0
do 101 i=3600,4320000,3600
t=real(i)
day=t/86400.
Do 102 j=100,1,-1
r=real(j)*0.01

s5 = -0.13813511810472D-24*exp(-0.25D0*R1/De/t)*r**20*R1**20*De**4
#*t**4-0.624999999920351D-1*exp(-0.25D0*R1/De/t)*r**4*R1**2*De**22
#*t**22-0.941830350714D-25*exp(-0.25D0*R1/De/t)*r**24*R1**20*De**4*
#t**4-0.6055075024483637D-8*exp(-0.25D0*R1/De/t)*r**14*R1**8*De**16
#*t**16-0.4277458914802414D-17*exp(-0.25D0*R1/De/t)*r**20*R1**15*De
#*t**9-0.8554917832141746D-16*exp(-0.25D0*R1/De/t)*r**20*R1**14*
#De**10*t**10

s4 = s5-0.5518948590027452D-11*exp(-0.25D0*R1/De/t)*r**12*R1**11*D
#e**13*t**13-0.221016188967552D-21*exp(-0.25D0*R1/De/t)*r**18*R1**1
#8*De**6*t**6-0.313943450238D-26*exp(-0.25D0*R1/De/t)*r**22*R1**21*
#De**3*t**3-0.2986444042563099D-14*exp(-0.25D0*R1/De/t)*r**22*R1**1
#2*De**12*t**12-0.4050623972350771D-20*exp(-0.25D0*R1/De/t)*r**22*R
#1**17*De**7*t**7+0.5000000000189973D0*r**2*R1*De**23*t**23+0.24220
#30010047147D-7*r**14*R1**7*De**17*t**17

s3 = s4+0.756884377981176D-9*r**16*R1**8*De**16*t**16+0.6249999999
#920351D-1*r**4*R1**2*De**22*t**22+0.5208333333584074D-2*r**6*R1**3
#*De**21*t**21+0.3255208333569325D-3*r**8*R1**4*De**20*t**20+0.1627
#604166467548D-4*r**10*R1**5*De**19*t**19+0.6781684024834019D-6*r**
#12*R1**6*De**18*t**18+0.2102456605573737D-10*r**18*R1**9*De**15*t
**15+0.5256141514251456D-12*r**20*R1**10*De**14*t**14+0.11945776166
#44702D-13*r**22*R1**11*De**13*t**13+0.2488703368485468D-15*r**24*R
#1**12*De**12*t**12-0.199999999949143D1*exp(-0.25D0*R1/De/t)*De**2
#4*t**24-0.3096822228515625D-31*exp(-0.25D0*R1/De/t)*r**24*R1**24-0
#.2864369809019474D-18*exp(-0.25D0*R1/De/t)*r**16*R1**16*De**8*t**8

s5 = -0.2649095323568345D-8*exp(-0.25D0*R1/De/t)*r**10*R1**9*De**1
#5*t**15-0.2299561912564291D-12*exp(-0.25D0*R1/De/t)*r**12*R1**12*D

```

```

#e**12*t**12-0.2422030010047147D-7*exp(-0.25D0*R1/De/t)*r**14*R1**7
#*De**17*t**17-0.1971053068002853D-11*exp(-0.25D0*R1/De/t)*r**16*R1
***11*De**13*t**13-0.9165983388862317D-17*exp(-0.25D0*R1/De/t)*r**1
#6*R1**15*De**9*t**9-0.171098356579412D-15*exp(-0.25D0*R1/De/t)*r**
#18*R1**14*De**10*t**10
s4 = s5-0.7956582802831872D-20*exp(-0.25D0*R1/De/t)*r**18*R1**17*D
#e**7*t**7-0.1103789718259182D-9*exp(-0.25D0*R1/De/t)*r**12*R1**10*
#De**14*t**14-0.6307369817355439D-10*exp(-0.25D0*R1/De/t)*r**14*R1*
**10*De**14*t**14-0.14864746696875D-29*exp(-0.25D0*R1/De/t)*r**24*R
#1**23*De*t-0.2933114684309095D-15*exp(-0.25D0*R1/De/t)*r**14*R1**1
#4*De**10*t**10-0.6159540837112523D-14*exp(-0.25D0*R1/De/t)*r**16*R
#1**13*De**11*t**11-0.1971053068002853D-12*exp(-0.25D0*R1/De/t)*r**
#14*R1**12*De**12*t**12
s5 = s4-0.8212721114035934D-14*exp(-0.25D0*R1/De/t)*r**14*R1**13*D
#e**11*t**11-0.1642544223441416D-13*exp(-0.25D0*R1/De/t)*r**20*R1**
#12*De**12*t**12-0.2119276258474139D-7*exp(-0.25D0*R1/De/t)*r**12*R
#1**8*De**16*t**16-0.2025311986175386D-20*exp(-0.25D0*R1/De/t)*r**2
#4*R1**17*De**7*t**7-0.1368786852762142D-14*exp(-0.25D0*R1/De/t)*r*
**20*R1**13*De**11*t**11-0.1194577616644702D-13*exp(-0.25D0*R1/De/t
#)*r**22*R1**11*De**13*t**13
s2 = s5-0.1627604166467548D-3*exp(-0.25D0*R1/De/t)*r**6*R1**5*De**
#19*t**19+0.1999999999949143D1*De**24*t**24-0.4069010416803099D-5*e
#xp(-0.25D0*R1/De/t)*r**10*R1**6*De**18*t**18-0.5208333333584074D-2
**exp(-0.25D0*R1/De/t)*r**6*R1**3*De**21*t**21-0.1356336805601033D-
#4*exp(-0.25D0*R1/De/t)*r**6*R1**6*De**18*t**18-0.1302083333554576D
#-2*exp(-0.25D0*R1/De/t)*r**6*R1**4*De**20*t**20-0.1627604166467548
#D-4*exp(-0.25D0*R1/De/t)*r**10*R1**5*De**19*t**19+s3
s5 = -0.5086263020845316D-6*exp(-0.25D0*R1/De/t)*r**10*R1**7*De**1
#7*t**17-0.8138020832337739D-4*exp(-0.25D0*R1/De/t)*r**8*R1**5*De**
#19*t**19-0.5475147411048567D-13*exp(-0.25D0*R1/De/t)*r**18*R1**12*
#De**12*t**12-0.5256141514251456D-11*exp(-0.25D0*R1/De/t)*r**18*R1*
**10*De**14*t**14-0.8477105032628096D-6*exp(-0.25D0*R1/De/t)*r**8*R
#1**7*De**17*t**17-0.1017252604042217D-4*exp(-0.25D0*R1/De/t)*r**8*
#R1**6*De**18*t**18
s4 = s5-0.1562500000138645D-1*exp(-0.25D0*R1/De/t)*r**4*R1**3*De**
#21*t**21-0.6570176891228747D-12*exp(-0.25D0*R1/De/t)*r**18*R1**11*
#De**13*t**13-0.5298190646502461D-7*exp(-0.25D0*R1/De/t)*r**8*R1**8
**De**16*t**16-0.342196713158824D-14*exp(-0.25D0*R1/De/t)*r**18*R1*
**13*De**11*t**11-0.1953125000014749D-2*exp(-0.25D0*R1/De/t)*r**4*R
#1**4*De**20*t**20-0.3255208333569325D-3*exp(-0.25D0*R1/De/t)*r**8*
#R1**4*De**20*t**20-0.756884377981176D-9*exp(-0.25D0*R1/De/t)*r**16
#*R1**8*De**16*t**16
s5 = s4-0.7129098191337357D-17*exp(-0.25D0*R1/De/t)*r**18*R1**15*D
#e**9*t**9-0.1231908167422505D-12*exp(-0.25D0*R1/De/t)*r**16*R1**12

```

```

#*De**12*t**12-0.2365263681349732D-10*exp(-0.25D0*R1/De/t)*r**16*R1
#**10*De**14*t**14-0.189221094495294D-9*exp(-0.25D0*R1/De/t)*r**16*
#R1**9*De**15*t**15-0.1324547661784173D-9*exp(-0.25D0*R1/De/t)*r**1
#0*R1**10*De**14*t**14-0.2546106496906199D-18*exp(-0.25D0*R1/De/t)*
#r**18*R1**16*De**8*t**8
s3 = s5-0.1695421007159848D-6*exp(-0.25D0*R1/De/t)*r**12*R1**7*De*
#*17*t**17-0.2566475349008294D-15*exp(-0.25D0*R1/De/t)*r**16*R1**14
#*De**10*t**10-0.261619541865D-26*exp(-0.25D0*R1/De/t)*r**24*R1**21
#*De**3*t**3-0.843879994239744D-22*exp(-0.25D0*R1/De/t)*r**24*R1**1
#8*De**6*t**6-0.7777198026913481D-17*exp(-0.25D0*R1/De/t)*r**24*R1*
#*14*De**10*t**10-0.6540488546625D-28*exp(-0.25D0*R1/De/t)*r**24*R1
#**22*De**2*t**2-0.45207856834272D-23*exp(-0.25D0*R1/De/t)*r**22*R1
#**19*De**5*t**5
s5 = -0.55254047241888D-23*exp(-0.25D0*R1/De/t)*r**20*R1**19*De**5
#*t**5-0.194429950672837D-17*exp(-0.25D0*R1/De/t)*r**22*R1**15*De**
#9*t**9-0.4238552517582506D-7*exp(-0.25D0*R1/De/t)*r**10*R1**8*De**
#16*t**16-0.5256141514251456D-12*exp(-0.25D0*R1/De/t)*r**20*R1**10*
#De**14*t**14-0.500000000189973D0*exp(-0.25D0*R1/De/t)*r**2*R1*De*
#*23*t**23-0.71350784145D-28*exp(-0.25D0*R1/De/t)*r**22*R1**22*De**
#2*t**2-0.1314035378879979D-12*exp(-0.25D0*R1/De/t)*r**20*R1**11*De
#**13*t**13
s4 = s5-0.6365266242265498D-20*exp(-0.25D0*R1/De/t)*r**20*R1**17*D
#e**7*t**7-0.2102456605573737D-10*exp(-0.25D0*R1/De/t)*r**18*R1**9*
#De**15*t**15-0.1989145700707968D-21*exp(-0.25D0*R1/De/t)*r**20*R1*
#*18*De**6*t**6-0.9721497533641851D-19*exp(-0.25D0*R1/De/t)*r**22*R
#1**16*De**8*t**8-0.3110879210765392D-16*exp(-0.25D0*R1/De/t)*r**22
#*R1**14*De**10*t**10-0.30138571222848D-23*exp(-0.25D0*R1/De/t)*r**
#24*R1**19*De**5*t**5-0.3733055053045317D-15*exp(-0.25D0*R1/De/t)*r
#**22*R1**13*De**11*t**11
s5 = s4-0.1446651418696704D-21*exp(-0.25D0*R1/De/t)*r**22*R1**18*D
#e**6*t**6-0.2488703368485468D-15*exp(-0.25D0*R1/De/t)*r**24*R1**12
#*De**12*t**12-0.1782274547834339D-18*exp(-0.25D0*R1/De/t)*r**20*R1
#**16*De**8*t**8-0.1766063548834154D-8*exp(-0.25D0*R1/De/t)*r**12*R
#1**9*De**15*t**15-0.6480998355761234D-18*exp(-0.25D0*R1/De/t)*r**2
#4*R1**15*De**9*t**9-0.1255773800952D-24*exp(-0.25D0*R1/De/t)*r**22
#*R1**20*De**4*t**4
s1 = s5-0.4050623972350771D-19*exp(-0.25D0*R1/De/t)*r**24*R1**16*D
#e**8*t**8-0.6781684024834019D-6*exp(-0.25D0*R1/De/t)*r**12*R1**6*D
#e**18*t**18+s3-0.756884377981176D-9*exp(-0.25D0*R1/De/t)*r**14*R1*
#*9*De**15*t**15-0.6221758421530785D-16*exp(-0.25D0*R1/De/t)*r**24*
#R1**13*De**11*t**11-0.3942106136005707D-11*exp(-0.25D0*R1/De/t)*r*
#*14*R1**11*De**13*t**13+s2-0.1249999999730379D0*exp(-0.25D0*R1/De/
#t)*r**2*R1**2*De**22*t**22
s2 = 1/De**23/t**23/R1

```

```

t0 = s1*s2
C=C0/(2.*De*t)*exp(-r**2/(4.*De*t))*t0
C1=C0*(1.-exp(-a**2*R/(4.*De*t)))
write(11,201)day,c,c1,q4,q5

102 continue
101 continue
201 format(f25.10,5x,f25.10,5x,f25.10,5x,f25.10,5x,f25.10)
stop
end

```

• Program (2D – Instantaneous Disk Source) : Equation 3-17

```

fd1 :=fopen("Equation3-17.dat",WRITE);
C0:=63200.;
De:=0.96*10E-06;
a:=1.0;
t:=3600.0;
R1:=1.0;

for r from 0.1 by 0.1 to 2.0 do
f1:=evalf(int(Bessell(0,u*a)*Bessell(1,u*r)*(exp(-(De*t*x^2)/(R1)),x=0..infinity);
c1:=a*C0*f1;
c2:=c1/C0;
fprintf(fd1,"%f    %f    %f    %f\n",t,r,c1,c2);
end do;
fclose(fd1);

```

• Program (2D – Instantaneous Disk Source – Q(t)) : Equation 3-16c

```

double precision t0,c,de,c0,a,t,r1,s1,s2,s3,s4,s5,s6,s7,s8
Open(11,file="2D-fig-4-7N.dat")
De=0.96*10E-06
C0=63200.0
a=1.0
Q=198548.656
pi=3.141592654
R1=1.0
do 101 i=3600,4320000,3600
t=real(i)

```

```
day=t/86400.
```

```
q20=0.0
```

```
c2=0.0
```

```
Do 102 j=100,1,-1
```

```
r=real(j)*0.01
```

```
s5 = -0.13813511810472D-24*exp(-0.25D0*R1/De/t)*r**20*R1**20*De**4
#t**4-0.624999999920351D-1*exp(-0.25D0*R1/De/t)*r**4*R1**2*De**22
#t**22-0.941830350714D-25*exp(-0.25D0*R1/De/t)*r**24*R1**20*De**4*
#t**4-0.6055075024483637D-8*exp(-0.25D0*R1/De/t)*r**14*R1**8*De**16
#t**16-0.4277458914802414D-17*exp(-0.25D0*R1/De/t)*r**20*R1**15*De
#t**9*t**9-0.8554917832141746D-16*exp(-0.25D0*R1/De/t)*r**20*R1**14*
#De**10*t**10
```

```
s4 = s5-0.5518948590027452D-11*exp(-0.25D0*R1/De/t)*r**12*R1**11*D
#e**13*t**13-0.221016188967552D-21*exp(-0.25D0*R1/De/t)*r**18*R1**1
#8*De**6*t**6-0.313943450238D-26*exp(-0.25D0*R1/De/t)*r**22*R1**21*
#De**3*t**3-0.2986444042563099D-14*exp(-0.25D0*R1/De/t)*r**22*R1**1
#2*De**12*t**12-0.4050623972350771D-20*exp(-0.25D0*R1/De/t)*r**22*R
#1**17*De**7*t**7+0.500000000189973D0*r**2*R1*De**23*t**23+0.24220
#30010047147D-7*r**14*R1**7*De**17*t**17
```

```
s3 = s4+0.756884377981176D-9*r**16*R1**8*De**16*t**16+0.6249999999
#920351D-1*r**4*R1**2*De**22*t**22+0.5208333333584074D-2*r**6*R1**3
#*De**21*t**21+0.3255208333569325D-3*r**8*R1**4*De**20*t**20+0.1627
#604166467548D-4*r**10*R1**5*De**19*t**19+0.6781684024834019D-6*r**
#12*R1**6*De**18*t**18+0.2102456605573737D-10*r**18*R1**9*De**15*t**
#15+0.5256141514251456D-12*r**20*R1**10*De**14*t**14+0.11945776166
#44702D-13*r**22*R1**11*De**13*t**13+0.2488703368485468D-15*r**24*R
#1**12*De**12*t**12-0.199999999949143D1*exp(-0.25D0*R1/De/t)*De**2
#4*t**24-0.3096822228515625D-31*exp(-0.25D0*R1/De/t)*r**24*R1**24-0
#.2864369809019474D-18*exp(-0.25D0*R1/De/t)*r**16*R1**16*De**8*t**8
```

```
s5 = -0.2649095323568345D-8*exp(-0.25D0*R1/De/t)*r**10*R1**9*De**1
#5*t**15-0.2299561912564291D-12*exp(-0.25D0*R1/De/t)*r**12*R1**12*D
#e**12*t**12-0.2422030010047147D-7*exp(-0.25D0*R1/De/t)*r**14*R1**7
#*De**17*t**17-0.1971053068002853D-11*exp(-0.25D0*R1/De/t)*r**16*R1
#t**11*De**13*t**13-0.9165983388862317D-17*exp(-0.25D0*R1/De/t)*r**1
#6*R1**15*De**9*t**9-0.171098356579412D-15*exp(-0.25D0*R1/De/t)*r**
#18*R1**14*De**10*t**10
```

```
s4 = s5-0.7956582802831872D-20*exp(-0.25D0*R1/De/t)*r**18*R1**17*D
#e**7*t**7-0.1103789718259182D-9*exp(-0.25D0*R1/De/t)*r**12*R1**10*
#De**14*t**14-0.6307369817355439D-10*exp(-0.25D0*R1/De/t)*r**14*R1*
#t**10*De**14*t**14-0.14864746696875D-29*exp(-0.25D0*R1/De/t)*r**24*R
#1**23*De**t-0.2933114684309095D-15*exp(-0.25D0*R1/De/t)*r**14*R1**1
#4*De**10*t**10-0.6159540837112523D-14*exp(-0.25D0*R1/De/t)*r**16*R
```

```

#1**13*De**11*t**11-0.1971053068002853D-12*exp(-0.25D0*R1/De/t)*r**
#14*R1**12*De**12*t**12
s5 = s4-0.8212721114035934D-14*exp(-0.25D0*R1/De/t)*r**14*R1**13*D
#e**11*t**11-0.1642544223441416D-13*exp(-0.25D0*R1/De/t)*r**20*R1**
#12*De**12*t**12-0.2119276258474139D-7*exp(-0.25D0*R1/De/t)*r**12*R
#1**8*De**16*t**16-0.2025311986175386D-20*exp(-0.25D0*R1/De/t)*r**2
#4*R1**17*De**7*t**7-0.1368786852762142D-14*exp(-0.25D0*R1/De/t)*r**
#*20*R1**13*De**11*t**11-0.1194577616644702D-13*exp(-0.25D0*R1/De/t
#)*r**22*R1**11*De**13*t**13
s2 = s5-0.1627604166467548D-3*exp(-0.25D0*R1/De/t)*r**6*R1**5*De**
#19*t**19+0.1999999999949143D1*De**24*t**24-0.4069010416803099D-5*e
#xp(-0.25D0*R1/De/t)*r**10*R1**6*De**18*t**18-0.5208333333584074D-2
#*exp(-0.25D0*R1/De/t)*r**6*R1**3*De**21*t**21-0.1356336805601033D-
#4*exp(-0.25D0*R1/De/t)*r**6*R1**6*De**18*t**18-0.1302083333554576D
#-2*exp(-0.25D0*R1/De/t)*r**6*R1**4*De**20*t**20-0.1627604166467548
#D-4*exp(-0.25D0*R1/De/t)*r**10*R1**5*De**19*t**19+s3
s5 = -0.5086263020845316D-6*exp(-0.25D0*R1/De/t)*r**10*R1**7*De**1
#7*t**17-0.8138020832337739D-4*exp(-0.25D0*R1/De/t)*r**8*R1**5*De**
#19*t**19-0.5475147411048567D-13*exp(-0.25D0*R1/De/t)*r**18*R1**12*
#De**12*t**12-0.5256141514251456D-11*exp(-0.25D0*R1/De/t)*r**18*R1*
#*10*De**14*t**14-0.8477105032628096D-6*exp(-0.25D0*R1/De/t)*r**8*R
#1**7*De**17*t**17-0.1017252604042217D-4*exp(-0.25D0*R1/De/t)*r**8*
#R1**6*De**18*t**18
s4 = s5-0.1562500000138645D-1*exp(-0.25D0*R1/De/t)*r**4*R1**3*De**
#21*t**21-0.6570176891228747D-12*exp(-0.25D0*R1/De/t)*r**18*R1**11*
#De**13*t**13-0.5298190646502461D-7*exp(-0.25D0*R1/De/t)*r**8*R1**8
#*De**16*t**16-0.342196713158824D-14*exp(-0.25D0*R1/De/t)*r**18*R1*
#*13*De**11*t**11-0.1953125000014749D-2*exp(-0.25D0*R1/De/t)*r**4*R
#1**4*De**20*t**20-0.3255208333569325D-3*exp(-0.25D0*R1/De/t)*r**8*
#R1**4*De**20*t**20-0.756884377981176D-9*exp(-0.25D0*R1/De/t)*r**16
#*R1**8*De**16*t**16
s5 = s4-0.7129098191337357D-17*exp(-0.25D0*R1/De/t)*r**18*R1**15*D
#e**9*t**9-0.1231908167422505D-12*exp(-0.25D0*R1/De/t)*r**16*R1**12
#*De**12*t**12-0.2365263681349732D-10*exp(-0.25D0*R1/De/t)*r**16*R1
#**10*De**14*t**14-0.189221094495294D-9*exp(-0.25D0*R1/De/t)*r**16*
#R1**9*De**15*t**15-0.1324547661784173D-9*exp(-0.25D0*R1/De/t)*r**1
#0*R1**10*De**14*t**14-0.2546106496906199D-18*exp(-0.25D0*R1/De/t)*
#r**18*R1**16*De**8*t**8
s3 = s5-0.1695421007159848D-6*exp(-0.25D0*R1/De/t)*r**12*R1**7*De*
#*17*t**17-0.2566475349008294D-15*exp(-0.25D0*R1/De/t)*r**16*R1**14
#*De**10*t**10-0.261619541865D-26*exp(-0.25D0*R1/De/t)*r**24*R1**21
#*De**3*t**3-0.843879994239744D-22*exp(-0.25D0*R1/De/t)*r**24*R1**1
#8*De**6*t**6-0.7777198026913481D-17*exp(-0.25D0*R1/De/t)*r**24*R1*
#*14*De**10*t**10-0.6540488546625D-28*exp(-0.25D0*R1/De/t)*r**24*R1

```

```

***22*De**2*t**2-0.45207856834272D-23*exp(-0.25D0*R1/De/t)*r**22*R1
***19*De**5*t**5
s5 = -0.55254047241888D-23*exp(-0.25D0*R1/De/t)*r**20*R1**19*De**5
#*t**5-0.194429950672837D-17*exp(-0.25D0*R1/De/t)*r**22*R1**15*De**
#9*t**9-0.4238552517582506D-7*exp(-0.25D0*R1/De/t)*r**10*R1**8*De**
#16*t**16-0.5256141514251456D-12*exp(-0.25D0*R1/De/t)*r**20*R1**10*
#De**14*t**14-0.5000000000189973D0*exp(-0.25D0*R1/De/t)*r**2*R1*De*
#*23*t**23-0.71350784145D-28*exp(-0.25D0*R1/De/t)*r**22*R1**22*De**
#2*t**2-0.1314035378879979D-12*exp(-0.25D0*R1/De/t)*r**20*R1**11*De
***13*t**13
s4 = s5-0.6365266242265498D-20*exp(-0.25D0*R1/De/t)*r**20*R1**17*D
#e**7*t**7-0.2102456605573737D-10*exp(-0.25D0*R1/De/t)*r**18*R1**9*
#De**15*t**15-0.1989145700707968D-21*exp(-0.25D0*R1/De/t)*r**20*R1*
#*18*De**6*t**6-0.9721497533641851D-19*exp(-0.25D0*R1/De/t)*r**22*R
#1**16*De**8*t**8-0.3110879210765392D-16*exp(-0.25D0*R1/De/t)*r**22
#*R1**14*De**10*t**10-0.30138571222848D-23*exp(-0.25D0*R1/De/t)*r**
#24*R1**19*De**5*t**5-0.3733055053045317D-15*exp(-0.25D0*R1/De/t)*r
***22*R1**13*De**11*t**11
s5 = s4-0.1446651418696704D-21*exp(-0.25D0*R1/De/t)*r**22*R1**18*D
#e**6*t**6-0.2488703368485468D-15*exp(-0.25D0*R1/De/t)*r**24*R1**12
#*De**12*t**12-0.1782274547834339D-18*exp(-0.25D0*R1/De/t)*r**20*R1
***16*De**8*t**8-0.1766063548834154D-8*exp(-0.25D0*R1/De/t)*r**12*R
#1**9*De**15*t**15-0.6480998355761234D-18*exp(-0.25D0*R1/De/t)*r**2
#4*R1**15*De**9*t**9-0.1255773800952D-24*exp(-0.25D0*R1/De/t)*r**22
#*R1**20*De**4*t**4
s1 = s5-0.4050623972350771D-19*exp(-0.25D0*R1/De/t)*r**24*R1**16*D
#e**8*t**8-0.6781684024834019D-6*exp(-0.25D0*R1/De/t)*r**12*R1**6*D
#e**18*t**18+s3-0.756884377981176D-9*exp(-0.25D0*R1/De/t)*r**14*R1*
#*9*De**15*t**15-0.6221758421530785D-16*exp(-0.25D0*R1/De/t)*r**24*
#R1**13*De**11*t**11-0.3942106136005707D-11*exp(-0.25D0*R1/De/t)*r**
#*14*R1**11*De**13*t**13+s2-0.1249999999730379D0*exp(-0.25D0*R1/De/
#t)*r**2*R1**2*De**22*t**22
s2 = 1/De**23/t**23/R1
t0 = s1*s2

C=C0/(2.*De*t)*exp(-r**2/(4.*De*t))*t0
C1=C0*(1.-exp(-a**2*R/(4.*De*t)))

if (r .eq. 1.) then
q10=pi*c
c2=c
go to 999
endif

```



```

if (r .eq. 0.01) then
  q30=pi*(0.01**2)*(c1-c)
  go to 1000
endif

q1=pi*((r)**2)*(c-c2)
q20=q20+q1
c2=c
1000 write(*,*) "r equal to 0.01"
if(r .eq. 0.01)then
  q3=q10+q20+q30
  q4=Q-q3
  q5=1-q3/Q
  write(11,201)day,c,q3,q4,q5
endif
999 write(*,*) "r equal to 1"
102 continue
101 continue
201 format(f25.10,5x,f25.10,5x,f25.10,5x,f25.10,5x,f25.10)
stop
end

```

• Program (2D – Instantaneous Disk Source – Q(t)) : Equation 3-18a

```

fd1 :=fopen("D:\MSthesis\Program\Maple\Equation2-16-Q-Value.dat",WRITE);
C0:=63200;
De:=0.96*10E-06;
a:=1.0;
R1:=1.0;
pi:=3.141592654;
Q:=198548.656;
for t from 300 by 300 to 86400 do
f0:=evalf(int((BesselJ(1,a*u)^2/u)*exp(-De*t*u**2/R1),u=0..infinity));
f1:=2.*pi*a^2*C0*f0;
q1:=1-((Q-f1)/Q);
o1:=1-f1/Q;
day:=t/86400.;
fprintf(fd1,"%f      %f      %f      %fn",day,f1,q1,o1);
end do;

```

• Program (3D – Instantaneous Disk Source) : Equation 3-20

```

double precision t0,c,de,c0,a,t,r1,s1,s2,s3,s4,s5,s6,s7,s8
Open(11,file="3DI-Equation3-20.dat")
De=0.96*10E-06
pi=3.141592654
C0=63200.0
a=1.0
z=0.0
R1=1.0
q=(pi*a**2*C0)/(2*pi*a)

Do I = 86400, 2592000, 86400
day=t/86400.

Do 102 j=1,50
r=real(j)*0.1

s5 = -0.13813511810472D-24*exp(-0.25D0*R1/De/t)*r**20*R1**20*De**4
**t**4-0.6249999999920351D-1*exp(-0.25D0*R1/De/t)*r**4*R1**2*De**22
**t**22-0.941830350714D-25*exp(-0.25D0*R1/De/t)*r**24*R1**20*De**4*
**t**4-0.6055075024483637D-8*exp(-0.25D0*R1/De/t)*r**14*R1**8*De**16
**t**16-0.4277458914802414D-17*exp(-0.25D0*R1/De/t)*r**20*R1**15*De
**9*t**9-0.8554917832141746D-16*exp(-0.25D0*R1/De/t)*r**20*R1**14*
#De**10*t**10
s4 = s5-0.5518948590027452D-11*exp(-0.25D0*R1/De/t)*r**12*R1**11*D
#e**13*t**13-0.221016188967552D-21*exp(-0.25D0*R1/De/t)*r**18*R1**1
#8*De**6*t**6-0.313943450238D-26*exp(-0.25D0*R1/De/t)*r**22*R1**21*
#De**3*t**3-0.2986444042563099D-14*exp(-0.25D0*R1/De/t)*r**22*R1**1
#2*De**12*t**12-0.4050623972350771D-20*exp(-0.25D0*R1/De/t)*r**22*R
#1**17*De**7*t**7+0.5000000000189973D0*r**2*R1*De**23*t**23+0.24220
#30010047147D-7*r**14*R1**7*De**17*t**17
s3 = s4+0.756884377981176D-9*r**16*R1**8*De**16*t**16+0.6249999999
#920351D-1*r**4*R1**2*De**22*t**22+0.5208333333584074D-2*r**6*R1**3
#*De**21*t**21+0.3255208333569325D-3*r**8*R1**4*De**20*t**20+0.1627
#604166467548D-4*r**10*R1**5*De**19*t**19+0.6781684024834019D-6*r**
#12*R1**6*De**18*t**18+0.2102456605573737D-10*r**18*R1**9*De**15*t
**15+0.5256141514251456D-12*r**20*R1**10*De**14*t**14+0.11945776166
#44702D-13*r**22*R1**11*De**13*t**13+0.2488703368485468D-15*r**24*R
#1**12*De**12*t**12-0.1999999999949143D1*exp(-0.25D0*R1/De/t)*De**2
#4*t**24-0.3096822228515625D-31*exp(-0.25D0*R1/De/t)*r**24*R1**24-0
#2864369809019474D-18*exp(-0.25D0*R1/De/t)*r**16*R1**16*De**8*t**8
s5 = -0.2649095323568345D-8*exp(-0.25D0*R1/De/t)*r**10*R1**9*De**1
#5*t**15-0.2299561912564291D-12*exp(-0.25D0*R1/De/t)*r**12*R1**12*D

```

```

#e**12*t**12-0.2422030010047147D-7*exp(-0.25D0*R1/De/t)*r**14*R1**7
#De**17*t**17-0.1971053068002853D-11*exp(-0.25D0*R1/De/t)*r**16*R1
**11*De**13*t**13-0.9165983388862317D-17*exp(-0.25D0*R1/De/t)*r**1
#6*R1**15*De**9*t**9-0.171098356579412D-15*exp(-0.25D0*R1/De/t)*r**
#18*R1**14*De**10*t**10
s4 = s5-0.7956582802831872D-20*exp(-0.25D0*R1/De/t)*r**18*R1**17*D
#e**7*t**7-0.1103789718259182D-9*exp(-0.25D0*R1/De/t)*r**12*R1**10*
#De**14*t**14-0.6307369817355439D-10*exp(-0.25D0*R1/De/t)*r**14*R1*
**10*De**14*t**14-0.14864746696875D-29*exp(-0.25D0*R1/De/t)*r**24*R
#1**23*De*t-0.2933114684309095D-15*exp(-0.25D0*R1/De/t)*r**14*R1**1
#4*De**10*t**10-0.6159540837112523D-14*exp(-0.25D0*R1/De/t)*r**16*R
#1**13*De**11*t**11-0.1971053068002853D-12*exp(-0.25D0*R1/De/t)*r**
#14*R1**12*De**12*t**12
s5 = s4-0.8212721114035934D-14*exp(-0.25D0*R1/De/t)*r**14*R1**13*D
#e**11*t**11-0.1642544223441416D-13*exp(-0.25D0*R1/De/t)*r**20*R1**
#12*De**12*t**12-0.2119276258474139D-7*exp(-0.25D0*R1/De/t)*r**12*R
#1**8*De**16*t**16-0.2025311986175386D-20*exp(-0.25D0*R1/De/t)*r**2
#4*R1**17*De**7*t**7-0.1368786852762142D-14*exp(-0.25D0*R1/De/t)*r*
**20*R1**13*De**11*t**11-0.1194577616644702D-13*exp(-0.25D0*R1/De/t
#)*r**22*R1**11*De**13*t**13
s2 = s5-0.1627604166467548D-3*exp(-0.25D0*R1/De/t)*r**6*R1**5*De**
#19*t**19+0.1999999999949143D1*De**24*t**24-0.4069010416803099D-5*e
#xp(-0.25D0*R1/De/t)*r**10*R1**6*De**18*t**18-0.5208333333584074D-2
**exp(-0.25D0*R1/De/t)*r**6*R1**3*De**21*t**21-0.1356336805601033D-
#4*exp(-0.25D0*R1/De/t)*r**6*R1**6*De**18*t**18-0.1302083333554576D
#-2*exp(-0.25D0*R1/De/t)*r**6*R1**4*De**20*t**20-0.1627604166467548
#D-4*exp(-0.25D0*R1/De/t)*r**10*R1**5*De**19*t**19+s3
s5 = -0.5086263020845316D-6*exp(-0.25D0*R1/De/t)*r**10*R1**7*De**1
#7*t**17-0.8138020832337739D-4*exp(-0.25D0*R1/De/t)*r**8*R1**5*De**
#19*t**19-0.5475147411048567D-13*exp(-0.25D0*R1/De/t)*r**18*R1**12*
#De**12*t**12-0.5256141514251456D-11*exp(-0.25D0*R1/De/t)*r**18*R1*
**10*De**14*t**14-0.8477105032628096D-6*exp(-0.25D0*R1/De/t)*r**8*R
#1**7*De**17*t**17-0.1017252604042217D-4*exp(-0.25D0*R1/De/t)*r**8*
#R1**6*De**18*t**18
s4 = s5-0.1562500000138645D-1*exp(-0.25D0*R1/De/t)*r**4*R1**3*De**
#21*t**21-0.6570176891228747D-12*exp(-0.25D0*R1/De/t)*r**18*R1**11*
#De**13*t**13-0.5298190646502461D-7*exp(-0.25D0*R1/De/t)*r**8*R1**8
**De**16*t**16-0.342196713158824D-14*exp(-0.25D0*R1/De/t)*r**18*R1*
**13*De**11*t**11-0.1953125000014749D-2*exp(-0.25D0*R1/De/t)*r**4*R
#1**4*De**20*t**20-0.3255208333569325D-3*exp(-0.25D0*R1/De/t)*r**8*
#R1**4*De**20*t**20-0.756884377981176D-9*exp(-0.25D0*R1/De/t)*r**16
**R1**8*De**16*t**16
s5 = s4-0.7129098191337357D-17*exp(-0.25D0*R1/De/t)*r**18*R1**15*D
#e**9*t**9-0.1231908167422505D-12*exp(-0.25D0*R1/De/t)*r**16*R1**12

```

```

#*De**12*t**12-0.2365263681349732D-10*exp(-0.25D0*R1/De/t)*r**16*R1
#**10*De**14*t**14-0.189221094495294D-9*exp(-0.25D0*R1/De/t)*r**16*
#R1**9*De**15*t**15-0.1324547661784173D-9*exp(-0.25D0*R1/De/t)*r**1
#0*R1**10*De**14*t**14-0.2546106496906199D-18*exp(-0.25D0*R1/De/t)*
#r**18*R1**16*De**8*t**8
s3 = s5-0.1695421007159848D-6*exp(-0.25D0*R1/De/t)*r**12*R1**7*De*
#*17*t**17-0.2566475349008294D-15*exp(-0.25D0*R1/De/t)*r**16*R1**14
#*De**10*t**10-0.261619541865D-26*exp(-0.25D0*R1/De/t)*r**24*R1**21
#*De**3*t**3-0.843879994239744D-22*exp(-0.25D0*R1/De/t)*r**24*R1**1
#8*De**6*t**6-0.777198026913481D-17*exp(-0.25D0*R1/De/t)*r**24*R1*
#*14*De**10*t**10-0.6540488546625D-28*exp(-0.25D0*R1/De/t)*r**24*R1
#**22*De**2*t**2-0.45207856834272D-23*exp(-0.25D0*R1/De/t)*r**22*R1
#**19*De**5*t**5
s5 = -0.55254047241888D-23*exp(-0.25D0*R1/De/t)*r**20*R1**19*De**5
#*t**5-0.194429950672837D-17*exp(-0.25D0*R1/De/t)*r**22*R1**15*De**
#9*t**9-0.4238552517582506D-7*exp(-0.25D0*R1/De/t)*r**10*R1**8*De**
#16*t**16-0.5256141514251456D-12*exp(-0.25D0*R1/De/t)*r**20*R1**10*
#De**14*t**14-0.500000000189973D0*exp(-0.25D0*R1/De/t)*r**2*R1*De*
#*23*t**23-0.71350784145D-28*exp(-0.25D0*R1/De/t)*r**22*R1**22*De**
#2*t**2-0.1314035378879979D-12*exp(-0.25D0*R1/De/t)*r**20*R1**11*De
#**13*t**13
s4 = s5-0.6365266242265498D-20*exp(-0.25D0*R1/De/t)*r**20*R1**17*D
#e**7*t**7-0.2102456605573737D-10*exp(-0.25D0*R1/De/t)*r**18*R1**9*
#De**15*t**15-0.1989145700707968D-21*exp(-0.25D0*R1/De/t)*r**20*R1*
#*18*De**6*t**6-0.9721497533641851D-19*exp(-0.25D0*R1/De/t)*r**22*R
#1**16*De**8*t**8-0.3110879210765392D-16*exp(-0.25D0*R1/De/t)*r**22
#*R1**14*De**10*t**10-0.30138571222848D-23*exp(-0.25D0*R1/De/t)*r**
#24*R1**19*De**5*t**5-0.3733055053045317D-15*exp(-0.25D0*R1/De/t)*r
#**22*R1**13*De**11*t**11
s5 = s4-0.1446651418696704D-21*exp(-0.25D0*R1/De/t)*r**22*R1**18*D
#e**6*t**6-0.2488703368485468D-15*exp(-0.25D0*R1/De/t)*r**24*R1**12
#*De**12*t**12-0.1782274547834339D-18*exp(-0.25D0*R1/De/t)*r**20*R1
#**16*De**8*t**8-0.1766063548834154D-8*exp(-0.25D0*R1/De/t)*r**12*R
#1**9*De**15*t**15-0.6480998355761234D-18*exp(-0.25D0*R1/De/t)*r**2
#4*R1**15*De**9*t**9-0.1255773800952D-24*exp(-0.25D0*R1/De/t)*r**22
#*R1**20*De**4*t**4
s1 = s5-0.4050623972350771D-19*exp(-0.25D0*R1/De/t)*r**24*R1**16*D
#e**8*t**8-0.6781684024834019D-6*exp(-0.25D0*R1/De/t)*r**12*R1**6*D
#e**18*t**18+s3-0.756884377981176D-9*exp(-0.25D0*R1/De/t)*r**14*R1*
#*9*De**15*t**15-0.6221758421530785D-16*exp(-0.25D0*R1/De/t)*r**24*
#R1**13*De**11*t**11-0.3942106136005707D-11*exp(-0.25D0*R1/De/t)*r*
#*14*R1**11*De**13*t**13+s2-0.1249999999730379D0*exp(-0.25D0*R1/De/
#t)*r**2*R1**2*De**22*t**22
s2 = 1/De**23/t**23/R1

```

```

t0 = s1*s2

C=(q*sqrt(R1**3)/(4*sqrt(pi*De**3*t**3)))*exp(-r**2*R1/(4.*De*t))*
#exp(-z**2*R1/(4.*De*t))*t0
c1=c/C0
write(11,201)r,c1,c,day
102 continue
201 format(f25.10,5x,f25.10,5x,f25.10,5x,f25.10)
stop
end

```

• Program (3D – Instantaneous Disk Source) : Equation 3-21

```

fd1 :=fopen("3DI-Equation3-21.dat",WRITE);
C0:=63200.;
De:=0.96*10E-06;
a:=1.0;
pi:=3.141592654;
R1:=1.0;
z:=0.0;
r:=0.;
for t from 86400 by 86400 to 2592000 do
day:=t/86400.;
f1:=evalf(int(exp((-De*t*x^2)/R1)* BesselJ(0,x*r)* BesselJ(1,x*a),x=0..infinity));
q:=C0/2.;

C:=((a*q)/(2*sqrt(pi*De*t))*exp((-z^2*R1)/(4*De*t))*f1;
C1:=C/C0;
fprintf(fd1,"%f    %f    %f    %f    \n",day,C1,f1,t);
end do;
fclose(fd1);

```

• Program (3D – Instantaneous Disk Source – Diffusive Loss): Equation 3-24c

```

double precision t0,c,de,c0,a,t,r1,s1,s2,s3,s4,s5,s6,s7,s8
Open(11,file="3D-I-Diffusive-loss.dat")
De=(0.96*10E-06)*0.3
pi=3.141592654
C0=63200.0
a=1.0
z=0.0
Q1=198548.656
R1=1.0
thetam=0.4
q=(pi*(a**2)*C0)/(2*pi*a)
do 101 i=1800,90000,1800
t=real(i)
thr=t/3600.
q20=0.0
c2=0.0

Do 102 j=100,1,-1
r=real(j)*0.01

s5 = -0.13813511810472D-24*exp(-0.25D0*R1/De/t)*r**20*R1**20*De**4
**t**4-0.6249999999920351D-1*exp(-0.25D0*R1/De/t)*r**4*R1**2*De**22
**t**22-0.941830350714D-25*exp(-0.25D0*R1/De/t)*r**24*R1**20*De**4*
**t**4-0.6055075024483637D-8*exp(-0.25D0*R1/De/t)*r**14*R1**8*De**16
**t**16-0.4277458914802414D-17*exp(-0.25D0*R1/De/t)*r**20*R1**15*De
**9*t**9-0.8554917832141746D-16*exp(-0.25D0*R1/De/t)*r**20*R1**14*
#De**10*t**10
s4 = s5-0.5518948590027452D-11*exp(-0.25D0*R1/De/t)*r**12*R1**11*D
#e**13*t**13-0.221016188967552D-21*exp(-0.25D0*R1/De/t)*r**18*R1**1
#8*De**6*t**6-0.313943450238D-26*exp(-0.25D0*R1/De/t)*r**22*R1**21*
#De**3*t**3-0.2986444042563099D-14*exp(-0.25D0*R1/De/t)*r**22*R1**1
#2*De**12*t**12-0.4050623972350771D-20*exp(-0.25D0*R1/De/t)*r**22*R
#1**17*De**7*t**7+0.500000000189973D0*r**2*R1*De**23*t**23+0.24220
#30010047147D-7*r**14*R1**7*De**17*t**17
s3 = s4+0.756884377981176D-9*r**16*R1**8*De**16*t**16+0.6249999999
#920351D-1*r**4*R1**2*De**22*t**22+0.5208333333584074D-2*r**6*R1**3
**De**21*t**21+0.3255208333569325D-3*r**8*R1**4*De**20*t**20+0.1627
#604166467548D-4*r**10*R1**5*De**19*t**19+0.6781684024834019D-6*r**
#12*R1**6*De**18*t**18+0.2102456605573737D-10*r**18*R1**9*De**15*t**
**15+0.5256141514251456D-12*r**20*R1**10*De**14*t**14+0.11945776166
#44702D-13*r**22*R1**11*De**13*t**13+0.2488703368485468D-15*r**24*R
#1**12*De**12*t**12-0.199999999949143D1*exp(-0.25D0*R1/De/t)*De**2

```

```

#4*t**24-0.3096822228515625D-31*exp(-0.25D0*R1/De/t)*r**24*R1**24-0
#.2864369809019474D-18*exp(-0.25D0*R1/De/t)*r**16*R1**16*De**8*t**8
s5 = -0.2649095323568345D-8*exp(-0.25D0*R1/De/t)*r**10*R1**9*De**1
#5*t**15-0.2299561912564291D-12*exp(-0.25D0*R1/De/t)*r**12*R1**12*D
#e**12*t**12-0.2422030010047147D-7*exp(-0.25D0*R1/De/t)*r**14*R1**7
#*De**17*t**17-0.1971053068002853D-11*exp(-0.25D0*R1/De/t)*r**16*R1
***11*De**13*t**13-0.9165983388862317D-17*exp(-0.25D0*R1/De/t)*r**1
#6*R1**15*De**9*t**9-0.171098356579412D-15*exp(-0.25D0*R1/De/t)*r**
#18*R1**14*De**10*t**10
s4 = s5-0.7956582802831872D-20*exp(-0.25D0*R1/De/t)*r**18*R1**17*D
#e**7*t**7-0.1103789718259182D-9*exp(-0.25D0*R1/De/t)*r**12*R1**10*
#De**14*t**14-0.6307369817355439D-10*exp(-0.25D0*R1/De/t)*r**14*R1*
**10*De**14*t**14-0.14864746696875D-29*exp(-0.25D0*R1/De/t)*r**24*R
#1**23*De*t-0.2933114684309095D-15*exp(-0.25D0*R1/De/t)*r**14*R1**1
#4*De**10*t**10-0.6159540837112523D-14*exp(-0.25D0*R1/De/t)*r**16*R
#1**13*De**11*t**11-0.1971053068002853D-12*exp(-0.25D0*R1/De/t)*r**
#14*R1**12*De**12*t**12
s5 = s4-0.8212721114035934D-14*exp(-0.25D0*R1/De/t)*r**14*R1**13*D
#e**11*t**11-0.1642544223441416D-13*exp(-0.25D0*R1/De/t)*r**20*R1**
#12*De**12*t**12-0.2119276258474139D-7*exp(-0.25D0*R1/De/t)*r**12*R
#1**8*De**16*t**16-0.2025311986175386D-20*exp(-0.25D0*R1/De/t)*r**2
#4*R1**17*De**7*t**7-0.1368786852762142D-14*exp(-0.25D0*R1/De/t)*r**
**20*R1**13*De**11*t**11-0.1194577616644702D-13*exp(-0.25D0*R1/De/t
#)*r**22*R1**11*De**13*t**13
s2 = s5-0.1627604166467548D-3*exp(-0.25D0*R1/De/t)*r**6*R1**5*De**
#19*t**19+0.1999999999949143D1*De**24*t**24-0.4069010416803099D-5*e
#xp(-0.25D0*R1/De/t)*r**10*R1**6*De**18*t**18-0.5208333333584074D-2
**exp(-0.25D0*R1/De/t)*r**6*R1**3*De**21*t**21-0.1356336805601033D-
#4*exp(-0.25D0*R1/De/t)*r**6*R1**6*De**18*t**18-0.1302083333554576D
#-2*exp(-0.25D0*R1/De/t)*r**6*R1**4*De**20*t**20-0.1627604166467548
#D-4*exp(-0.25D0*R1/De/t)*r**10*R1**5*De**19*t**19+s3
s5 = -0.5086263020845316D-6*exp(-0.25D0*R1/De/t)*r**10*R1**7*De**1
#7*t**17-0.8138020832337739D-4*exp(-0.25D0*R1/De/t)*r**8*R1**5*De**
#19*t**19-0.5475147411048567D-13*exp(-0.25D0*R1/De/t)*r**18*R1**12*
#De**12*t**12-0.5256141514251456D-11*exp(-0.25D0*R1/De/t)*r**18*R1*
**10*De**14*t**14-0.8477105032628096D-6*exp(-0.25D0*R1/De/t)*r**8*R
#1**7*De**17*t**17-0.1017252604042217D-4*exp(-0.25D0*R1/De/t)*r**8*
#R1**6*De**18*t**18
s4 = s5-0.1562500000138645D-1*exp(-0.25D0*R1/De/t)*r**4*R1**3*De**
#21*t**21-0.6570176891228747D-12*exp(-0.25D0*R1/De/t)*r**18*R1**11*
#De**13*t**13-0.5298190646502461D-7*exp(-0.25D0*R1/De/t)*r**8*R1**8
**De**16*t**16-0.342196713158824D-14*exp(-0.25D0*R1/De/t)*r**18*R1*
**13*De**11*t**11-0.1953125000014749D-2*exp(-0.25D0*R1/De/t)*r**4*R
#1**4*De**20*t**20-0.3255208333569325D-3*exp(-0.25D0*R1/De/t)*r**8*

```

```

#R1**4*De**20*t**20-0.756884377981176D-9*exp(-0.25D0*R1/De/t)*r**16
#*R1**8*De**16*t**16
s5 = s4-0.7129098191337357D-17*exp(-0.25D0*R1/De/t)*r**18*R1**15*D
#e**9*t**9-0.1231908167422505D-12*exp(-0.25D0*R1/De/t)*r**16*R1**12
#*De**12*t**12-0.2365263681349732D-10*exp(-0.25D0*R1/De/t)*r**16*R1
***10*De**14*t**14-0.189221094495294D-9*exp(-0.25D0*R1/De/t)*r**16*
#R1**9*De**15*t**15-0.1324547661784173D-9*exp(-0.25D0*R1/De/t)*r**1
#0*R1**10*De**14*t**14-0.2546106496906199D-18*exp(-0.25D0*R1/De/t)*
#r**18*R1**16*De**8*t**8
s3 = s5-0.1695421007159848D-6*exp(-0.25D0*R1/De/t)*r**12*R1**7*De*
#*17*t**17-0.2566475349008294D-15*exp(-0.25D0*R1/De/t)*r**16*R1**14
#*De**10*t**10-0.261619541865D-26*exp(-0.25D0*R1/De/t)*r**24*R1**21
#*De**3*t**3-0.843879994239744D-22*exp(-0.25D0*R1/De/t)*r**24*R1**1
#8*De**6*t**6-0.7777198026913481D-17*exp(-0.25D0*R1/De/t)*r**24*R1*
**14*De**10*t**10-0.6540488546625D-28*exp(-0.25D0*R1/De/t)*r**24*R1
***22*De**2*t**2-0.45207856834272D-23*exp(-0.25D0*R1/De/t)*r**22*R1
***19*De**5*t**5
s5 = -0.55254047241888D-23*exp(-0.25D0*R1/De/t)*r**20*R1**19*De**5
#*t**5-0.194429950672837D-17*exp(-0.25D0*R1/De/t)*r**22*R1**15*De**
#9*t**9-0.4238552517582506D-7*exp(-0.25D0*R1/De/t)*r**10*R1**8*De**
#16*t**16-0.5256141514251456D-12*exp(-0.25D0*R1/De/t)*r**20*R1**10*
#De**14*t**14-0.500000000189973D0*exp(-0.25D0*R1/De/t)*r**2*R1*De*
#*23*t**23-0.71350784145D-28*exp(-0.25D0*R1/De/t)*r**22*R1**22*De**
#2*t**2-0.1314035378879979D-12*exp(-0.25D0*R1/De/t)*r**20*R1**11*De
***13*t**13
s4 = s5-0.6365266242265498D-20*exp(-0.25D0*R1/De/t)*r**20*R1**17*D
#e**7*t**7-0.2102456605573737D-10*exp(-0.25D0*R1/De/t)*r**18*R1**9*
#De**15*t**15-0.1989145700707968D-21*exp(-0.25D0*R1/De/t)*r**20*R1*
#*18*De**6*t**6-0.9721497533641851D-19*exp(-0.25D0*R1/De/t)*r**22*R
#1**16*De**8*t**8-0.3110879210765392D-16*exp(-0.25D0*R1/De/t)*r**22
#*R1**14*De**10*t**10-0.30138571222848D-23*exp(-0.25D0*R1/De/t)*r**
#24*R1**19*De**5*t**5-0.3733055053045317D-15*exp(-0.25D0*R1/De/t)*r
***22*R1**13*De**11*t**11
s5 = s4-0.1446651418696704D-21*exp(-0.25D0*R1/De/t)*r**22*R1**18*D
#e**6*t**6-0.2488703368485468D-15*exp(-0.25D0*R1/De/t)*r**24*R1**12
#*De**12*t**12-0.1782274547834339D-18*exp(-0.25D0*R1/De/t)*r**20*R1
***16*De**8*t**8-0.1766063548834154D-8*exp(-0.25D0*R1/De/t)*r**12*R
#1**9*De**15*t**15-0.6480998355761234D-18*exp(-0.25D0*R1/De/t)*r**2
#4*R1**15*De**9*t**9-0.1255773800952D-24*exp(-0.25D0*R1/De/t)*r**22
#*R1**20*De**4*t**4
s1 = s5-0.4050623972350771D-19*exp(-0.25D0*R1/De/t)*r**24*R1**16*D
#e**8*t**8-0.6781684024834019D-6*exp(-0.25D0*R1/De/t)*r**12*R1**6D
#e**18*t**18+s3-0.756884377981176D-9*exp(-0.25D0*R1/De/t)*r**14*R1*
#*9*De**15*t**15-0.6221758421530785D-16*exp(-0.25D0*R1/De/t)*r**24*

```



```

#R1**13*De**11*t**11-0.3942106136005707D-11*exp(-0.25D0*R1/De/t)*r*
#*14*R1**11*De**13*t**13+s2-0.124999999730379D0*exp(-0.25D0*R1/De/
#t)*r**2*R1**2*De**22*t**22
s2 = 1/De**23/t**23/R1
t0 = s1*s2

c=(q*sqrt(R1**3)/(4*sqrt(pi*De**3*t**3)))*exp(-r**2*R1/
#(4.*De*t))*exp(-z**2*R1/(4.*De*t))*t0
c1=(q*sqrt(R1)/(2*sqrt(pi*De*t)))*(1.-exp(-a**2*R1/
#(4.*De*t)))*exp(-z**2*R1/(4.*De*t))

if (r .eq. 1.) then
q10=pi*c
c2=c
go to 999
endif
if (r .eq. 0.01) then
q30=pi*(0.01**2)*(c1-c)
go to 1000
endif
q2=pi*((r)**2)*(c-c2)
q20=q20+q2
c2=c
1000 write(*,*) " "

if(r .eq. 0.01)then
q3=q10+q20+q30
q4=Q1-q3
q5=thetam*(1-q3/Q1)
write(11,201)thr,c,q3,q4,q5
endif
999 write(*,*) " "
102 continue
101 continue
201 format(f25.10,5x,f25.10,5x,f25.10,5x,f25.10,5x,f25.10,5x,f25.10)
stop
end

```

• Program (3D – Continuous Disk Source) : Equation 3-27

```

fd1 :=fopen("equation3-27a.dat",WRITE);
fd2 :=fopen("equation3-27b.dat ",WRITE);

pi:=3.141592654;
for t from 0.2 by 0.2 to 10 do
for r from 0.0 by 0.25 to 1 do
E:=evalf((2./pi)*int((sqrt(1-r^2*sin(x)*sin(x))),x=0..pi/2));
for i from 1 by 1 to 75 do
val:=i;
U[i,1]:=1.;
C[0]:=1;

for j from 2 by 1 to val do
U[i,j]:=(U[i,j-1]*((i-j+2)*r)/(j-1));
end do;

T[i]:=U[i,1]+sum('(U[i,j-1]*((i-j+2)*r)/(j-1)))^2*((i-j+1)/i)',j1=2..val);
end do;

for k from 1 by 1 to 75 do
C[k]:=4^k*(2*k+1)*((k+1)!);
end do;

R:=(-1/(2*sqrt(pi*t)))*sum('((-1)^(k+1)/(C[k-1]*t^(k-1)))*T[k]',k'=1..75);
RT:=E+(-1/(2*sqrt(pi*t)))*sum('((-1)^(k+1)/(C[k-1]*t^(k-1)))*T[k]',k'=1..75);
fprintf(fd1,"%g          %g          %+15.10f\n",t,r,RT);
end do;
end do;

for t from 10.0 by 10.0 to 100 do
for r from 0.0 by 0.25 to 1 do

E:=evalf((2./pi)*int((sqrt(1-r^2*sin(x)*sin(x))),x=0..pi/2));

for i from 1 by 1 to 75 do
val:=i;
U[i,1]:=1.;
C[0]:=1;

for j from 2 by 1 to val do
U[i,j]:=(U[i,j-1]*((i-j+2)*r)/(j-1));
end do;

```

```

T[i]:=U[i,1]+sum('(U[i,j1-1]*(((i-j1+2)*r)/(j1-1)))^2*((i-j1+1)/i)',j1=2..val);
end do;

for k from 1 by 1 to 75 do
C[k]:=4^k*(2*k+1)*((k+1)!);
end do;
R:=(-1/(2*sqrt(pi*t)))*sum('((-1)^(k+1)/(C[k-1]*t^(k-1)))*T[k]',k'=1..75);
RT:=E+(-1/(2*sqrt(pi*t)))*sum('((-1)^(k+1)/(C[k-1]*t^(k-1)))*T[k]',k'=1..75);
fprintf(fd1,"%g          %g          %+15.10f\n",t,r,RT);
end do;
end do;

for t from 100. by 100. to 10000 do
for r from 0.0 by 0.25 to 1 do

E:=evalf((2./pi)*int((sqrt(1-r^2*sin(x)*sin(x))),x=0..pi/2));
for i from 1 by 1 to 75 do
val:=i;
U[i,1]:=1.;
C[0]:=1;

for j from 2 by 1 to val do
U[i,j]:=(U[i,j-1]*(((i-j+2)*r)/(j-1)));
end do;

T[i]:=U[i,1]+sum('(U[i,j1-1]*(((i-j1+2)*r)/(j1-1)))^2*((i-j1+1)/i)',j1=2..val);
end do;
for k from 1 by 1 to 75 do
C[k]:=4^k*(2*k+1)*((k+1)!);
end do;
R:=(-1/(2*sqrt(pi*t)))*sum('((-1)^(k+1)/(C[k-1]*t^(k-1)))*T[k]',k'=1..75);
RT:=E+(-1/(2*sqrt(pi*t)))*sum('((-1)^(k+1)/(C[k-1]*t^(k-1)))*T[k]',k'=1..75);
fprintf(fd1,"%g          %g          %+15.10f\n",t,r,RT);
end do;
end do;

for t from 10000. by 10000. to 100000 do
for r from 0.0 by 0.25 to 1 do
E:=evalf((2./pi)*int((sqrt(1-r^2*sin(x)*sin(x))),x=0..pi/2));
for i from 1 by 1 to 75 do
val:=i;
U[i,1]:=1.;
C[0]:=1;

```

```

for j from 2 by 1 to val do
U[i,j]:=U[i,j-1]*(((i-j+2)*r)/(j-1));
end do;

T[i]:=U[i,1]+sum('U[i,j1-1]*(((i-j1+2)*r)/(j1-1))^2*((i-j1+1)/i)',j1=2..val);
end do;

for k from 1 by 1 to 75 do
C[k]:=4^k*(2*k+1)*((k+1)!);
end do;

R:=(-1/(2*sqrt(pi*t)))*sum('((-1)^(k+1)/(C[k-1]*t^(k-1)))*T[k]','k'=1..75);
RT:=E+(-1/(2*sqrt(pi*t)))*sum('((-1)^(k+1)/(C[k-1]*t^(k-1)))*T[k]','k'=1..75);

fprintf(fd1,"%g          %g          %+15.10fn",t,r,RT);

end do;
end do;
fclose(fd1);

for t from 0.2 by 0.2 to 10 do
for r1 from 1.25 by 0.25 to 20 do

pi:=3.141592654;

E1:=evalf(int((sqrt(1-(1/r1)^2*sin(x))*sin(x)),x=0..pi/2));
K1:=evalf(int(1/(sqrt(1-(1/r1)^2*sin(x))*sin(x)),x=0..pi/2));
K:=evalf( (2.*r1)/pi)*(E1-(1-(1/r1)^2)*K1);

for i from 1 by 1 to 75 do
val:=i;
U[i,1]:=1.;
C[0]:=1;
for j from 2 by 1 to val do
U[i,j]:=U[i,j-1]*(((i-j+2)*r1)/(j-1));
end do;

T[i]:=U[i,1]+sum('U[i,j1-1]*(((i-j1+2)*r1)/(j1-1))^2*((i-j1+1)/i)',j1=2..val);
end do;

for k from 1 by 1 to 75 do
C[k]:=4^k*(2*k+1)*((k+1)!);
end do;

```

```

R0:=(-1/(2*sqrt(pi*t)))*sum('((-1)^(k+1)/(C[k-1]*t^(k-1)))*T[k]','k'=1..75);
RT0:=K+(-1/(2*sqrt(pi*t)))*sum('((-1)^(k+1)/(C[k-1]*t^(k-1)))*T[k]','k'=1..75);

fprintf(fd2,"%g          %g          %+15.10f\n",t,r1,RT0);
end do;
end do;

for t from 10.0 by 10.0 to 100 do
for r1 from 1.25 by 0.25 to 20 do
pi:=3.141592654;
E1:=evalf(int((sqrt(1-(1/r1)^2*sin(x)*sin(x))),x=0..pi/2));
K1:=evalf(int(1/(sqrt(1-(1/r1)^2*sin(x)*sin(x))),x=0..pi/2));
K:=evalf( (2.*r1)/pi)*(E1-(1-(1/r1)^2)*K1);
for i from 1 by 1 to 75 do
val:=i;
U[i,1]:=1.;
C[0]:=1;

for j from 2 by 1 to val do
U[i,j]=(U[i,j-1]*(((i-j+2)*r1)/(j-1)));
end do;
T[i]:=U[i,1]+sum('U[i,j-1]*(((i-j+2)*r1)/(j-1)))^2*((i-j+1)/i)',j=2..val);
end do;

for k from 1 by 1 to 75 do
C[k]:=4^k*(2*k+1)*((k+1)!);
end do;
R0:=(-1/(2*sqrt(pi*t)))*sum('((-1)^(k+1)/(C[k-1]*t^(k-1)))*T[k]','k'=1..75);
RT0:=K+(-1/(2*sqrt(pi*t)))*sum('((-1)^(k+1)/(C[k-1]*t^(k-1)))*T[k]','k'=1..75);
fprintf(fd2,"%g          %g          %+15.10f\n",t,r1,RT0);
end do;
end do;

for t from 100. by 100. to 10000 do
for r1 from 1.5 by 0.5 to 20. do

pi:=3.141592654;
E1:=evalf(int((sqrt(1-(1/r1)^2*sin(x)*sin(x))),x=0..pi/2));
K1:=evalf(int(1/(sqrt(1-(1/r1)^2*sin(x)*sin(x))),x=0..pi/2));
K:=evalf((2.*r1)/pi)*(E1-(1-(1/r1)^2)*K1);
for i from 1 by 1 to 75 do
val:=i;
U[i,1]:=1.;
C[0]:=1;

```

```

for j from 2 by 1 to val do
U[i,j]:=(U[i,j-1]*(((i-j+2)*r1)/(j-1)));
end do;
T[i]:=U[i,1]+sum('(U[i,j1-1]*(((i-j1+2)*r1)/(j1-1)))^2*((i-j1+1)/i)',j1=2..val);
end do;
for k from 1 by 1 to 75 do
C[k]:=4^k*(2*k+1)*((k+1)!);
end do;
R0:=(-1/(2*sqrt(pi*t)))*sum('((-1)^(k+1)/(C[k-1]*t^(k-1)))*T[k]',k'=1..75);
RT0:=K+(-1/(2*sqrt(pi*t)))*sum('((-1)^(k+1)/(C[k-1]*t^(k-1)))*T[k]',k'=1..75);
fprintf(fd2,"%g          %g          %+15.10f\n",t,r1,RT0);
end do;
end do;

```

• Program (3D – Continuous Disk Source – Diffusive Loss): Equation 3-33b

```

fd1 :=fopen("3D-C-MdT.dat",WRITE);
pi:=3.141592654;
C0:=63200.;
for t from 0.82944 by 0.82944 to 41.472 do
day:=t/0.82944;
qsum:=0.0;
for r from 1.0 by -0.05 to 0 do
E:=evalf((2./pi)*int((sqrt(1-r^2*sin(x))*sin(x)),x=0..pi/2));
for i from 1 by 1 to 75 do
val:=i;
U[i,1]:=1.;
C[0]:=1;
for j from 2 by 1 to val do
U[i,j]:=(U[i,j-1]*(((i-j+2)*r)/(j-1)));
end do;

T[i]:=U[i,1]+sum('(U[i,j1-1]*(((i-j1+2)*r)/(j1-1)))^2*((i-j1+1)/i)',j1=2..val);
end do;

for k from 1 by 1 to 75 do
C[k]:=4^k*(2*k+1)*((k+1)!);
end do;

R:=(-1/(2*sqrt(pi*t)))*sum('((-1)^(k+1)/(C[k-1]*t^(k-1)))*T[k]',k'=1..75);

```

```
RT:=E+(-1/(2*sqrt(pi*t)))*sum('((-1)^(k+1)/(C[k-1]*t^(k-1)))*T[k]', 'k'=1..75);
qsum1:=pi*r^2*RT;
qsum:=qsum+qsum1;
qrel:=qsum/E;
if(r = 0) then
fprintf(fd1,"%g %g %+15.10f %+15.10fn",day,RT,qsum/20,qrel/20);
end if;
end do;
end do;
fclose(fd1);
```

Appendix II. Analysis data for experiments 2 and 3.

Sample Number	Distance (cm)	Experiment 2		Experiment 3	
		Concentration (ppm)	Calibrated concentration (ppm)	Concentration (ppm)	Calibrated concentration (ppm)
1	1	91.1	92.08	128.8	112.65
2	1	19.6	19.50	228	193.74
3	1.5	17.6	22.06	23.3	19.65
4	1.5	4.3	5.42	69.3	74.92
5	2	5.1	6.04	12.9	15.20
6	2	3.1	3.43	47.6	42.85
7	3	2.5	2.68	22.4	29.30
8	3	1.9	2.01	9.4	8.26
9	5	ND	ND	6	6.40
10	5	ND	ND	ND	ND
11	6	ND	ND	4.1	5.54
12	6	ND	ND	ND	ND
13	9	1.8	2.02	4.5	4.70
14	9	2	1.95	ND	ND
15	3	ND	ND	3.1	2.8
16	3.6	ND	ND	ND	ND
17	5	ND	ND	ND	ND
18	6.7	ND	ND	ND	ND
19	8.5	ND	ND	ND	ND
20	6	ND	ND	ND	ND
21	6.32	ND	ND	ND	ND
22	7.21	ND	ND	ND	ND
23	8.48	ND	ND	ND	ND
24	10	ND	ND	ND	ND